

# **Geological evolution of the Strandja Massif (Thrace, Turkey)**

Dissertation  
zur Erlangung des Grades eines Doktors der Naturwissenschaften

der Geowissenschaftlichen Fakultät  
der Eberhard-Karls-Universität Tübingen

vorgelegt von  
GÜRSEL SUNAL  
aus Ankara/Türkei

2008

Tag der mündlichen Prüfung: 16.12.2008

Dekan: Prof. Prof. Dr. Peter Grathwohl

1. Berichterstatter: Prof. Dr. Dr. h.c. M. Satir

2. Berichterstatter: Prof. Dr. B.A. Natal'in

## Contents

Abstract	1
Kurzfassung	3
Introduction	5
Geological Overview	7
Analytical techniques	12
Summary of the Publications	14
References	20
Supplementary	25
<u>Chapter 1:</u> Paleozoic magmatic events in the Strandja Massif, NW Turkey	25
<u>Chapter 2:</u> Paleotectonic position of the Strandja massif, northwest Turkey, and surrounding continental blocks, based on zircon Pb-Pb age studies	65
<u>Chapter 3:</u> Diachronous metamorphism and exhumation in a contractional orogen: the Strandja Massif, NW Turkey	117

## **Acknowledgements**

I would like to express my thanks to all of those who have been involved in my research here at Tübingen University. My sincere appreciation goes to my advisors Prof. Dr. Dr. h. c. Muharrem Satır and Prof. Dr. Boris A. Natal'in for their guidance and for the opportunities that they made available to me. Their knowledge and patience allowed me to expand my geologic background and apply it to a great research opportunity. Helps of G. Bartholomä during mineral separation and XRF studies, H. Taubault during XRF measurements, W. Siebel, E. Reitter and T.T.B. Nguyen during isotopic measurements are gratefully appreciated. I also wish to thank B. Steinhilber, G. Stoschek and U. Wahl for their friendship and invaluable help during my study in the institute. I would also like to express my thanks to my best friend M. Kibaroglu. I thoroughly enjoyed working with him as a officemate and discussing geologic and social topics. E. Toraman is thanked for his friendship, assists in the field and constructive comments during whole extend of this study. A. Dikbaş and O. Wonderschmidt are thanked for the field studies. Thank goes to G. Topuz whose background in metamorphic and igneous petrogenesis was invaluable. I thank R. Altherr for friendly access to electron microprobe facility in Heidelberg. I also wish to thank A.İ. Okay, S. Akyüz, P. Bons and W. Siebel for their constractive comments and corrections during the preperation of the manuscripts. V. Morgan is thanked for her help with the English.

This research was funded by TÜBİTAK (The Scientific and Technical Research Council of Turkey, Project no: YDABCAG 101Y010) and resulted from the cooperative study between Istanbul Technical University (ITU Research fond, Project no: 11-07-128), Turkey and University of Tübingen, Germany.

Lastly I wish to thank my family for their love and support. This PhD thesis is dedicated to memory of my father Şevket Sunal and to love of my mother Suzan Sunal.

## Abstract

The Strandja Massif is located in the NW part of Turkey. The massif is bounded by the Thrace basin to the south, the Istanbul Zone to the east and the Black Sea to the north. It is roughly a NW-SE trending mountain belt, ca. 200 km long and 90 km wide. The tectonic position of the massif is interpreted as a western part of the Pontide belt. The main aim of this study focuses on the formation history of metamorphic rocks of the Strandja Massif using structural, petrological, geochemical, and radiogenic dating methods.

The Strandja Massif mainly consist of two assemblages (the basement and the cover), which can be distinguished to each other with their rock association, age, and pre-metamorphic unconformity defined between them. The basement constitutes Paleozoic metasediments (biotite and garnet-biotite schists) and orthogneisses (hornblende-biotite, biotite-muscovite, and muscovite orthogneisses) whereas the cover association compound of Mesozoic metaclastic rocks.

Metamorphic grade decreases from the epidote-amphibolite facies in the south to the albite-epidote amphibolite/greenschist-facies transition in the north. Estimated  $P$ - $T$  conditions reach 485-530 °C and 0.60-0.80 GPa in the south and ~450-500 °C in the northern part. Rb-Sr muscovite ages decrease systematically northwards from 162 to 142 Ma. The Rb-Sr biotite ages also decrease systematically from 153 Ma in the south to 134 in the north. These ages point out diachronous metamorphism and cooling. Structural features such as (i) consistent south-dipping foliation, (ii) southwest to southeast-plunging stretching lineation, (iii) top to north shear sense, and ductile shear zones suggest compressional deformation coupled with exhumation.

Various types of orthogneisses constitute a significant part of the metamorphic basement. Their modal compositions correspond to quartz diorite, tonalite, granodiorite and trondhjemite. Geochemical data suggest a calc-alkaline trend of differentiation. Isotopic dating using the single zircon Pb-Pb evaporation method has shown that there are two magmatic events; one occurred within a short time interval between  $312\pm 2$  and  $315\pm 5$  Ma and another one is dated as  $257\pm 6$  Ma, which shows extensive magmatic activity in the study area during the late Carboniferous and Permian intervals. These magmatic activities indicate existence of a mature magmatic arc.

For the deposition age of the basement metasediments, evaporation Pb-Pb ages of detrital zircons are used. According to that protholite age of garnet-biotite schists of the

metamorphic basement were deposited later than 430 Ma and prior to 315 Ma whereas biotite schists exposed along the southern boundary of the basement were restricted between 300 and 271 Ma.

Pb-Pb detrital zircon ages have been used for revealing tectonic history and initial position of the Strandja massif. Age data derived from detrital zircons vary between 430 and 2700 Ma, which reveal to heterogeneous source areas. Detrital zircon ages of the Strandja Massif are correlative with both the Avalonian and the Armorican tectonic units of Western Europe. The presence of Mesoproterozoic zircon ages in the metasediments of the Strandja massif indicates that the proximity of the Strandja massif to Avalonian (or Baltica) derived units occurred during the late Silurian-Carboniferous interval.

## **Kurzfassung**

Das Strandja-Massiv liegt im Nordwesten der Türkei und wird vom Thrakien-Becken im Süden, von der Istanbul-Zone im Osten und vom Schwarzen Meer im Norden abgegrenzt. Es bildet eine NW-SO streichenden Gebirgsgürtel, ca. 200 km lang und 90 km breit. Tektonisch betrachtet wird das Massiv als westlicher Ausläufer des Pontischen Gebirgsgürtels angesehen. Diese Arbeit befasst sich mit der Entwicklungsgeschichte der metamorphen Gesteine des Strandja Massivs. Seine Gesteine wurden mit Hilfe von strukturgeologischen, petrographischen, geochemischen und radiometrischen Methoden untersucht.

Das Massiv besteht hauptsächlich aus zwei Einheiten (Basement und Decke), die sich bezüglich ihrer Gesteinsvergesellschaftung, des Alters und einer pre-metamorphen Diskordanz voneinander unterscheiden. Die Basement-Einheit besteht im Wesentlichen aus Paläozoischen Metasedimenten (Biotit- und Granat-Biotit-Schiefer) und Orthogneissen (Hornblende-Biotit-, Biotit-Muskovit- und Muskovit-Orthogneissen), während sich die Deckeneinheit aus Mesozoischen, metaklastischen Gesteinen, wie etwa Metakonglomeraten und Metasandsteinen, zusammensetzt.

Der Metamorphosegrad nimmt von einer Epidot-Amphibolit-Fazies im Süden zu einer Albit-Epidot-Amphibolit/Grünschiefer-Fazies im Norden ab. Geschätzte P-T Bedingungen reichen von 485-530 °C / 0.60-0.80 GPa in Süden bis zu ~ 450-500 °C im Norden. Rb-Sr Muskovit Alter zeigen eine systematische Abnahme von 162 Ma auf 142 Ma nach Norden hin. Die Rb-Sr Biotit Alter nehmen ebenfalls systematisch von 153 Ma im Süden auf 134 Ma im Norden ab. Diese Alterdaten deuten auf eine diakrone Metamorphose und Abkühlung hin. Mehrere strukturelle Merkmale, wie z.B. (i) einstimmig nach Süden einfallende Foliation, (ii) S-SE streichende Lineation und (iii) nordvergente Verscherung und duktilen Scherzonen deuten auf Kompression während der Exhumierung hin.

Die Orthogneisse, die den wesentlichen Bestandteil der Basement-Einheit ausmachen, weisen Modalbestände auf, die einem Quarz-Diorit, Tonalit, Granodiorit und Trondhjemite entsprechen. Geochemisch lässt sich eine kalk-alkalischer Differenziationstrend erkennen. Pb-Pb Evaporationsdatierungen an magmatischen Zirkonen erbrachten Alterswerte, die auf zwei getrennte magmatischen Aktivitäten hin deuten. Die erste erfolgte von 312±2 Ma bis zu 315±5 Ma, und die zweite ca. bei 257±6 Ma. Diese deutet auf einen weit verbreiteten Magmatismus während des Spätkarbons und Frühperms hin. Dieser Magmatismus lässt sich auf eine Bildung in einem reifen magmatischen Bogen zurückführen.

Die Sedimentationsalter der Metasedimente im Basement wurden anhand von Pb-Pb Evaporationsaltern von detritischen Zirkonen eingegrenzt, demnach erfolgte die Ablagerung der Protolithe der Granat-Biotit-Schiefer zwischen 430 und 315 Ma, während die Sedimentation der Protolithe der Biotit-Schiefer im südlichen Teil des Arbeitsgebietes zwischen 300 Ma und 271 Ma eingegrenzt werden konnte.

Pb-Pb Alterswerte detritischer Zirkone wurden zur Ermittlung der ursprünglichen geotektonischen Stellung des Strandja-Massivs verwendet. Ihre Alterswerte variieren zwischen 430 Ma und 2700 Ma, was auf sehr heterogene Einzugsgebiete zurückschliessen lässt. Vergleichbare Alterswerte sind aus den sogenannten tektonischen Einheiten Avalonia und Armorika in West-Europa bekannt. Die Anwesenheit von mesoproterozoischen Zirkonen in den Metasedimenten deutet darauf hin, dass sich das Strandja-Massiv der tektonischen Einheit Avalonia während des Spätsilur-Karbon-Intervalls annäherte.



## Introduction

This study has been proposed and supervised by Prof. Dr. Dr. h.c. Muharrem Satır and Prof. Dr. Boris Natal'in. The main aim of this study in the geology of metamorphic rocks in the Strandja Massif, NW Turkey, because they haven't been well-studied previously. At the same time, the Strandja Massif has a key location allowing to resolve first order global and local tectonic problems. For instance, the position of the Paleo-Tethyan suture, the continuity of the Hercynian structures from Bulgaria to Turkey and the Gondwanian versus Asiatic origin of Precambrian and Paleozoic basements of the region. Among the local problems we should name the protolith age of metamorphic rocks, timing of metamorphism and magmatism, and thus, exhumation history of the metamorphic rocks.

The main methods we used include detailed geological mapping, petrography, petrology, and U-Pb and Rb-Sr geochronology. They allowed us to understand tectonics of the region, and to correlate with the neighboring regions such as the Sakar-Strandja Zone in Bulgaria and the Rhodope Massif in Greece and Bulgaria. The frame of this study comprises events starting from pre-Cambrian to late Mesozoic.

This thesis consists of three chapters each focusing on different geologic problem of the region.

- The first chapter deals with Variscan and post-Variscan events within the study area. For this, the magmatic rocks assigned in the previous workers to the metamorphic basement of the Strandja Massif have been classified in terms of petrological criteria. Then classified magmatic rocks have been dated using zircon evaporation technique revealing the completely new dataset for the region. Finally, geochemical properties of magmatic rocks have been used for determination of their tectonic settings. As a result of this study, the Variscan tectonics recorded in the Strandja Massif were re-evaluated and correlated with the neighboring regions.
- The second chapter is devoted to the results of the detrital zircon analysis that were performed in the region for the first time. Discovering the Ordovician as depositional time and wide older spectrum of ages allowed us estimate the paleotectonic position of the Strandja Massif and the surrounding regions. Besides the detrital zircons, the xenocrystic zircons from the magmatic rocks have been used as tracers. The zircon

dataset from Paleozoic rocks of the Strandja Massif has been correlated with available data sets belonging to Tectonic zones in Europe, Turkey and the main cratons within Africa, Baltica and S. America. The zones belonging to Gondwana-Land were compared and classified according to the compiled zircon ages.

- The Mesozoic aged Cimmeride events have been presented in the third chapter. In this period the study area was metamorphosed and penetratively deformed. Deformation formed N-verging stacking in the whole region. Being able to understand the geologic history of this period, we used Rb-Sr dating and metamorphic petrology. Facies analyses were carried out via EPMA and optical petrology. Finally, we combined geochemical and petrologic data with structural data.

## Geological Overview

The Strandja Massif is located in the NW part of Turkey. The massif is bounded by the Thrace basin to the south, the Istanbul Zone to the east and waters of Black Sea to the north. It is roughly a NW-SE trending massif and its continuation crosses the Turkish-Bulgaria border (Fig. 1 and 2). In Bulgarian side, the relevant structures are either named as the “Strandja Massif” or the “Sakar-Strandja Massif” (Chatalov, 1988; Chatalov, 1991; Yanev, 2000 ; Gerdjikov, 2005) (Fig. 1 and 2). In Turkey, the name “Strandja Massif” was first used by Pamir and Baykal (1947).

Tectonic assemblage of Turkey was formed by the collision of continental blocks or zones departed from Gondwana-Land, or more specifically Africa and S America, during the different geological intervals (Şengör and Yılmaz, 1981; Şengör et al., 1984). Tethyan amalgamations are the most widely studied and known tectonic events in the region. The Tethysides were resulted by two different ocean closures, namely Paleo- and Neo-Tethys, respectively. The Cimmerides were formed at the expense of the closure of the Paleo-Tethys while the Alpine belt is the result of the Neo-Tethyan evolution. Hercynian events (now started to be called as Variscan) were also extensively studied but traces of this event were poorly preserved. The tectonic position of the massif is interpreted as a western part of the Pontide belt that occupies northern Turkey, southern Black Sea coast (Ketin, 1966). Şengör and Yılmaz (1981), re-evaluated Turkish geology in terms of plate tectonics approach, and interpreted the Pontides in the frame of Paleo- and Neo-Tethyan closure (Cimmeride and Alpine orogeny). They stressed the importance of the suture zones which divide the Anatolides from the Pontides. In addition, they proposed role of the Paleo-Tethyan events on the formation of the Pontides.

The Strandja Massif consists of two parts; the high grade basement units with Kırklareli type metagranites which are mainly Paleozoic in age and the cover units which were represented by epi-continental clastics and allochthonous Triassic phylittes with metabasics (Aydın, 1982; Chatalov, 1988; Chatalov, 1991 ; Okay et al., 2001; Natal'in et al., 2005). The basement made up of different types of orthogneisses, biotite paragneisses and amphibolites whereas the cover consists of clastic and calcareous sediments. The first radiometric dates related with the rocks of the Strandja Massif were reported by Aydın (1982). This study was done in the Kırklareli region and comprises Rb-Sr whole-rock dates of Kırklareli metagranite ( $244 \pm 11$  Ma) with mineral-whole-rock Rb-Sr ( $155 \pm 2$  Ma) metamorphic ages. Later studies mainly used ages reported by Aydın (1982) and paleontologically determined ages from the

Bulgarian side of the Strandja Massif. The recent study has published by Okay et al. (2001). They dated basement rocks exposed in the Kırklareli region using Pb-Pb evaporation and Rb-Sr methods. They claimed that the Kırklareli type plutons emplaced in different intervals in the late Carboniferous and early Permian (309-271 Ma). They also dated a migmatite sample and found ages  $299 \pm 15$  and  $276 \pm 12$  Ma for the high grade early metamorphism. This early metamorphic phase idea was also shared by Natal'in et al. (2005). They reported early formed foliation in the basement rocks and interpreted this to be a pre-Mesozoic deformation. The metamorphic age for the Mesozoic metamorphism and deformation given by Okay et al. (2001) confirmed the reported dates by Aydın (1982).

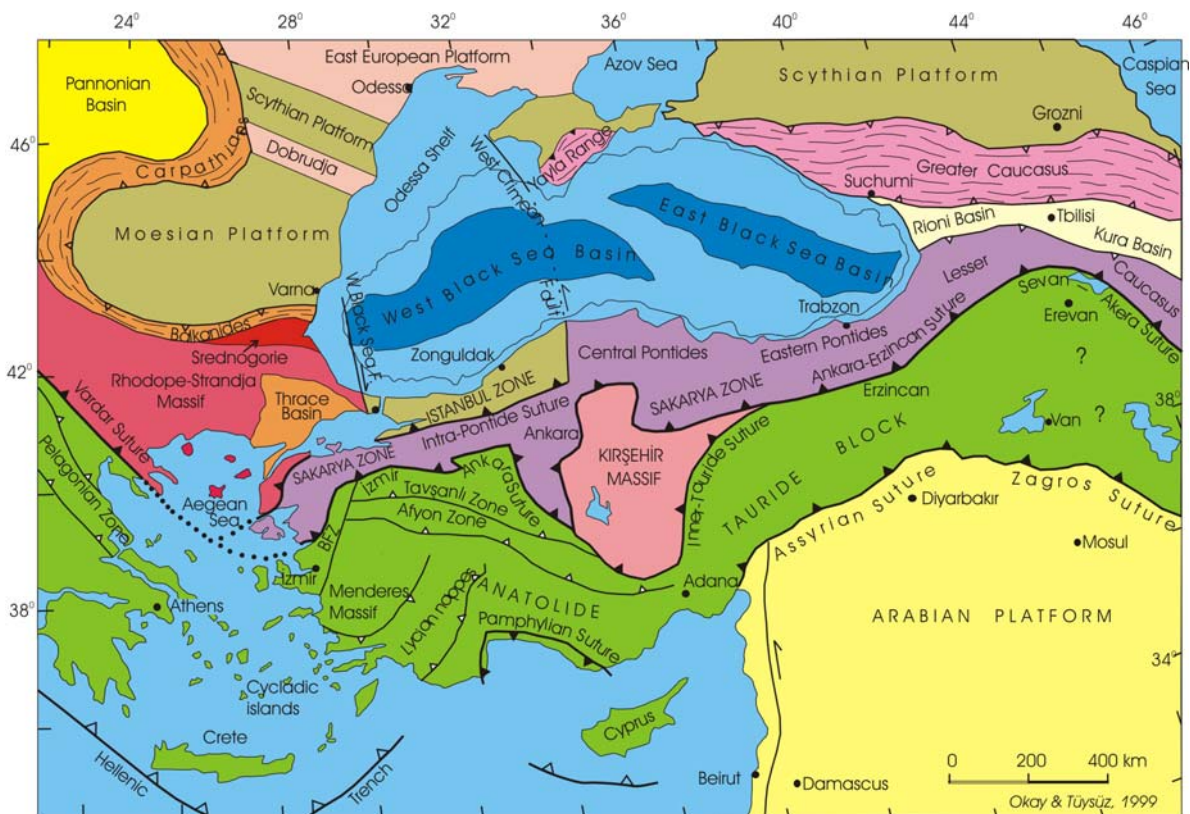


Fig. 1. Tectonic map of Turkey and its surroundings (after Okay and Tüysüz, 1999).

The Paleozoic and pre-Paleozoic history of the Strandja Massif were very unclear. The basement of the Strandja Massif was previously described as only by associations of rock types without considering their origin (Aydın, 1982; Çağlayan et al., 1988; Türkecan and Yurtsever, 2002 ). In addition, the age constraints were constructed only basic rock relations

(stratigraphy) and comparisons with the similar rocks exposed in Bulgarian side of the Strandja Massif (Chatalov, 1988; Chatalov, 1991). The basement, as it was previously described, consist of ortho and para-gneisses, migmatites?, and amphibolites (Aydın, 1982; Çağlayan et al., 1988; Okay et al., 2001; Türkecan and Yurtsever, 2002). No attempts have been performed to classify these rock types and map them. One of the recent studies of Okay et al. (2001) has shown that some of the intrusions in the Strandja Massif are late Paleozoic in age (namely Variscan). However, the problems addressed in the next paragraphs by various authors mainly stayed as debates. For example, Gondwanian origin of the Strandja Massif was never studied. In this thesis, especially in the first two chapters, we concentrated our efforts on solving these problems.

Mid-Mesozoic deformational events in the Strandja Massif were interpreted in the frame of the Cimmeride orogenic system (Şengör et al., 1984). The Strandja Massif belongs to the Mediterranean Cimmerides and is a part of the Anatolian Cimmerides subdivision (Şengör et al., 1984). The Cimmerian continent drifted from north Gondwana-Land as a narrow continental strip with the coeval opening of the Neo-Tethyan Ocean to the south. The Cimmeride orogeny occurred because of the collision of the Cimmerian Continent (Şengör, 1979) with Eurasia via northward subduction of the Paleo-Tethyan Ocean beneath the southern Eurasian margin. The Cimmerian Continent can be traced from the Carpathians in the west, and to northern China in the east (Şengör et al., 1984). The history of the Cimmeride orogeny is much clearer in the part between northern China and Iran than the western part of Iran. Metamorphic belts in this orogenic system are the Taurides, the Sakarya Zone, the Rhodopes, the Strandja Massif, and the Carpathians. In previous studies, the Central Pontides (northern Turkey) are also believed to be part of the Paleo-Tethyan suture but Okay et al. (2006) has claimed that because of the tectonic imbrications of both Neo- and Paleo-Tethyan accretionary complexes in the central Pontides, the Cimmeride orogeny indicates an accretionary nature rather than a collisional one. According to this interpretation, the Küre nappe (cf. Şengör et al., 1984) that is located in the northern path of the Central Pontides consists of accretionary complex with ophiolitic rocks.

Natal'in et al. (2005) interpreted the tectonics of the Strandja Massif without a Cimmerian collision and proposed that the region evolved within the frame of the Silk-Road arc developed in the southern part of Eurasia. These different interpretations assume that before the time of the main deformation of the Strandja Massif, it belonged either to southern Eurasia or northern Gondwana. The Cimmeride idea of Şengör et al. (1984) infers that the Strandja Massif was a part of the Cimmerian continent that was departed from Gondwana and

collided with Eurasia. However, Natal'in et al. (2005) has located the Strandja Massif to the southern part of Eurasia and interpreted the orogenic event in terms of arc shaving or sliding events formed during the development of the Silk-Road arc.

There are many points of debate concerning both continuation of the Cimmeride suture (orogeny) in the Eastern Europe and the type of the Cimmeride orogeny in the Mediterranean Cimmerides. In southern Asia, sutures of Cimmeride orogeny and the distribution of the Cimmerian continent is much clearer than the Mediterranean ones. The main reason of such confusion in the western continuation of the Cimmeride orogeny is that this region represents the western tip of the Paleo-Tethyan ocean that has a wedge shape pinching out to the west where different orogenic systems converging to each other (Şengör et al., 1984).

Hercynian orogeny (Variscan?) of the Western Europe can be traced to the Eastern Europe and it is believed that the traces of this orogeny also observed in the Balkan region and northern Turkey (Carrigan et al., 2003; Cherneva and Georgieva, 2005; Topuz et al., 2007). Moreover, Şengör et al., (1984 and 1988) has proposed that synchronously with the Hercynian orogeny (post collisional magmatics), in the northeastern part of Gondwana-Land (present North Africa), an another orogenic system (subduction related) was developing (present Rhodopes Strandja, Sakarya, and Caucasus). Şengör et al., (1988) have proposed that Eastern Europe and the whole Anatolian territory represents Hercynian-Cimmeride transitional region. The main difference between Hercynian and the orogeny occurred in the northeastern Gondwana-Land is that the Hercynian orogeny was collisional but other one was subduction related (Andean type). Aside from that, Natal'in and Şengör (2005) has proposed that later than the mentioned orogenies, the Silk-Road arc started to develop in the southern part of the Eurasian margin. This orogeny is Alpid type which means that during the oblique subduction of the Paleo-Tethys under the southern margin of Eurasia, and strike-slip motion was one of the main components of the system. This yielded strike-slip bounded slivers and shaving along the arc and created accretion of the different parts of the arc to each other. In the eastern part of the Cimmerian orogenic system is much simpler but the western tip of the wedge shaped termination of the Paleo-Tethys brought them together. Complexities arise in the region affected later overprinting deformations (Alpine orogeny). The Alpine orogeny either displaced former orogenic belts or erased their structural features.

There is no Alpine metamorphic overprint in the Strandja Massif. However, the Rhodope Massif (Fig. 2), which is one of the known pieces of the Cimmeride orogeny, has strongly effected by the Alpine metamorphism (Gebauer and Liati., 1997; Lips et al., 1998; Liati and Gebauer., 2001; Liati, 2005). Therefore the Strandja Massif is an adequate region

for the evaluation of the Cimmeride orogeny. In the Strandja Massif, the main vergence of the late Jurassic-early Cretaceous deformations is to the north, with considerable right-lateral motion (Natal'in et al., 2005). Natal'in et al. (2005) has suggested that the region has an inverted metamorphic grading. In the southern part of the studied area, rocks of the basement are structurally over the cover rocks that are located in the north, which means that the main movement was result of the southern forces. This led us to consider that collision between the Strandja Massif and the continent that is placed to the south of it occurred via northward subduction of the Paleo-Tethyan Ocean.

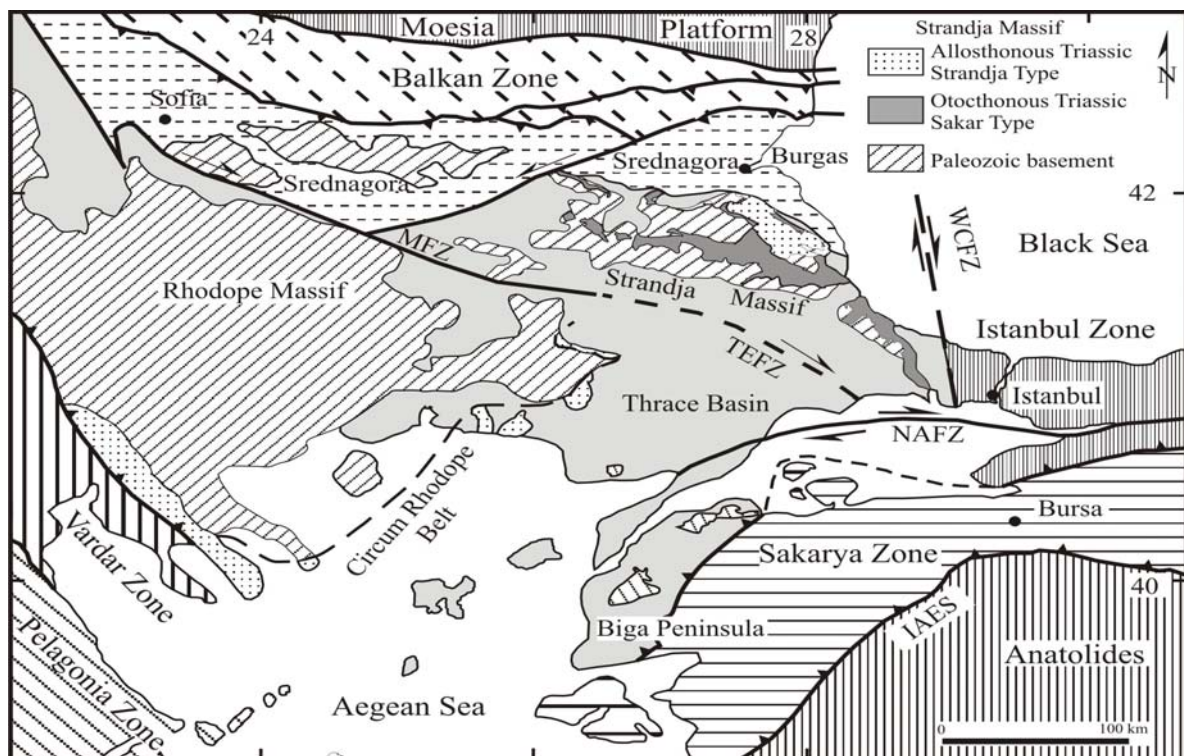


Fig. 2. Main tectonic units of the northern Aegean, the Balkanides and NW Turkey (modified after Okay and Satır 2000). Tectonic zones and massifs indicated in the map and their connection or relation have been discussed in the text. IAES: Izmir-Ankara-Erzincan suture, NAF: North Anatolian Fault, MFZ: Maritsa Fault, WCFZ: West Crimean Fault.

In the Balkan region, there are many places that are interpreted in the frame of the Cimmeride orogeny; from south to north, some regions of the Anatolide-Tauride block (Şengör et al., 1984), Crete (Şengör et al., 1984; Stampfli and Borel, 2002), the Vardar Zone (Stampfli and Borel, 2002), the Sakarya Zone, the Rhodope massif (Robertson and Dixon, 1984; Şengör et al., 1984; Turpaud and Reischmann, 2005; Liati, 2005), and the Carpathian

belt (Şengör et al., 1984 and 1988) (Fig. 1 and 2). Unfortunately the majority of these regions have been affected by the Alpine events. It is not easy to define their paleopositions and their original links between to each others. It is also hard to determine the vergence of the deformation that was gained during the Cimmeride orogeny. Because of that many researchers could not have possibly reconstructed the Cimmerian continent and the Cimmeride suture to its original position.

## **Analytical techniques**

The whole-rock powders were split from 1-5 kg of crushed rocks. Major and trace elements were determined by x-ray fluorescence spectrometry at the University of Tübingen, Germany. For this study rock powders was mixed with Li<sub>2</sub>B<sub>2</sub>O<sub>7</sub> (1.5:7.5) and then were fused at 1150°C into glass discs. Total iron is expressed as Fe<sub>2</sub>O<sub>3</sub>. Loss of ignition (LOI) was calculated after heating the sample powder to 1000°C for 1 hour.

For single-zircon Pb-evaporation, chemically untreated grains were analyzed using a double Re filament configuration as suggested by Kober (1986, 1987). For cathodoluminescence (CL) studies, zircons were mounted in epoxy resin and polished down to expose grain interiors. CL images were obtained by Technocyn 8200 Mk 4 Luminascope fitted with an Alcatel Vacuum Pump and JEOL JXA-8900RL electron microprobe, using an accelerating voltage of 15 kV and a beam current of 15 nA. Each zircon was embedded in a Re evaporation filament and placed in front of a 1 mm wide Re ionization filament. Each grain was heated first at 1350 °C for 5-10 minute for removal of common (Pb<sup>204</sup>) and radiogenic Pb hosted in less stable phases (e.g. in crystal domains affected by radiation damage) that have low activation energies (Kober, 1986). During repeated evaporation-deposition cycles in 20 °C steps, Pb is deposited on ionization filament for the measurements starting at about 1380 °C (all of the heating steps are unproved). Only high counts, generally 20,000-250,000 per second for <sup>206</sup>Pb, were used for age evaluations. Pb isotopes were dynamically measured in a sequence of 206-207-208-204-206-207 with a secondary electron multiplier. Correction of the common lead contribution to measured <sup>207</sup>Pb/<sup>206</sup>Pb ratios was made according to the two-stage growth model of Stacey and Kramers (1975). Further detailed information on the method is given in Chen et al. (2002) and Siebel et al. (2003). All isotopic ratios were measured in static mode on a Finnigan-MAT 262 multicollector mass spectrometer at the Department of Geochemistry, Tübingen University, Germany.



For conventional U–Pb analysis, non-magnetic zircon populations consisting of morphologically identical grains were washed in hot 6N HCl and hot 7N HNO<sub>3</sub> prior to remove surface contamination. Further detailed information on method is given in Chen et al. (2002) and Siebel et al. (2003).

The age calculations were created using the Isoplot program (Ludwig, 2003). The errors of <sup>207</sup>Pb/<sup>206</sup>Pb ages are given by the 2σ (2 sigma) standard deviation. The <sup>207</sup>Pb/<sup>206</sup>Pb evaporation ages during the course of measurements for Redwitzites granite from the Bohemian massif yielded an average age of 322.8 ± 4.1 Ma, similar to those age ranges reported by Siebel (1994) and Siebel et al. (2003).

Mineral analyses were performed at Heidelberg University using a CAMECA SX-51 microprobe equipped with five wavelength-dispersive spectrometers and an additional Si-Li detector (Oxford Instruments). Operating conditions were 15 kV accelerating voltage and 20 nA beam current. Counting times were usually 10 s except for Mg, Ca, Al (20 s) and Ti (30 s) in spinel. Beam diameter was usually ~1 μm except for feldspar analyses which were performed with a defocused beam (5–10 μm). Raw data were corrected for matrix effects with the help of the PAP algorithm (Pouchou and Pichoir 1984, 1985) implemented by CAMECA. Synthetic and natural standards were used for calibration before each measurement session. Detection limits are generally on the order of 0.1 wt% of the element under consideration.

Mineral separation (biotite, muscovite) were carried out using conventional techniques including crushing, sieving, magnetic separator and heavy liquids. Rb-Sr isotopic analyses were performed with a FINNIGAN MAT-262 multicollector mass spectrometer in Tübingen. Rb and Sr contents of whole rocks were determined by XRF, using lithium borate fusion discs with accuracy better than 2%. Rb and Sr concentrations of mineral separates were determined by isotopic dilution. Sr and light rare-earth elements were isolated on quartz columns by conventional ion exchange chromatography with a 5 ml resin bed of Bio Rad AG 50W-X12, 200–400 mesh. Sr was loaded with a Ta-HF activator on preconditioned W filaments and was measured in single-filament mode. Analyses of 28 separate loads of the NBS987 Sr standard yielded <sup>87</sup>Sr/<sup>86</sup>Sr ratio of 0.710259±0.000012. Total procedural blanks were <200 pg for Sr was loaded with a Si-gel onto a pre-conditioned Re filament and measured at ~1,300 °C in single-filament mode. Age determinations are based on <sup>87</sup>Rb decay constant of 1.42x10<sup>-11</sup> /yr (Steiger and Jäger 1977). Fractionation was corrected by normalizing the <sup>86</sup>Sr/<sup>88</sup>Sr ratios to 0.1194. The input errors for age computations are 1% (2σ) for <sup>87</sup>Rb/<sup>86</sup>Sr ratios and 0.003% (2σ) for <sup>87</sup>Sr/<sup>86</sup>Sr ratios. Rb–Sr age calculations were performed using the Isoplot 3.0 program produced by Ludwig (2003).

## Summary of the Publications

The thesis comprises three different parts related mainly to the basement of the Strandja Massif. First two chapters are related with the geology of the basement rocks, their ages, chemistry, petrology, and provenances. The first two chapters were published in international journals. The last chapter is related with the basement and the cover units, their petrology, ages, metamorphic conditions, exhumations and tectonic positions in the frame of the Eastern Balkan region (Fig. 2).

### Chapter 1: Paleozoic magmatic events in the Strandja Massif, NW Turkey

This paper published in the *Geodinamica Acta* Journal by coauthors Boris Natal'in, Muharrem Satir and Erkan Toraman. This chapter mainly deals with the Late Paleozoic evolution of the Strandja Massif. The basement of the Strandja Massif has been known for a long time. The rock types were classified according to their petrographic characters (such as gneiss, schists, and amphibolites). In our study we classified these units considering their protholith rock types, and petrological and structural features. In our classification we established that the basement of the Strandja Massif comprises several types of orthogneisses, most of which were missed in the previous studies. These orthogneisses intruded into the basement paragneisses, and garnet-biotite schist. Finally, all of the rocks were intruded by the Kırklareli type monzonitic granites (metagranites). Three different types of orthogneisses have been distinguished in the studied area: hornblende-biotite orthogneiss, biotite-muscovite orthogneiss, and leucocratic (Q-feldspatic) orthogneiss. Geochronology revealed that all these units were formed in the late Carboniferous (between 310-315 Ma). We also dated one sample from the Kırklareli metagranite and confirmed Permian ages obtained in previous papers (Aydın, 1982; Okay et al., 2001).

The orthogneisses are medium-grained rocks, greenish gray to gray in color. They consist of quartz (10-25%), albite-oligoclase (35-40%), biotite (5-15%), hornblende-actinolite (5-10%), epidote (15-20%), chlorite (3-5%), and muscovite (5%) with ratio between light and dark minerals similar to granite-granodiorite. Mafic dykes and schlierens of amphibolite are common feature of these rocks. The biotite-muscovite granite gneisses are medium grained, greenish-gray to gray in color. Their mineral composition is similar to the hornblende-biotite orthogneisses except the absence of hornblende and a greater content of muscovite (5-10%). The leucocratic orthogneisses consist of quartz (35-45%), plagioclase (35-45%), K-feldspar

(15-25%), muscovite (10-15%), chlorite (2-4%), biotite (<1 %), and opaque minerals (1-2%). The Kırklareli monzogranites consist of quartz (25-30 %), plagioclase (13-20 %), K-feldspar (35-47 %), biotite (5-10 %), muscovite (2-4 %), epidote, chlorite and others (1-2 %). The characteristic feature of these rocks is porphyric fabric with large (4 cm) pink crystals of K-feldspar.

The hornblende-biotite gneiss are tonalite and quartz-monzodiorite in compositions. The biotite- muscovite gneiss is represented in granite-granodiorite fields. Similar to the biotite muscovite gneiss, the leucocratic gneiss also reveals a granodioritic composition. Geochemical features of the late Carboniferous granitoids reveal a calc-alkaline nature. The hornblende-biotite gneisses are all enclosed in the metaluminous field and show I type character whereas both biotite-muscovite and leucocratic gneisses are slightly peraluminous in character and aligned along the I-S division line.

The Kırklareli metagranites of Permian age are K-feldspar bearing monzonitic granites. They are I type and metaluminous. In the field they show different petrological and structural features relative to the other units. In places they have their original textural features. Moreover depending on the stress intensity their textures vary from deformed granite to augen K-feldspar gneiss. It is also possible to see xenoliths of the country metamorphic rocks.

Although we have a limited dataset, we can set some constraints on the evolution of the late Carboniferous granitoids. The major element geochemistry of the late Carboniferous granitoids shows a typical basic to acidic evolution trend. They are either metaluminous or slightly peraluminous, I type character. All these features suggest either arc magmatism or syn- to post collisional magmatic activity. Considering ages of the granitoids and geodynamic evolution of the region, we speculate that Late Carboniferous is the time of arc magmatism. Furthermore, the Kırklareli metagranite of Permian age shows similar geochemical features with the late Carboniferous ones. These metagranites were interpreted as post-collisional by Okay et al. (2001). However, these rocks do not contain inherited zircons that put a strong argument to its post-collisional character.

## Chapter 2: Paleotectonic Position of the Strandja Massif and Surrounding Continental Blocks Based on Zircon Pb-Pb Age Studies

This chapter deals with the pre-Ordovician evolution of the Strandja Massif and the surrounding continental blocks. This study has been published in International Geological Review. In this study we used Pb-Pb evaporation zircon ages to understand the origin of the Strandja Massif. Three samples have been collected from the study area, two samples from

the central part and one from the south. The samples belong to the central part are garnet biotite schists intruded by biotite-muscovite granite gneiss (see Chapter 1 for details). The sample from the southern part is a biotite schist with amphibolite layers. In this part of the region, biotite schists are cut by Permian Kırklareli metagranite. In addition, inherited zircon ages obtained from the late Carboniferous granitoids were used (see Chapter 1 for details). We also compiled available zircon age data published in the geological literature related to surrounding continental blocks and main massifs or zones located in Europe. In addition, zircon ages belong to the main cratonic areas that were possible sources for the majority of the European massifs, were also compiled. The correlation between various provinces was based mainly on age distributions (genetic maps) rather than individual peaks. This method provides a better control for major tectonic, magmatic, and metamorphic events recorded in the zircon populations and better view of gaps. These gaps are considered as a key indicator in the evolution of zircon populations.

One of the outcomes of this study is evaluation of the detrital and inherited zircon data in the provenance studies. There are many published papers concerned with statistical usage of the detrital data (e.g. Sircombe, 2004; Andersen, 2005). Inherited ages were also used as a tracer for provenance studies, but comparison of both data was not well-considered. Detrital zircon data are strongly dependent on the lateral sediment transport and reworking of the sediments several times (e.g. Okay and Ergun, 2005). For example, Avigad et al. (2003) has inferred that Achaean zircons of the Kibaran orogeny in central Africa transported approximately 5000 km to the north and were found in Cambrian sandstones in Israel (NE Africa). This is even two times longer than the longest extension of Turkey. This distant transport of the detrital zircons used in provenance studies brings together mixing of different components, making interpretation more problematic. However inherited zircons in magmatic rocks intruded into terrestrial settings represents up to 80 km thick continental crust. Beside that continental crust is 35-40 km thick in average. The inheritance mechanism of zircons in a magma are generally depends on several factors. Zircons may be assimilated from country rocks by an ascending magma. Another way of inheritance is remelting of the deeper parts of the continental crust. One more way to add inherited zircons to magma is recycling of early formed crust through subduction system. In any circumstance, inherited zircons reveal limited sources and thus better constraints when compared to detrital zircons. In the case of the Strandja Massif, inherited zircons clearly indicated a NE African affinity, but detrital zircon data revealed a more complex pattern. Having both data gave us even better determination of

the source of the rocks (inherited zircons) and mixing of different components during sedimentary processes in their geological evolution.

Results showed that many of the massifs surrounding the Aegean region have strong N African affinity (eastern Gondwana-Land) and a close similarity with European massifs such as the Saxothuringian, the Sudetes, and SW Iberia. The outcome of this study is that knowing that the Meso-Proterozoic gap that was claimed in the previous studies must be narrower than it was assumed. We renewed zircon age distribution patterns considering recent publications. Another result of this study is that the Istanbul Zone is characterized by an enigmatic distribution when compared with the other massifs around the Aegean region. The only equivalent massif in Europe is the Rhenohercynian Massif of N Germany (Ecker gneiss complex). This suggests that the Rhenohercynian Massif has NW African and northern of South American affinity (western Gondwana-Land).

Another goal of this study was to determine the deposition age of the protolith of the basement biotite schists. Their age estimate considerably varied in the previous studies from Precambrian to Carboniferous (Çağlayan et al., 1988; Okay et al., 2001; Türkecan and Yurtsever, 2002). We used detrital zircon Pb-Pb ages and constrained the deposition age of the basement schists. The garnet biotite schists, which are exposed in the central part of the study area, were deposited during the Silurian to Carboniferous interval. The biotite schists with amphibolites, which are exposed in the south of the study area, were deposited in the interval between late Carboniferous and Permian.

### Chapter 3: Compression and diachronous cooling in a Late Jurassic-Early Cretaceous metamorphic belt (the Strandja Massif, NW Turkey)

In this chapter metamorphism and cooling events occurred in the Strandja Massif have been studied. This study was submitted to the Journal of Geology. Mid-Mesozoic metamorphism and related deformation in the studied area was interpreted within the frame of the Cimmeride orogeny. Metamorphism in the study area has been known for years but was not studied in detail. In previous studies the age of deformation or cooling of the region has been given, but due to insufficient number of ages the cooling history or related deformation history was unsubstantiated. These two parameters are widely used in the geological literature for understanding exhumation style for different metamorphic regions.

The Strandja Massif has two metamorphic domains; high grade metamorphic rocks to the south and low grade metamorphic rocks to the north. In previous studies metamorphic grades have been constrained as amphibolite facies for the high grade rocks and greenschist for the low ones (Aydın, 1982, Okay et al., 2001). Age of deformation or cooling ages of rocks were estimated as 155 Ma (Aydın, 1982, Okay et al., 2001).

In this study we collected 21 samples from the whole region for Rb-Sr mica chronology. These samples were used in petrological investigations as well.

Our study has shown that the metamorphic conditions in the south reached up to epidote-amphibolite facies. Estimated P-T conditions are 0.50-0.80 Gpa and 485-530 °C. The low grade rocks located to the north are in greenschist-facies with P-T estimates of 0.40- 0.70 Gpa and <485°C.

Cooling of the study area is diachronous. The Cooling ages from epidote-amphibolite-facies to greenschist-facies domain, Rb-Sr biotite- and muscovite cooling ages, become consistently younger from south to north, from 153 to 134 Ma and from 162 to 143 Ma, respectively. This is also compatible with the structural data collected from the study area which show N-vergent movement. These ages point out that in the vertical scale there is ~10 Ma difference between the biotite and muscovite ages, whereas in horizontal scale from south to north the difference is about 20 Ma. The vertical scale can be deduced from closure temperature of biotite and muscovite minerals in the Rb-Sr isotopic system. This age difference can correspond to a 200 °C difference of biotite and muscovite Rb-Sr closure temperatures. In a given geothermal gradient this temperature difference can be converted into the vertical scale. Moreover, a horizontal age difference reveals timing of tectonic events within the region. According to cooling ages and closure temperatures of biotite and muscovite it can be stated that the cooling rate is ~20 °C/Ma.

Similar metamorphic grades and ages are also reported in Bulgaria and Greece. The continuation of the Strandja Massif to Bulgaria was evaluated by several authors (Chatalov, 1988; Chatalov, 1991 ; Yanev, 2000 ; Gerdjikov, 2005). They reported similar rock types and metamorphic facies in these regions. Rb-Sr and K-Ar ages ranges from 170 to 130 Ma (Lilov and Maliakov, 2001; Lilov et al., 2004; Bonev et al., 2008). Unfortunately, it is not possible to correlate cooling or exhumation pattern of these region with our study area since the reported ages from these units are evaluated using different geochronological systems, thus can not be correlated. Furthermore, for many regions such as Bulgarian Strandja, deformation and cooling were occurred during mid-Mesozoic.

Mid-Mesozoic metamorphism and related deformations recorded in the Strandja Massif are in close connection with similar events recorded in the Rhodope Massif. The Rhodope Massif is regarded as a nappe stack (e.g. Burg et al., 1996; Ricou et al., 1998; van Hinsbergen et al., 2005), consisting of three main tectonic units (e.g. Liati and Mposkos, 1990; Magganas et al., 1991; Liati and Seidel, 1996; Liati and Gebauer, 1999; Mposkos and Kostopoulos, 2001; Magganas, 2002; Liati et al., 2002; Liati, 2005; Bonev and Stampfli, 2003 and 2008): (i) The lowermost tectonic unit comprises orthogneiss, pelitic gneiss, schist and local eclogitic amphibolite, subjected first to a low-*T* eclogite-facies metamorphism overprinted by lower amphibolite to upper greenschist-facies metamorphism, (ii) the overlying tectonic unit consists of interlayered amphibolite, marble, metapelitic schist and various gneisses enclosing eclogite and metaperidotite lenses which underwent high-*T* eclogite to ultrahigh-pressure metamorphism, followed by amphibolite- to granulite-facies overprint, (iii) the uppermost tectonic unit, on the other hand, is made up greenschist-facies phyllite, metabasite, rocks with local serpentinite, metagabbro and blueschists (also known as the Circum-Rhodope Belt).

The Rhodope Massif represents subduction, accretion and arc development. All the units belonging to these tectonic domains were later imbricated to each other and now are seen as different tectonic nappes. The Strandja Massif represents the back-arc basin of an island arc formed in the Rhodope Massif. Southward vergence did not affect the entire Rhodope Massif. Furthermore in the Strandja Massif, northward vergence developed as a retro-wedge deformation. The mid-Mesozoic tectonic frame of the region is interpreted as double-sided deformation of the foreland (the Rhodopes) and the hinterland domains of the Vardar Ocean.

## References

- Andersen, T., 2005. Detrital zircons as tracers of sedimentary provenance: limiting conditions from statistics and numerical simulation. *Chemical Geology*, 216: 249–270.
- Aydın, Y., 1982. Geology of the Yıldız (Istranca) Mountains. Thesis, Istanbul Technical University, İstanbul, 1982, 106 pp.
- Avigad, D., Kolodner, K., McWilliams, M., Persing, H., Weissbrod, D., 2003. Origin of northern Gondwana Cambrian sandstone revealed by detrital zircon SHRIMP dating. *Geological Society of America*, 31 (3); 227–230.
- Bonev, N.G., Stampfli, G.M., 2003. New structural and petrologic data on Mesozoic schists in the Rhodope (Bulgaria): geodynamic implications. - *C. R. Geoscience* 335 (8), 691-699.
- Bonev, N., Spikings, R., Moritz, R., Marchev, P., 2008. Structural and  $^{40}\text{Ar}/^{39}\text{Ar}$  age constraints on the Kulidjik nappe: a record of an early Alpine thrust tectonics in the northeastern Rhodope Massif, Bulgaria. *Donald D. Harrington Symposium Geology of the Aegean*, April 28-30.
- Bonev, N.G., Stampfli, G.M., 2008. Petrology, geochemistry and geodynamic implications of Jurassic island arc magmatism as revealed by mafic volcanic rocks in the Mesozoic low-grade sequence, eastern Rhodope, Bulgaria. *Lithos*, 100 (1-4), 210-233.
- Burg, J.P., Ricou, L.E., Ivanov, Z., Godfriaux, I., Dimov, D. and Klain, L., 1996. Syn-metamorphic nappe complex in the Rhodope Massif: Structure and kinematics. *Terra Nova* 8, 6-15.
- Carrigan, C.W., Mukasa, S.B., Haydoutov, I., Kolcheva, K., 2003. Ion microprobe U-Pb zircon ages of pre-Alpine rocks in the Balkan, Sredna Gora, and Rhodope terranes of Bulgaria: Constraints on Neoproterozoic and Variscan tectonic evolution. *J. Czech Geol. Soc.*, 48, 32-33.
- Çağlayan, A.M., Şengün, M., Yurtsever, A., 1988. Main Fault systems shaping the Istranca Massif, Turkey, *J. Pure Appl. Sci. Ser. A Geosci.* 21, 145-154.
- Chatalov, G., 1988. Recent developments I the geology of the Strandja Zone in Bulgaria. *Bull. Tech. Univ. Istanbul* 41, 433-466.
- Chatalov, A.G., 1991. Triassic in Bulgaria- a review, in Special issue on tectonics, In: JF Dewey (ed). *Bull. of the Tech. Uni. of Istanbul*, 44 (1-2), 103-135.



- Chen, F., Siebel, W., Satir, M., Terzioğlu, N., Saka K., 2002. Late Proterozoic continental accretion in the north-western Turkey: evidence from zircon U–Pb and Pb–Pb dating and Nd–Sr isotopes. *Int. J. Earth Sci.* 91, 469-481.
- Cherneva, Z., Georgieva, M., 2005. Metamorphosed Hercynian granitoids in the Alpine structures of the Central Rhodope, Bulgaria: geotectonic position and geochemistry, *Lithos*, 2 (1-2), 149-168.
- Gebauer, D. and Liati, A., 1997. Geochronological evidence for Mesozoic rifting and oceanization followed by Eocene subduction in the Rhodope Complex (Northern Greece). *Terra Nova* 9 (Abstract supplement 1):10.
- Gerdjikov, I., 2005. Alpine metamorphism and granitoid magmatism in the Strandja zone: new data from the Sakar unit, SE Bulgaria, *Turkish J. Earth Sci.* 14, 167-183.
- Ketin, İ., 1966. Anadolu'nun tektonik birlikleri. *M.T.A. Derg.* 66, 75-88.
- Kober, B., 1986. Whole-grain evaporation for  $^{207}\text{Pb}/^{206}\text{Pb}$  age investigations on single zircons using a double-filament thermal ion source. *Contrib. Mineral. Petrol.* 93, 481-490.
- Kober, B., 1987. Single-zircon evaporation combined with  $\text{Pb}^+$  emitter-bedding for  $^{207}\text{Pb}/^{206}\text{Pb}$ -age investigations using thermal ion mass spectrometry, and implications to zirconology. *Contrib. Mineral. Petrol.* 96, 63-71.
- Liati, A., Mposkos, E., 1990. Evolution of the eclogites in the Rhodope zone of northern Greece. *Lithos* 25, 89–99.
- Liati, A., Seidel, E., 1996. Metamorphic evolution and geochemistry of kyanite eclogites in central Rhodope, northern Greece. *Contrib Mineral Petrol* 123, 293-307.
- Liati, A. and Gebauer, D., 1999. Constraining the prograde and retrograde P–T–t path of Eocene HP-rocks by SHRIMP dating of different zircon domains: inferred rates of heating, burial, cooling and exhumation for central Rhodope, northern Greece. *Contrib Mineral Petrol* 135, 340–354.
- Liati, A. and Gebauer, D., 2001. Palaeozoic as well as Mesozoic sedimentation and polymetamorphism in Central Rhodope (N' Greece) as inferred from U–Pb SHRIMP-dating of detrital zircons. *EUG 11, Journal of Conference Abstracts* 6, 315.
- Liati, A., Gebauer, D., Wysoczanski, R., 2002. U–Pb SHRIMP-dating of zircon domains from UHP mafic rocks in the Rhodope zone (N' Greece); evidence for Early Cretaceous crystallization and Late Cretaceous metamorphism. *Chem Geol* 184, 281–300.

- Liati, A., 2005. Identification of repeated Alpine (ultra) high-pressure metamorphic events by U-Pb SHRIMP geochronology and REE geochemistry of zircon: the Rhodope zone of Northern Greece. *Contributions to Mineralogy and Petrology* 150, 608-630.
- Lilov, P., Maliakov, Y., 2001. Données de géochronologie isotopique sur les métadiabases du Strandja, C.R. Acad. Bulg. Sci. 54 (7), 67-70.
- Lilov, P., Maliakov, Y., Balogh, K., 2004. K-Ar dating of metamorphic rocks from Strandja Massif, SE Bulgaria. Bulgarian Academy of Sciences, Geochemistry, Mineralogy and Petrology 41, 107-120.
- Lips, A. L. W., White, S. H. & Wijbrans, J. R. 1998. Ar<sup>40</sup>-Ar<sup>39</sup> laserprobe direct dating of discrete deformational events: a continuous record of Early Alpine tectonics in the Pelagonian Zone, NW Aegean area, Greece. *Tectonophysics*, 298, 133-153.
- Ludwig, K.R., 2003. Isoplot 3.0, a geochronological toolkit for Microsoft Excel, Berkeley Geochronology Center, Special Publication. No. 4.
- Magganas, A.C., Sideris, C., Kokkinakis, A., 1991. Marginal basin–volcanic arc origin of metabasic rocks of the Circum-Rhodope Belt, Thrace, Greece. *Mineralogy and Petrology* 44, 235–252.
- Magganas, A.C., 2002. Constraints on the petrogenesis of Evros ophiolite extrusives, NE Greece. *Lithos* 65(1-2), 165-182.
- Mposkos, E.D., Kostopoulos, D.K., 2001. Diamond, former coesite and supersilicic garnet in metasedimentary rocks from the Greek Rhodope: a new ultrahigh-pressure metamorphic province established. *Earth and Planetary Science Letters* 192(4), 497-506.
- Natal'in, B.A., Sunal, G., Toraman, E., 2005. The Strandja arc: anatomy of collision after long-lived arc parallel tectonic transport, In: Sklyarov EV (ed) *Structural and Tectonic Correlation across the Central Asia Orogenic Collage: North-Eastern Segment. Guidebook and abstract volume of the Siberian Workshop IGCP-480, IEC SB RAS, Irkutsk*, pp 240-245.
- Natal'in, B.A., Şengör, A. M. C. 2005. Late Palaeozoic to Triassic evolution of the Turan and Scythian platforms: The pre-history of Palaeo-Tethyan closure, *Tectonophysics*, 404, 175-202.
- Okay, A.I., Tüysüz, O., 1999. Tethyan sutures of northern Turkey. In: B. Durand, L. Jolivet, F. Horvath and M. Seranne (Editors), *The Mediterranean Basins: Tertiary Extension within the Alpine Orogen*. Geological Society, London, Special Publication, 156, pp. 475-515.

- Okay, A.I., Satır, M., 2000. Upper Cretaceous eclogite facies metamorphic rocks from the Biga Peninsula, northwest Turkey. *Turkish Journal of Earth Sciences* 9, 47-56.
- Okay, A.I., Satır, M., Tüysüz, O., Akyüz, S., Fukun, C., 2001. The tectonics of the Strandja Massif: late-Variscan and mid-Mesozoic deformation and metamorphism in the Northern Aegean. *Int. J. Earth Sciences* 90, 217-233.
- Okay, A.I., Satır, M., Siebel, S., 2006. Pre-Alpide Palaeozoic and Mesozoic orogenic events in the Eastern Mediterranean region, Geological Society, London, *Memoirs* 32, 389-405.
- Okay, N., Ergun, B., 2005. Source of the basinal sediments in the Marmara Sea investigated using heavy minerals in the modern beach sands (1-2): 1-15.
- Pamir, H. N. and Baykal, F., 1947. The geological structure of the Strandja Massif. – *Bulletin of the Geological Society of Turkey*, 1, 7-43.
- Pouchou, J. L., Pichoir, F. 1984. A new model for quantitative analyses. I. Application to the analysis of homogeneous samples. *La Recherche Aérospatiale*. 3: 13–38.
- Pouchou, J.L., Pichoir, F. 1985. “PAP” (f-r-Z) correction procedure for improved quantitative microanalysis. In: Armstrong, J. T. ed. *Microbeam analysis*. San Francisco Press. pp 104–106.
- Ricou, L.E., Burg, J.P., Godfriaux, I., Ivanov, Z., 1998. Rhodope and Vardar: the metamorphic and the olistostromic paired belts related to the Cretaceous subduction under Europe. *Geodinamica Acta* 11, 285-309.
- Robertson, A. H. F. and Dixon, J. E., 1984. Introduction: aspects of the geological evolution of the eastern Mediterranean. In *The geological evolution of the Eastern Mediterranean* (eds. J. E. Dixon and A. H. F. Robertson), pp. 1-74. Geological Society of London Special Publication no. 17.
- Şengör, A.M.C., 1979. Mid-Mesozoic closure of Permo-Triassic Tethys and its implications: *Nature*, c. 279, 590-593.
- Şengör, A.M.C., Yılmaz, Y., 1981. Tethyan evolution of Turkey: A plate tectonic approach. *Tectonophysics* 75, 181-241.
- Şengör, A.M.C., Yılmaz, Y., Sungurlu, O., 1984. Tectonics of the Mediterranean Cimmerides: nature and evolution of the western termination of Paleo-Tethys. In: Dixon JE and Robinson AHF (eds.) *The geological evolution of the Eastern Mediterranean*. Geological Society of London Special Publication 17, pp 77-112.

- Şengör, A.M.C., Altner, D., Cin, A., Ustaömer, T., Hsü, K.J., 1988. Origin and assembly of the Tethyside orogenic collage at the expense of Gondwana Land. In: Audley-Charles MG, Hallam A (eds) Gondwana and Tethys. Geol Soc Lond Spec Publ 37:119–181.
- Siebel, W., 1994. Inferences about magma mixing and thermal events from isotopic variations in Redwitzites near the KTB site. KTB Rep 94(3), 157-164.
- Siebel, W, Chen, F., Satır, M., 2003. Late-Variscan magmatism revisited: new implications from Pb-evaporation zircon ages on the emplacement of redwitzites and granites in NE Bavaria, International Journal of Earth Sciences 92, 36-53.
- Sircombe, K.N., 2004. AGEDISPLAY: an EXCEL workbook to evaluate and display univariate geochronological data using binned frequency histograms and probability density distributions. Computers and Geosciences, 30: (1), 21-31.
- Stacey, J.S., Kramers, J.D., 1975. Approximation of terrestrial lead isotope evolution by a two stage model. Earth Planet. Sci. Lett. 26, 207-221.
- Stampfli, G. M. and Borel, G. D., 2002. A plate tectonic model for the Paleozoic and Mesozoic constrained by dynamic plate boundaries and restored synthetic oceanic isochrons. Earth and Planetary Science Letters, 196, 17-33.
- Steiger, R. H, and Jäger, E. 1977. Subcommittee on geochronology: Convention on the use of decay constants in geo- and cosmochemistry. Earth and Planetary Science Letters. 36: 359-362.
- Topuz, G., Altherr, R., Schwarz, W-H., Dokuz, A., Meyer, H-P., 2007. Variscan amphibolite-facies metamorphic rocks from the Kurtoğlu metamorphic complex (Gümüşhane area, Eastern Pontides, Turkey) International Journal of Earth Sciences, 96, 861-873.
- Türkcan, A., Yurtsever, A., 2002. Geological map of Turkey. Istanbul. General Directorate of Mineral Research and Exploration, Ankara.
- Turpaud, P. & Reischmann, T., 2005. Relationships between crustal blocks and UHP relics, an example from Northern Greece. Geophysical Research Abstracts, 7, 04353.
- van Hinsbergen, D.I.J., Hafkenscheid, E., Spakman, W., Meulen Kamp, J.E., Wortel, R., 2005. Nappe stacking resulting from subduction of oceanic and continental lithosphere below Greece. Geology 33, 325-328.
- Yanev, S., 2000. Palaeozoic terranes of the Balkan Peninsula in the framework of Pangea assembly. Palaeogeography, Palaeoclimatology, Palaeoecology 161, 151-177.

## Supplementary

### Chapter 1: Paleozoic magmatic events in the Strandja Massif, NW Turkey

Gürsel Sunal <sup>a,b,\*</sup>, Boris A. Natal'in <sup>a</sup>, Muharrem Satır <sup>b</sup>, Erkan Toraman <sup>c, d</sup>

<sup>a</sup> Istanbul Technical University, Department of Geology, TR-34390 Istanbul, Turkey  
(corresponding author)

Phone: +90-212-2856162

Fax: +90-212-2856210

<sup>b</sup> Universität Tübingen, Institut für Geowissenschaften, Wilhelmstrasse 56, D-72074  
Tübingen, Germany

<sup>c</sup> Department of Earth and Atmospheric Sciences, Saint Louis University, 329 Macelwane  
Hall 3507 Laclede Ave. St. Louis, MO 63103 USA

<sup>d</sup> ITU Eurasia Institute of Earth Sciences, TR-34390 Istanbul, Turkey

\* Corresponding Author

Published in Geodinamica Acta

Idea:	30%
Problem:	40%
Production of Data:	70%
Evaluation and Interpretation:	60%
Preparation of the manuscript:	70%

### ***Abstract***

The Strandja massif consists of metamorphic basement intruded by large Early Permian plutons of the Kırklareli type and overlain by Triassic metasedimentary cover. Together with its continuation in Bulgaria this massif forms an important link between the Pontides and the orogenic belts of Europe. Various types of orthogneisses constitute a significant part of the metamorphic basement however these rocks have until now escaped a particular study and therefore the Paleozoic history of the massif is essentially unknown. In this study these rocks are classified and mapped as hornblende-biotite, biotite-muscovite, and leucocratic orthogneisses. Their modal compositions correspond to quartz diorite, tonalite, granodiorite and trondhjemite. Geochemical data suggest a calc-alkaline trend of differentiation and metaluminous character of the parent magmas. Isotopic dating using the single zircon evaporation method has shown that magmatic ages of these orthogneisses cluster within a short time interval between 312 and 315 Ma in the Carboniferous. At the same time inherited ages of magmatic zircons in these rocks record a long lived magmatic activity between 320 and 650 Ma. We infer that the Carboniferous orthogneisses were formed in a magmatic arc that evolved atop of a mature continental basement. Previously established ([1, 2]) Early Permian magmatic event has been confirmed by additional age determinations constraining it at  $257\pm 6$  Ma. Tectonic setting of this episode is also interpreted as subduction related taking into consideration its geochemical features and relationships with surrounding tectonic units.

**Keywords: Carboniferous granitoids/ Strandja Massif/ single zircon Pb/Pb evaporation ages**

## 1. Introduction

The Strandja massif occupies the northern half of the Thrace province of northwestern Turkey and neighboring regions of Bulgaria (Fig. 1b). In Bulgaria, its continuation is known as a Balkan terrane consisting of Paleozoic rocks [3-5]. In Turkey, the Strandja massif is interpreted as a part of the Pontides [6] that is an orogenic belt consisting of fragments of the Cimmerian microcontinent of Gondwanian origin, which collided with Eurasia during the early Mesozoic Cimmerian orogeny [7]. This interpretation of the Pontides is still shared by many researches while others infer that the Strandja massif along with the Istanbul zone belonged to the Laurasian margin during the Late Paleozoic and Mesozoic [8, 9].

Summaries on geology of the massif have been provided by [1, 2, 10-12]. According to these studies the Strandja massif consists of the metamorphosed basement that is intruded by granites and unconformably overlain by the Triassic to Jurassic metasedimentary cover. Timing of tectonic events was constrained by the following isotopic age determinations. Aydın [1] reported  $244 \pm 11$  Ma Rb-Sr whole-rock age for the Kırklareli metagranites that intrude the basement. Using zircon evaporation method Okay et al. [2] dated the same granites as well as the Kula pluton located to the north as  $271 \pm 2$  Ma old (mean of 5 and 2 grains respectively). The Üsküp metagranites that are exposed to the east of the Kırklareli pluton yielded  $309 \pm 24$  Ma (ages obtained from a single grain). Zircons from country rock gneisses yielded somewhat younger ages –  $266 \pm 14$ ,  $239 \pm 16$  Ma (single grain), and  $278 \pm 19$  Ma (single grain). A single zircon from migmatites associated with the metagranites yielded four different ages  $299 \pm 15$ ,  $276 \pm 12$ ,  $239 \pm 12$ , and  $221 \pm 14$  Ma. Two last age determinations have been considered as unreliable because of the inferred Triassic age of the sedimentary cover (Okay et al., 2001). The Kırklareli granites also yielded biotite K-Ar ages of 150-149 Ma, Rb-Sr biotite whole-rocks age of 144 Ma [1, 10], and Rb-Sr biotite and whole-rock age of  $155 \pm 2$  Ma [2]. All of these ages were interpreted as the age of regional metamorphism.

This limited database explains why the Paleozoic tectonic history of the Strandja massif was never discussed in detail. Concerning the Permian magmatism, Şengör et al. [13] interpret it as subduction-related paired with a south-dipping subduction zone while Okay et al. [2] consider it as collisional.

Various gneisses and schists metamorphosed in amphibolite facies have been described in the Paleozoic basement [1, 12]. Interpretations of their ages vary from the Precambrian [11, 14) to “late Variscan” [2]. A significant part of these rocks is represented by orthogneisses some which were interpreted as metamorphic equivalents of the early Permian granites [12]. Our geological mapping and structural studies have shown that the main part of the so-called Teke Dere group that unites all country rocks of the early Permian granites [12] consists of orthogneisses suggesting a long magmatic history of the Strandja massif in a magmatic arc tectonic setting [15].

The goal of this study is to present new data on geochronology and petrology of orthogneisses constituting a significant portion of the Paleozoic basement of the Strandja massif. Using zircon evaporation method and conventional U-Pb method we have established a prolonged history of the Paleozoic magmatic activity with peaks at  $314.7 \pm 2.6$ ,  $312.3 \pm 1.7$ , and  $257 \pm 6.2$  Ma. Inherited zircons in orthogneisses suggest an additional magmatic episode around 350 Ma. These data allow a better correlation of the tectonic activity of the Strandja massif with surrounding regions and newly obtained geochemical data impose constraints on tectonic settings of the massif in the Paleozoic.

## **2. Tectonic units of the studied area**

Similar to previous studies we recognized in the studied area the Paleozoic basement, early Permian Kırklareli granites, and overlying them the Triassic metasedimentary cover. The basement consists of biotite-muscovite paragneisses, biotite schists, amphibolites, and several types of orthogneisses three of which were formed before the emplacement of the



Kırklareli granites (Fig. 1a, [16]). These rocks strike northwest and have consistent moderate dips to the southwest. The Kırklareli granites form a large (25x14 km) pluton slightly elongated in the east-west direction. Along its margins, the granites are converted to mylonitic gneisses. The Triassic metasedimentary cover starts with metaconglomerates containing clasts of granite gneisses, quartzites, quartz, and schists. They grade up into quartz-rich metasandstones containing lens-shape bodies of metaconglomerates and diamictites. These rocks are metamorphosed in greenschist facies. Clasts in metaconglomerates and diamictites have their own foliation indicating an episode of metamorphism and deformation preceding the accumulation of the massif cover. The age of cover rocks is inferred from long-distance correlations with Bulgarian part of the Strandja massif [12, 2] where Triassic fossils have been found in rocks of a similar lithology [3, 17].

Original relationships between tectonic units are almost completely obliterated by the late Mesozoic deformations and metamorphism that occurred between 136 and 171 Ma (Natal'in et al., in preparation). The late Mesozoic deformation and metamorphism formed penetrative foliation that in many places strikes at a high angle to lithological boundaries. It reworked earlier formed fabric and mineral assemblages hindering the reconstruction of the Paleozoic-early Mesozoic history of the Strandja massif.

In following sections we give a description of the orthogneisses in the basement and Kırklareli granite. Information on other rock units and structural history of the region will be published elsewhere (Natal'in et al., in preparation).

### **2.1. Hornblende- biotite orthogneisses**

The hornblende-biotite orthogneisses constitute two elongated bodies in the western part of the studied area (Fig. 1a). Generally, these rocks reveal strong foliation and mineral lineation, but in places they are massive and preserve their original magmatic fabric. The orthogneisses are medium grained rocks, greenish gray to gray in color. They consist of

quartz (10-25%), albite-oligoclase (35-40%), biotite (5-15%), hornblende-actinolite (5-10%), epidote (15-20%), chlorite (3-5%), and muscovite (5%) with ratio between light and dark minerals similar to granite-granodiorite. Mafic dykes and schlierens of amphibolite are common feature of these rocks. Composition of amphibolites varies from dioritic to gabbroic(Hbl-Bt schlieren in Table 1 and Fig. 2). Amphibole is bluish-green in color; plagioclase is strongly decomposed. The schlierens vary in shape form equidimensional to strongly elongate. The elongated schlierens occurring in weakly foliated and lineated rocks suggest their origin because of magma flow [18, 19]. The schlierens and mafic dykes may be interpreted as evidence of magma mixing during the formation of the parent granitoids [20, 19]. In places, xenoliths of biotite schists similar to country rocks were observed.

## **2.2. Biotite-muscovite orthogneisses**

The biotite-muscovite orthogneisses form a large body in the northern part of the mapped area (Fig. 1a). Similar to the hornblende-biotite orthogneisses they are represented by foliated and weakly foliated or unfoliated rocks. They preserve good evidence for magmatic origin of rocks. The weakly to unfoliated granite constitute lens shape bodies that vary from ten meter to 500 m across.

The biotite-muscovite granite gneisses are medium grained, greenish-gray to gray in color. Their mineral composition is similar to the hornblende-biotite orthogneisses except the absence of hornblende and a greater content of muscovite (5-10%). Weakly strained rocks are very homogenous while foliated rocks sometimes reveal a vague compositional layering. In contrast to the hornblende-biotite granite gneisses schlierens and biotite xenoliths are absent in the biotite-muscovite granite gneisses.

### **2.3. Leucocratic orthogneisses and granites**

The hornblende-biotite and biotite-muscovite orthogneisses as well as surrounding metasedimentary rocks are cut by dykes of leucocratic granite gneisses and granites. Thickness of these dykes varies from several centimeters to several tens meters. A closely spaced swarm of this rock is shown in Fig. 1a. In places the leucocratic granitic rocks are strongly foliated and folded. At the same time some bodies are not foliated at all though they cut foliated granite gneisses. These rocks are enigmatic because foliation in granite gneisses is Mesozoic in age. Presence of metamorphic muscovite in the leucocratic rocks suggest that these rocks somehow were affected by metamorphism but resisted deformation. Leucocratic orthogneisses consist of quartz (35-45%), plagioclase (35-45%), K-feldspar (15-25%), muscovite (10-15%), chlorite (2-4%), biotite (<1 %), and opaque minerals (1-2%).

The leucocratic granites and granite gneisses are mainly exposed within the medial Paleozoic gneisses and among Paleozoic metasediments to the south of the Kırklareli granites. They are absent within the Kırklareli pluton.

### **2.4. Kırklareli metagranites**

The Kırklareli monzogranites constitute a large (23x15 km) pluton located to the north of Kırklareli (Fig. 1b). Its western part occurs in the map area (Fig. 1a). The Kırklareli monzogranites consist of quartz (25-30 %), plagioclase (13-20 %), K-feldspar (35-47 %), biotite (5-10 %), muscovite (2-4 %), epidote, chlorite and others (1-2 %). The characteristic feature of these rocks is porphyric fabric with large (4 cm) pink crystals of K-feldspar. These crystals make the magmatic origin of rocks obvious however the granites usually reveal clear metamorphic foliation dipping to the south at moderate angles. Quartz always has undulose extinction and often recrystallized into fine-grained aggregates. Plagioclase is strongly altered. K-feldspar is often characterized by microcline twining and marginal replacement by myrmekites. Biotite is brown to dark green in color. Kinking and bending of its crystal,

grains shredding along cleavage planes, displaced cleavage fragments of former grains that form wedge shape terminations are very common for biotites in thin sections. Some times biotite forms typical folia wrapping around K-feldspar. All of these structural features indicate solid state deformation of the Kırklareli granites in accord with criteria described by Vernon [20]. Muscovite replaces the biotite and we disagree with a previously published conclusion on its magmatic origin [2].

Migmatites are widespread along the southern margin of the Kırklareli pluton. There, intrusive contacts of the granites and country rocks were also observed. In the north and northwest the Kırklareli granites are framed by mylonitic granite gneisses (Fig. 1a). These fine- to medium-grained rocks are very homogeneous in composition and often contain floating porphyroblasts of pink K-feldspar as well as lower strained lenses of porphyric granites similar to the Kırklareli type. We interpret them as a part of the pluton affected by ductile shearing.

### **3. Two episodes of magmatic activity**

All orthogneisses and Kırklareli metagranites reveal penetrative foliation that has consistent attitude (Fig. 1a). This foliation has Mesozoic age as it is evident from available isotopic dating [1, 10, 2]. In places, the hornblende-biotite and Biotite-muscovite granite gneisses preserve two foliations made of biotite. This foliation is absent in the Kırklareli granites. The earlier foliation indicates an episode of metamorphism and deformation separating emplacement of formation of parent rocks of hornblende- and biotite-muscovite orthogneisses and the intrusion of the Kırklareli granites. The absence of leucocratic granite gneisses in the Kırklareli pluton suggests that they were formed together with the hornblende-biotite and biotite-muscovite orthogneisses. Geological relationships have been confirmed by isotopic dating indicating the Carboniferous age of the hornblende-biotite, the biotite-muscovite and the leucocratic orthogneisses (see below) and the Permian age of the Kırklareli

granite (our data and data presented by Aydın [10] and Okay et al. [2]). These two groups of rocks are distinct in terms of their geochemical signature.

#### **4. Analytical techniques**

The whole-rock powders were split from 1-5 kg of crushed rocks. Major and trace elements were determined by x-ray fluorescence spectrometry at the University of Tübingen, Germany. For this study rock powders was mixed with Li<sub>2</sub>B<sub>2</sub>O<sub>7</sub> (1.5:7.5) and then were fused at 1150°C into glass discs. Total iron is expressed as Fe<sub>2</sub>O<sub>3</sub>. Loss of ignition (LOI) was calculated after heating the sample powder to 1000°C for 1 hour.

Zircons were extracted from rock samples by standard mineral separation techniques; Wilfley table, heavy liquids, Frantz isodynamic separator and were finally handpicked under a binocular microscope. Then a fraction with grain sizes 63-200 µm was classified according to crystal properties (i.e. euhedral morphology, lack of overgrowth and visible inclusions). For cathodoluminescence (CL) studies, zircons were mounted in epoxy resin and polished down to expose grain interiors. CL images were obtained by Technocyn 8200 Mk 4 Luminascope fitted with an Alcatel Vacuum Pump. The chamber is mounted on a Zeiss Microscope which has had the normal stage replaced by CL chamber.

For single-zircon Pb-evaporation, chemically untreated, grains were analyzed using a double Re filament configuration suggested by Kober [21, 22]. Note that a group of zircons used for the evaporation is not the same that was used for CL studies. We simply rely of identity of these two groups in our interpretations of ages. Each zircon was embedded in a Re evaporation filament and placed in front of a 1 mm wide Re ionization filament. Then it was heated first at 1350 °C for 5-10 min for removal of common and radiogenic Pb hosted in less stable phases (e.g. in crystal domains affected by radiation damage), which have low activation energies [21]. During repeated evaporation-deposition cycles in 20 °C steps Pb is deposited to ionization filament for the measurements starting at about 1380 °C. Only high

counts, generally 20.000-200.000 per second for  $^{206}\text{Pb}$  were used for age evaluations. Pb isotopes were dynamically measured in a sequence of 206-207-208-204-206-207 with a secondary electron multiplier. Correction of the common lead contribution to measured  $^{207}\text{Pb}/^{206}\text{Pb}$  ratios is made in accord with the two-stage growth model of Stacey and Kramers [23]. Further detailed information on method is given in Chen et al. [24], Okay et al. [2], and Siebel et al. [25]. All isotopic ratios were measured in static mode on a Finnigan-MAT 262 multicollector mass spectrometer at the Tübingen University, Germany.

The  $^{207}\text{Pb}/^{206}\text{Pb}$  ages are based on the means of all measurements evaluated and the errors are given by the  $2\sigma$  (2 sigma) standard deviation. The age and error for several grains from the same sample are given as weighted mean and error of the weighted mean, respectively.  $^{207}\text{Pb}/^{206}\text{Pb}$  evaporation ages during the course of measurements for Redwitzites granites yielded an average age of  $322.8 \pm 4.1$  Ma, similar to those age ranges reported by Siebel [26] and Siebel et al. [25].

For conventional U–Pb analysis, non-magnetic zircon populations consisting of morphologically identical grains were washed in hot 6N HCl and hot 7N HNO<sub>3</sub> prior to remove surface contamination. Further detailed information on method is given in Chen et al. [24], Siebel et al. [25], and Nguyen et al. [27].

## **5. Results**

### **5.1. Major and trace element geochemistry**

#### ***5.1.1. Carboniferous magmatism***

Chemical composition of the hornblende-biotite and biotite-muscovite granite gneisses is shown in (Table 1). Modal compositions the hornblende-biotite granite gneisses fall in the tonalites and quartz monzodiorite fields when plotted on quartz – alkali-feldspar – plagioclase (QAP) diagram (Figure 2a, [28]). Compositions of the biotite-muscovite and leucocratic

orthogneisses form a cluster within the granodiorite field (Fig.2a). On the anorthite – albite – orthoclase (AAO) diagram [29] the hornblende-biotite orthogneisses are within the tonalite and granodiorite fields (Fig. 2b). The biotite-muscovite orthogneisses are scattered in the granite, trondjemite, and granodiorite fields while leucocratic orthogneisses fall in the trondjemite field (Fig. 2b).

The hornblende-biotite gneisses contain about 50-60 wt. % SiO<sub>2</sub> and 14-19 wt. % Al<sub>2</sub>O<sub>3</sub>. Low content of SiO<sub>2</sub> was obtained from schlierens. The biotite-muscovite orthogneisses are more felsic in composition. Their SiO<sub>2</sub> content in the biotite-muscovite gneisses range between 66-76 wt. % and they have relatively low Al<sub>2</sub>O<sub>3</sub> contents of 14-15 wt. %. The leucocratic gneiss reveal yet higher SiO<sub>2</sub> contents (76-80 wt. %) and further decrease of the Al<sub>2</sub>O<sub>3</sub> contents between 12 and 15 wt.%.

XMgO [MgO/(Fe<sub>2</sub>O<sub>3</sub><sup>tot</sup> \*0.9+MgO)] values vary between 0.51 and 0.68 in the hornblende-biotite gneisses, and between 0.39 and 0.51 in the biotite-muscovite gneiss (Table 1). The aluminum saturation index [ASI = molecular Al<sub>2</sub>O<sub>3</sub>/(CaO+Na<sub>2</sub>O+K<sub>2</sub>O)] ranges from 0.63 to 0.91 in the hornblende-biotite gneisses, and from 1.07 to 2.26 in the biotite-muscovite gneisses (Figure 3b and Table 1). XMgO [MgO/( Fe<sub>2</sub>O<sub>3</sub><sup>tot</sup> \*0.9+MgO)] values of the leucocratic gneisses vary between 0.33 and 0.56, and ASI values between 1.1 and 1.2 (Figure 3b and Table 1). Note that all three types of orthogneisses follow a single trend on the AFM diagram being within the calc-alkaline field (Figure 3a)

### ***5.1.2. Permian magmatism***

In a ternary Quartz-Alkalifeldspar- Plagioclase (Q-A-P) diagram (Figure 2a, [28]), the Kırklareli K-feldspar metagranites form a tight group within the monzogranite field. On the normative anorthite– albite–orthoclase diagram [29] they are in the granite field (Figure 2b). Comparing with the previously described rock types the Kırklareli metagranites have a more restricted content of SiO<sub>2</sub> – 70-74 wt. % and Al<sub>2</sub>O<sub>3</sub> – 13-15 wt. % (Table 1). Their XMgO

$[\text{MgO}/(\text{Fe}_2\text{O}_3^{\text{tot}} * 0.9 + \text{MgO})]$  values vary between 0.28 and 0.36 (Table 1) and ASI values between 0.9-1 (Figure 3b and Table 1). Similar to hornblende-biotite, biotite-muscovite, and leucocratic orthogneisses the K-feldspar metagranites shows calc-alkaline affinity, occurring on the trend defined for the older magmatic complexes (Figure 3a).

## 5.2 Geochronology

Figure 4 shows the general distribution of ages obtained by single grain evaporation method in the Strandja Massif. Scattered and inherited ages are also indicated in this diagram.

### 5.2.1. Carboniferous granitoids

#### 5.2.1.1. Biotite-Muscovite gneiss

Only one sample Gk117 has been used for isotopic age determinations of these rocks (see Fig. 1 for location). All zircons extracted from this sample have prismatic partly corroded crystals with 1:2 and 1:3 aspect ratios (Figure 5a). Their cathodoluminescence (CL) images show magmatic oscillatory zoning indicating a magmatic origin (Figure 5a). Three distinct populations have been recognized: 1) dark brown, semi-transparent; 2) colorless to light brown, transparent; and 3) greenish, semi-transparent. The only grain of the first population yields 460 and 472 Ma ages (grain 1 in Table 2). The second population has mixed ages varying from 318 to 460 Ma (grains 2, 3, 4, 13 in Table 2) increasing with an increase of the evaporation temperature. Greenish and semi-transparent crystals yield ages of 306 and 319 Ma (grains 7, 10, 11, 12 in Table 2). The CL images of zircons do not exhibit any inherited core except grain 1a in Fig. 5 that shows a dark body which is difficult to interpret. However old ages especially those obtained with the increase of evaporation temperature suggest the presence of inherited core in the analyzed zircons.

Consistent ages of greenish zircons reflect the magmatic ages of the biotite-muscovite orthogneisses. It has a weighted average mean of  $314.7 \pm 2.6$  Ma (mean of 6 grains and 9



heating steps, Table 2, Figure 6a). In all of the zircon images a high CL zone is surrounded by low CL on the outer side which is parallel with oscillatory zoning in the inner parts of crystals. Both of these zones may indicate a metamorphic overprint [30] and thus explain a scatter of magmatic ages between 309 and 319 Ma.

#### ***5.2.1.2. Hornblende- Biotite gneiss***

Two samples (Gk115 and Gk35) of the hornblende-biotite gneisses have been dated using single-zircon  $^{207}\text{Pb}/^{206}\text{Pb}$  stepwise-evaporation method (see Fig. 1 for location). All zircons in these samples are idiomorphic and prismatic. They are classified into two groups: 1) colorless or light brown, transparent and translucent (Fig. 5 b-1 and 2), and 2) dark brown, semi-transparent, euhedral prismatic grains (Fig. b-3 and 4). Cathodoluminescence images show that all grains exhibit oscillatory magmatic zoning testifying the magmatic origin of the zircons. A presence of inherited rounded core in the grain b1 (Fig. 5b1) suggests that some zircons contain older cores incorporated during the formation and emplacement of the hornblende-biotite granites. Note that the inherited core also has the oscillatory magmatic zoning. All of the grains exhibit low CL outer rims representing a metamorphic overprint.

Six grains in the sample Gk115 gave young ages between 309 and 316 Ma at all evaporation steps. All of these grains belong to the first morphological group. Grains 11 and 14 of the same group revealed increasing of ages with increase of the evaporation temperature. Grains 3 and 7 (first group) of the sample Gk35 have similar behavior. The increase of ages in these grains reflects the presence of inherited cores. Old dates in these grains are difficult to interpret because they may indicate ages of inherited cores or mixed ages of the cores and young magmatic overgrowth. Zircons of the second group (grains 8, 9 and 16 in the sample Gk115 and grains 3 and 7 in sample Gk35) yielded ages older than 340 Ma at all heating steps (Table 3). These zircons represent xenocrysts incorporated by granitic magma from older intrusions.

Fig. 6b shows a histogram of  $^{206}\text{Pb}/^{207}\text{Pb}$  ratios obtained from both samples and plotted on the same diagram. Note that peaks of the sample Gk 115 and Gk 35 fit each other giving age of  $312.3 \pm 1.7$  Ma (weighted mean of 13 grains, 20 heating steps). We accept this date as the magmatic age of the hornblende-biotite orthogneisses.

Beside the single zircon evaporation method, we used a conventional U-Pb method (Table 4, Fig. 6d). Each fraction consists of four to seven zircons of the same morphological features. Fractions 1-3, and 5 represent the first group and fraction 4 belongs to the second one (Table 4). Obtained ages do not form a reliable single discordia line (Fig. 6d). Calculated upper and lower intercept ages gave high errors and high a MSWD value. Three fractions lie near the concordia. The fraction 1 reveals U loss and gives U-Pb ages of 308 and 315 Ma which is in accordance with the magmatic ages obtained by the single zircon evaporation method. Fractions 3 and 5 yield U-Pb ages of 330/334 and 390/399 Ma, respectively. These ages are more concordant than the ages of the previous fraction. The age of the fraction 3 may have a geological meaning because some of the evaporated zircons have similar ages of 330-355 Ma. These ages may reflect a long time interval during which the hornblende- biotite granites were forming. We interpret the age of the fraction 5 (399 Ma) as the age of inherited zircons or as a mixed age of several zircons. Fractions 2 and 4 (Table 4) reflect inherited or mixed zircon ages. Following [31] we calculated a forced regressions through 308 Ma to evaluate a possible age range of inherited zircons (Fig. 6d). This gives a range between 650 and 1300 Ma which is in accordance with the inherited zircon ages obtained by the single zircon evaporation method.

### ***5.2.1.3. Leucocratic gneiss***

The age of the leucocratic gneisses is poorly constrained because of fewer amounts of zircons. Only two grains have been extracted from the sample Gk39 (see Fig. 1 for location). The grain 1 (Table 5) gave  $313.3 \pm 10$  Ma in the first heating step and older ( $\sim 350$  Ma) ages at

higher evaporation temperatures. The grain 2 yielded only old ages more than 648 Ma (Table 5). Taking the geological relationships into account we infer that 313 Ma is a magmatic age of the leucocratic orthogneisses. The scatter of older inherited or mixed ages in the sample Gk 39 is similar to the scatter in hornblende-biotite and biotite-muscovite orthogneisses. This feature makes the leucocratic gneisses different from the Kırklareli granites.

### **5.2.2. Permian granitoids**

The Kırklareli granites have already been dated by Aydın [1, 10] and Okay et al. [2] as 245 Ma and ~271 Ma accordingly. In this study we have obtained ages intermediate between these reported dates. Only one sample (Gk 18) has been used for single zircon evaporation method. This sample is an augen gneiss consisting of quartz, porphyroblasts of strongly altered and in places completely recrystallized K-feldspar, altered plagioclase, brown muscovite, epidote, sphene, and rutile.

Zircons of this sample form a uniform population represented by brown, semi-transparent, and euhedral, prismatic crystals. CL images of selected grains are shown in Figure 5c. Clear oscillatory magmatic zoning is characteristic for all selected grains.

All evaporated grains yielded ages between 253.8 and 276.1 Ma (Table 6) which give weighted average mean of  $257 \pm 6.2$  Ma (Fig. 6c) that is similar to Okay et al. [2] data. Neither ours nor Okay et al. [2] studies who used the same zircon evaporation technique have revealed a large scatter of ages typical for the presence of inherited zircon core. Interestingly, grains 1 and 2 show decrease of ages with the rise of the evaporation temperature.

## **6. Discussion**

Geological mapping, structural and geochemical studies, and isotopic dating indicate that the Paleozoic history of the Strandja massif included Carboniferous and Permian episodes of magmatic activity. The Permian magmatic episode has been established by previous studies

[1, 10, 12, 2] and confirmed by this study. The Carboniferous episode is described for the first time.

The Carboniferous hornblende-biotite, biotite-muscovite, and leucocratic orthogneisses yield approximately same ages of 312-314 Ma. These rocks have not been mapped in the previous studies [12, 2] therefore it is difficult to estimate their total volume in the basement of the Strandja massif. However, it is worth noting that in the studied area they constitute about 70% of the basement thus indicating that deciphering their nature is crucial for the understanding of the tectonic history of the Strandja massif.

Geochemical data suggest the evolution of Carboniferous magmas followed a calc-alkaline trend starting with granitoids from which the hornblende-biotite orthogneisses were formed and ending with the granites that now occur as the leucocratic gneisses. Crosscutting relationships of the leucocratic gneisses with the hornblende-biotite and biotite-muscovite orthogneisses supports this inference however relationships between two later types are reworked by Mesozoic deformations. Relationships between major elements indicate similarity of the hornblende-biotite orthogneisses with metaluminous I-type granitoids. The abundance of mafic schlierens suggests repeated injections of mafic magmas into an evolving magmatic chamber. The biotite-muscovite orthogneisses reveal peraluminous features and intermediate character between I- and S- types of granitoids. Finally, the leucocratic orthogneisses exhibits peraluminous, and S-type character. Taken together all of these features suggest that Carboniferous magmatic rocks evolved within a mature magmatic arc.

The mature crust of the Carboniferous arc can be inferred from abundant inherited zircon ages that have been detected in all of the Carboniferous metamorphic rocks. Some magmatic zircons from these rocks reveal consistent ages at all heating steps suggesting that these zircons are xenocrysts inherited from previously emplaced magmatic rocks. Zircon ages between 320 and 370 Ma obtained in this study (Figure 4 and 5, Table 2, 3, 4, and 5) are

correlative with magmatic ages of granitoids in neighboring regions of Bulgaria [32, 5] and they correspond to ages of magmatic rocks that are known as early Variscan granitoids in Europe [33, 34]. The time interval between 420 and 600 Ma is also almost completely covered by our dates (Fig. 4). Similar ages (~450, 560, 665, and 975 Ma) of inherited zircons have been reported by Carrigan et al. [35] in the Balkan tectonic unit of Bulgaria. These correlations suggest that inherited or mixed ages obtained in this study indicate a long-lived magmatic activity within the Strandja massif. The long-lived magmatic activity is a characteristic feature of the arc tectonic setting.

Major elements ratios show that the Kırklareli metagranites are of I-type being transitional between metaluminous and peraluminous granitoids (Figure 2 and 3, Table 1). Similar to the Carboniferous orthogneisses the Kırklareli metagranites show the calc-alkaline trend of differentiation (Fig. 3). These geochemical features are not too decisive for an interpretation of a possible tectonic setting. Considering tectonic evolution of Tethysides, Şengör et al. [13] interpret the Permian and Triassic magmatism of the Strandja massif as subduction related. Taking into consideration correlations with the Variscan belt Okay et al. [2] infer a post-collisional setting of the Kırklareli granites.

Okay et al. [2] also suggest the anatectic nature of these granites. We disagree with this conclusion for following reasons. 1) Migmatization relevant to the Kırklareli pluton occurs only along the southern margin of the intrusion where amount of migmatites rarely exceeds 10 % of total volume of country rocks. 2) Xenoliths of country rocks were observed only at margins of the pluton but they are absent in its internal parts. 3) The composition of the pluton is very homogenous suggesting that it represents a single magmatic phase.

In accord with this observation we want to add that all studied zircons in the Kırklareli metagranite (Table 6) reveal no inherited or mixed ages. Zircons studied by Okay et al. [2] both in Kırklareli and other plutons of this type have the same character. At the same time,

crosscutting relationships of the Kırklareli pluton with the country rocks are obvious from the geological map (Fig. 1). We infer that the formation of the Kırklareli magmas was due to influx of the high temperature mantle magmas to the base of the crust where it was contaminated with crustal components or facilitate generation of primary crystal magmas at elevated temperatures that remelted earlier formed zircons. The following emplacement of such magmas to high crustal levels caused the formation of the Kırklareli type plutons in the Strandja massif. The mechanism outlined is more suitable for subduction related tectonic setting. The presence of oceanic and arc related rocks within a Strandja type of Triassic in Bulgaria, in which a stratigraphic conformity with Paleozoic rocks is admitted, is another argument in favor of this inference [3, 17, 36, 13].

There is abundant literature on tectonic settings of the granitoids, their ages, and the timing of metamorphism in the Variscan belt of Europe [33-35, 37-47]. Magmatic activity there [25, 35, 40, 48-63] occurred over a time interval (320 to 290 Ma) which is similar to those in the Strandja massif. Taking into consideration S-type of intrusions the majority of researches assigned them to post-collisional tectonic settings. However, some researchers consider a possibility of subduction-related tectonic setting pointing to the presence of calc-alkaline character of some intrusions and their definite I-type (.e.g [51]) for magmatic rocks of 310 Ma in Bulgaria). Moreover, Matte [64] infers that during the Westphalian time (~318-303 Ma) the western part Variscan belt was characterized by the Himalayan-type mountain building while its eastern part was still represented by an Andean-type of active margins. Typical I-type granitoids in Variscan belt, their isotopic composition and REE abundances show either continental contribution to mantle derived magmas or remelting of lower continental crust. Some differentiation diagrams have been proposed to determine the tectonic settings of granitoids [65] but generally our samples fall to the junction subduction-related and syn-collisional granites [16]. This matter was discussed in detail by Förster et al. [66].

This correlation indicates that more work needs to be done for the solution of the first order questions concerning tectonic setting of the Carboniferous and Permian magmatism both in Strandja massif and surrounding regions.

## **7. Conclusions**

The Pb/Pb zircon evaporation studies of the orthogneisses constituting the Paleozoic basement of the Strandja massif have revealed a voluminous Carboniferous magmatic episode at 312 to 314 Ma. After an episode of metamorphism and deformation it was followed by emplacement of the early Permian ( $257\pm 6$  Ma) monzogranites of the Kırklareli type.

The Carboniferous magmatic rocks have geochemical features that allow considering them as subduction related. Ages of inherited magmatic zircons indicate a long lived magmatic activity within the Strandja massive that collaborate the inference about subduction nature of the medial Paleozoic magmatism. It also testifies that the basement of the arc was continental and included Precambrian protoliths.

The Permian magmatic rocks belong to calc-alkaline series but in contrast to the Carboniferous they have a narrower compositional range and on discrimination diagrams are located close the metaluminous/peraluminous boundary. Tectonic setting of these rocks in conjunction with geochemical features also allows interpreting them as subduction related.

## **8. Acknowledgements**

This study was supported by TÜBİTAK (The Scientific and Technical Research Council of Turkey, Project no: YDABCAG 101Y010) and resulted from the cooperative study between Istanbul Technical University, Turkey and University of Tübingen, Germany. G. Bartholomä and H. Taubald for the XRF analysis are gratefully acknowledged. We wish to thank W. Siebel and E. Reitter for help in isotopic measurements. We warmly thank T.T.B. Nguyen for help in mineral separation and isotopic measurements. We sincerely thank G.

Topuz for constructive comments on geochemistry part, and O. Vonderschmit and A. Dikbař for valuable assists in the field study. We also thank Prof. Aral Okay for his extensive comments on an earlier version of this paper that significantly improved it.

## 9. References

- [1] Aydın Y., Etude petrographique et geochimique de la partie centrale du Massif d'Istranca (Turquie), Thesis, University of Nancy (1974).
- [2] Okay A.I., Satır M., Tüysüz O., Akyüz S., Fukun C., The tectonics of the Strandja Massif: late-Variscan and mid-Mesozoic deformation and metamorphism in the Northern Aegean. *Int. J. Earth Sciences* 90 (2001) 217-233.
- [3] Chatalov G., Recent developments I the geology of the Strandja Zone in Bulgaria. *Bull. Tech. Univ. Istanbul* 41 (1988) 433-466.
- [4] Haydoutov I., Yanev S., The Protomoesian microcontinent of the Balkan Peninsula – a peri-Gondwanaland piece. *Tectonophys* 272 (1997) 303-313.
- [5] Yanev S., Palaeozoic terranes of the Balkan Peninsula in the framework of Pangea assembly. *Palaeogeography, Palaeoclimatology, Palaeoecology* 161 (2000) 151-177.
- [6] Ketin İ., Anadolu'nun tektonik birlikleri. *M.T.A. Derg.* 66 (1966) 75-88.
- [7] Şengör A.M.C., Yılmaz Y., Tethyan evolution of Turkey: A plate tectonic approach. *Tectonophysics* 75 (1981) 181-241.
- [8] Okay A.I., Satır M., Maluski H., Siyako M., Monie P., Metzger R., Akyüz S. Paleo- and Neo-Tethyan events in northwestern Turkey: geologic and geochronologic constraints. In: A. Yin and M. Harrison (Editors), *The Tectonic Evolution of Asia*. Rubey Colloquium. Cambridge University Press, Cambridge, 1996, pp. 420-441.



- [9] Okay A.I., Tüysüz O., Tethyan sutures of northern Turkey. In: B. Durand, L. Jolivet, F. Horvath and M. Seranne (Editors), *The Mediterranean Basins: Tertiary Extension within the Alpine Orogen*. Geological Society, London, Special Publication, 156, 1999, pp. 475-515.
- [10] Aydın Y., *Geology of the Yıldız (Istranca) Mountains*. Thesis, Istanbul Technical University, İstanbul, 1982, 106 p.
- [11] Yılmaz Y., Tüysüz O., Yiğitbas E., Genç Ş.C., Şengör A.M.C., *Geology and tectonic evolution of the Pontides*. In: A.G. Robinson (Editor), *Regional and Petroleum geology of the Black Sea and surrounding region*. AAPG Memoir 68, 1997, pp. 183-226.
- [12] Çağlayan A.M., Şengün M., Yurtsever A., *Main Fault systems shaping the Istranca Massif, Turkey*, J. Pure Appl. Sci. Ser. A Geosci. 21 (1988) 145-154.
- [13] Şengör A.M.C., Yılmaz Y., Sungurlu O., *Tectonics of the Mediterranean Cimmerides: Nature and evolution of the western termination of Paleo-Tethys*. In: J.E. Dixon and A.H.F. Robinson (Editors), *The geological evolution of the Eastern Mediterranean*. Geological Society of London Special Publication 17, 1984, pp. 77-112.
- [14] Türkcan A., Yurtsever A., *Geological map of Turkey*. Istanbul. General Directorate of Mineral Research and Exploration (2002), Ankara.
- [15] Natal'in B.A., Sunal G., Toraman E., *Dextral arc-parallel tectonic transport along the southern margin of Eurasian in the late Paleozoic-early Mesozoic*, 1st International Symposium of Istanbul Technical University the Faculty of Mines on Earth Sciences and Engineering 16-18 May, 2002, Istanbul Technical University (ITU) (2002) 80.
- [16] Natal'in B. A., Satir M., Sunal G., Toraman E., *Structural and metamorphic evolution of the Strandja massif*. Final report of the 101Y010 Project, Türkiye Bilimsel Teknik Araştırma Kurumu, Yer Deniz Atmosfer Bilimleri ve Çevre Araştırma Grubu Ankara, 2005.
- [17] Chatalov G.A., *Triassic in Bulgaria - A review*. Bulletin of the Technical University of Istanbul 44(1-2) (1991)103-135.

- [18] Paterson S.R., Pignotta G.S., Vernon R.H., The significance of microgranitoid enclave shapes and orientations. *Journal of Structural Geology*, 26(8) (2004)1465-1481.
- [19] Wiebe R.A., Collins W.J., Depositional features and stratigraphic sections in granitic plutons: implications for the emplacement and crystallization of granitic magma. *Journal of Structural Geology* 20(9-10) (1998) 1273-1289.
- [20] Vernon R.H., Review of Microstructural Evidence of Magmatic and Solid-State Flow. *Electronic Geosciences* 5 (2000).
- [21] Kober B., Whole-grain evaporation for  $^{207}\text{Pb}/^{206}\text{Pb}$  age investigations on single zircons using a double-filament thermal ion source. *Contrib. Mineral. Petrol.* 93 (1986) 481-490.
- [22] Kober B., Single-zircon evaporation combined with  $\text{Pb}^+$  emitter-bedding for  $^{207}\text{Pb}/^{206}\text{Pb}$ -age investigations using thermal ion mass spectrometry, and implications to zirconology. *Contrib. Mineral. Petrol.* 96 (1987) 63-71.
- [23] Stacey J.S., Kramers J.D., Approximation of terrestrial lead isotope evolution by a two stage model. *Earth Planet. Sci. Lett.* 26 (1975) 207-221.
- [24] Chen F., Siebel W., Satır M., Terzioğlu N., Saka K., Late Proterozoic continental accretion in the north-western Turkey: evidence from zircon U–Pb and Pb–Pb dating and Nd–Sr isotopes. *Int. J. Earth Sci.* 91 (2002) 469-481.
- [25] Siebel W, Chen F., Satır M., Late-Variscan magmatism revisited: new implications from Pb-evaporation zircon ages on the emplacement of redwitzites and granites in NE Bavaria, *International Journal of Earth Sciences* 92 (2003) 36-53.
- [26] Siebel W., Inferences about magma mixing and thermal events from isotopic variations in redwitzites near the KTB site. *KTB Rep* 94(3) (1994) 157-164.
- [27] Nguyen T.T.B., Satır M., Siebel W., Chen F., Granitoids in the Dalat zone, southern Vietnam: age constraints on magmatism and regional geological implications, *Int. J. Earth Sci. (Geol Rundsch)*, 93 (2004) 329-340.

- [28] Le Maitre R.W., A classification of Ingeous rocks and glossary of terms. Blackwell, Oxford, 1989,193 p.
- [29] O'Connor J.T., A classification for quartz-rich igneous rocks based on feldspar ratios. US Geol. Surv. Prof. Pap. B525 (1965) 79-84.
- [30] Nemchin A.A., Pidgeon R.T., Evolution of the Darling Range Batholith, Yilgarn Craton, Western Australia: a SHRIMP zircon study. J. Petrol. 38 (1997) 625-649.
- [31] Chen F., Todt W., Hann H. P., Zircon and Garnet Geochronology of Eclogites from the Moldanubian Zone of the Black Forest, Germany, The Journal of Geology 111 (2003) 207-222.
- [32] Zagorchev I.S., Rhodope controversies. Episodes 21(3) (1998)159-166.
- [33] Finger F., Roberts M.P., Haunschmid B., Schermaier A., Steyrer H.P., Variscan granitoids of central Europe: their typology, potential sources and tectonothermal relations. Mineral. Petrol., 61 (1997) 67-96.
- [34] Klötzli U.S., Koller F., Scharbert S., Höck V., Cadomian lower-crustal contributions to Variscan granite petrogenesis (South Bohemian pluton, Austria): Constraints from zircon typology and geochronology, whole-rock, and feldspar Pb-Sr isotope systematics. J. Petrol. 42 (2001) 1621-1642.
- [35] Carrigan C.W., Mukasa S.B., Haydoutov I., Kolcheva K., Age of Variscan magmatism from the Bulgarian sector of the orogen. Submitted to Lithos (2004) special volume on the Magmatic and Metamorphic Evolution of Central European Variscides.
- [36] Şengör A.M.C., The Cimmeride orogenic system and the tectonics of Eurasia. The Geological Society of America, Special Paper 195, 1984, 82 p.
- [37] O'Brien P.J., Carswell D.A., Gebauer D., Eclogite formation and distribution in the European Variscides. In: D.A. Carswell, Editor, Eclogite Facies Rocks, Blackie, Glasgow, 1990, pp. 204-224.

- [38] Kalt A., Hanel M., Schleicher H., Kramm U., Petrology and geochronology of eclogites from the Variscan Schwarzwald (F.R.G.). *Contrib Mineral. Petrol.* 115 (1994) 287–302.
- [39] Kalt A., Corfu F., Wijbrans J.R., Time calibration of a P–T path from a Variscan high-temperature low-pressure metamorphic complex (Bayerischer Wald, Germany), and the detection of inherited monazite. *Contrib. Mineral. Petrol.* 138 (2000) 143–163.
- [40] Kröner A., Hegner E., Hammer J., Haase G., Bielicki K.H., Krauss M., Eidam J., Geochronology and Nd-Sr systematics of Lusatian granitoids: significance for the evolution of the Variscan orogen in east-central Europe. *Geol. Rundsch. (Int. J. Earth Sci.)* 83 (1994) 357-376.
- [41] Kröner A., O'Brien P.J., Nemchin A.A., Pidgeon R.T., Zircon ages for highpressure granulites from South Bohemia, Czech Republic, and their connection to the Carboniferous high temperature processes. *Contrib. Mineral. Petrol.* 138 (2000) 127-142.
- [42] Schaltegger U., Magma pulses in the Central Variscan Belt: episodic melt generation and emplacement during lithospheric thinning. *Terra Nova* 9 (1997) 242-245.
- [43] Schaltegger U., U-Pb geochronology of the Southern Black Forest Batholith (Central Variscan Belt): timing of exhumation and granite emplacement. *Int. J. Earth Sci.* 88 (2000) 814-828.
- [44] Fernández-Suárez J., Dunning G.R., Jenner G.A., Gutiérrez-Alonso G., Variscan collisional magmatism and deformation in NW Iberia: constraints from U-Pb geochronology of granitoids. *J. Geol. Soc. London*, 157 (2000) 565-576.
- [45] von Raumer J.F., The Palaeozoic evolution in the Alps: from Gondwana to Pangea, *Geol Rundsch*, 87 (1998) 407–435.
- [46] Friedl G., Finger F., Paquette J.L., von Quadt A., McNaughton N.J., Fletcher I.R., Pre-Variscan geological events in the Austrian part of the Bohemian Massif deduced from U–Pb zircon ages, *Int. J. Earth Sci. (Geol Rundsch)* 93 (2004) 802–823.

- [47] Romer R.L., Rötzler J., P-T-t evaluation of ultrahigh-Temperature granulites from the Saxon Granulite Massif, Germany. Part II: Geochronology. *Journal of Petrology* 42 (2001) 2015-2032.
- [48] Peytcheva I., von Quadt A., U-Pb zircon dating of metagranites from Byala-reka region in the east Rhodopes, Bulgaria. *Proceedings of the XV Congress of the Carpatho- Balcan Geological Association*, Sept., 1995, Athens, Geol. Soc. Greece Special Publication, 4(2) (1995) 637-642.
- [49] Peytcheva I., Salnikova E., Kostitsyn Yu., Ovtcharova M., Sarov S., Metagranites from the Madan- Davidkovo dome, Central Rhodopes: U-Pb and Sr-Rb protholite and metamorphism dating. *ABCD-GEODE* (2000) 67.
- [50] Cherneva Z., Ovtcharova M., von Quadt A., Kolcheva K., Stancheva E., Sarov S., Peytcheva I., Monazite and zircon U-Pb ages of migmatites from the Arda River Valley, Central Rhodopian Dome, Bulgaria, in Daboveski and Ivanov, eds., *Modern Problems of the Bulgarian Geological Society, Annual Sci. Conf. Abstr.* (2002) 20-22.
- [51] Carrigan C.W., Mukasa S.B., Haydoutov I., Kolcheva K., Ion microprobe U-Pb zircon ages of pre-Alpine rocks in the Balkan, Sredna Gora, and Rhodope terranes of Bulgaria: Constraints on Neoproterozoic and Variscan tectonic evolution. *J. Czech Geol. Soc.*, 48 (2003) 32-33.
- [52] Gerdes A., Friedl G., Parrish R.R., Finger F., High-resolution geochronology of Variscan granite emplacement – the South Bohemian Batholith. *J. Czech Geol. Soc.*, 48 (2003) 53-54.
- [53] Azevedo M.R., Valle Aguado B., Schaltegger U., Nolan J., Medina J., Martins M.E., U-Pb zircon and monazite geochronology of Variscan magmatism related to synconvergence extension in central northern Portugal. *J. Czech Geological Soc.* 48 (2003), 16.

- [54] Schaltegger U., Corfu F., The age and source of late Hercynian magmatism in the central Alps: evidence from precise U-Pb ages and initial Hf isotopes. *Contrib. Mineral. Petrol.* 111 (1992) 329-344.
- [55] von Quadt A., Grünenfelder M. and Büchi H., U-Pb zircon ages from igneous rocks of the Bernina nappe system (Grisons, Switzerland). *Schweiz. Mineral. Petrogr. Mitt.*, 74 (1994) 373-382.
- [56] Siebel W., Constraints on Variscan granite emplacement in northeast Bavaria, Germany: further clues from a petrogenetic study of the Mitterteich granite. *Geol. Rundsch* 84 (1995) 384–398.
- [57] Siebel W., Trzebski R., Stettner G., Hecht L., Casten U., Höhndorf A., Müller P., Granitoid magmatism of the NW Bohemian massif revealed: Gravity data, composition, age relations and phase concept. *Geol. Rundsch.* 86(suppl) (1997) 45–63.
- [58] Cocherie A., Guerrot C., Rossi P.H., Single-zircon dating by step-wise Pb evaporation: comparison with other geochronological techniques applied to the Hercynian granites of Corsica, France. *Chem. Geol.* 101 (1992) 131–141.
- [59] Schmidberger S.S., Hegner E., Geochemistry and isotope systematics of calc-alkaline volcanic rocks from the Saar-Nahe basin (SW Germany) - implications for Late-Variscan orogenic development, *Contrib. Mineral. Petrol.* 135 (1999) 373-385.
- [60] Amov B., Arnaudov V., Lead isotope data on the Paleozoic granitoids and ore mineralization from western Balkan and Tran district. I. Isotope and geochronology. *Geol. Balc.* (1981) 11-2.
- [61] Kamenov B., von Quadt A., Peytcheva I., New insight into petrology, geochemistry, and dating of the Vejen pluton, Bulgaria. *Geochemistry, Mineralogy, and Petrology* 39 (2002) 3-26.

- [62] Peytcheva I., von Quadt A., Ovtcharova M., Handler R., Neubauer F., Salnikova E., Kostitsyn Y., Sarov S., Kolcheva K., Metagranitoids from the eastern part of the Central Rhodopean Dome (Bulgaria): U–Pb, Rb–Sr and  $^{40}\text{Ar}/^{39}\text{Ar}$  timing of emplacement and exhumation and isotope-geochemical features, *Mineralogy and Petrology* 82 (2004) 1-32.
- [63] Bonin B., Orogenic to Non-Orogenic Magmatic Events: Overview of the Late Variscan Magmatic Evolution of the Alpine Belt. *Turkish Journal of Earth Sciences*, 7 (1998) 133-143.
- [64] Matte P., Variscides between the Appalachians and the Urals: similarities and differences between Paleozoic subduction and collision belts. *Spec. Pap. Geol. Soc. Am.* 364 (2002) 239–251.
- [65] Pearce J.A., Harris N.B.W., Tindle A.G., Trace element discrimination diagrams for the tectonic interpretation of granitic rocks. *J. Petrol.* 25 (1984) 956-983.
- [66] Förster H.J., Tischendorf G., Trumbull R.B., An evaluation of the Rb vs. ( Y + Nb) discrimination diagram to infer tectonic setting of silicic igneous rocks, *Lithos*, 40 (1997) 261-293.
- [67] Maniar P.D., Piccoli P.M., Tectonic discrimination of granitoids. *Bulletin of the American Geological Society* 101 (1989) 635–643.
- [68] Shand S.J., *Eruptive Rocks*, D. Van Nostrand Company, New York, 1927, pp. 360.
- [69] Irvine T.N., Barager W.R.A., A guide to the chemical classification of the common volcanic rocks, *Canadian Journal of Earth Sciences* 8 (1971) 523-548.
- [70] Ludwig K.R., *Isoplot 3.0, A Geochronological Toolkit for Microsoft Excel*, Berkeley Geochronology Center Special Publication, 2003, No. 4.

### **Figure captions**

Figure 1. a- Simplified geological map of the study area (after Natal'in et al. [16]), b- Map shows main tectonic divisions and the position of the Strandja Massif in Marmara region.

Figure 2. Plot of normative compositions of the units in a- quartz-alkalifeldspar- plagioclase (Q-A-P) diagram (LeMaitre [28]), b- The normative anorthite-albite-orthoclase compositions of the units (O'Connor [29]). Hbl-Bt: hornblende-biotite; Bt-Ms: biotite-muscovite.

Figure 3. a- Plot of the Shand's index for granitoids in the study area. Discrimination fields for different types of granitoids (Maniar and Piccoli [67], Shand [68]) are shown. b- Tholeiitic-calc-alkaline description of the Irvine and Baragar [69]. Note that all of orthogneisses follow a single trend on the AFM diagram being within the calc-alkaline field. Abbreviations are the same as in *figure 2*.

Figure 4. Summary chart of the ages of the units derived from single grain evaporation method. Note that the ages older than 1.3 Ga. are not plotted in this diagram. Errors bars represent two-sigma standard deviations ( $2\sigma$ ). Abbreviations are the same as in *figure 2*.

Figure 5. CL images of selected grains of; a- biotite-muscovite orthogneiss, b- hornblende-biotite orthogneiss, and c- Kırklareli metagranite. All of the grains show oscillatory magmatic zoning. Figures 1a and 1b have core structures (for discussion see text).

Figure 6. Histograms showing the frequency distributions of radiogenic  $^{207}\text{Pb}/^{206}\text{Pb}$  ratios derived from evaporation of single zircon grains: a- biotite-muscovite orthogneiss, b- hornblende-biotite orthogneiss, and c- Kırklareli metagranite. d- U-Pb Concordia plots for zircon analyses of the hornblende-biotite orthogneiss (Gk 35). The upper intercept ages are calculated from zircon fractions taking a forced regression through 310 Ma. Ellipses indicate  $2\sigma$  errors. The data were calculated with ISOPLOT program (Ludwig [70]). Abbreviations are the same as in *figure 2*.



Table 1. Major and trace element compositions of the units. Hbl-Bt: hornblende-biotite; Bt-Ms: biotite-muscovite.

Sample	Bt-Ms orthogneiss					Hbl-Bt orthogneiss							Hbl-Bt schlieren		
	Gk117	Gk119	Gk120	Gk122	Gk125	Gk108	Gk111	Gk115	Gk116	Gk118	Gk35	Gk123	Gk114	Gk137	Gk138
SiO <sub>2</sub>	72.937	73.375	69.134	76.541	72.601	59.217	56.935	58.035	55.801	53.686	59.941	60.67	50.559	53.527	51.028
TiO <sub>2</sub>	0.242	0.39	0.579	0.159	0.481	0.764	0.691	0.856	0.838	1.293	0.747	0.73	1.081	0.981	0.798
Al <sub>2</sub> O <sub>3</sub>	14.799	14.889	15.055	14.374	14.182	16.501	15.618	17.493	16.545	18.927	17.302	17.409	18.072	15.455	14.755
Fe <sub>2</sub> O <sub>3</sub> <sup>tot</sup>	1.7	2.396	4.363	1.83	3.372	7.397	7.759	7.555	8.615	7.63	6.356	6.559	10.836	12.089	10.769
MnO	0.034	0.03	0.055	0.014	0.042	0.137	0.145	0.115	0.151	0.127	0.09	0.102	0.182	0.218	0.381
MgO	0.547	0.775	2.356	0.592	1.414	5.099	8.407	4.511	6.758	4.95	3.488	4.675	7.071	6.333	9.52
CaO	0.957	0.665	2.871	0.167	1.474	6.642	6.821	6.254	7.594	6.772	5.705	5.9	8.25	8.392	10.26
Na <sub>2</sub> O	3.641	4.36	3.996	0.484	4.11	3.111	2.82	3.329	3.247	3.44	3.05	3.697	2.72	2.528	2.429
K <sub>2</sub> O	5.219	3.555	2.111	4.852	2.998	1.441	1.859	2.204	1.502	3.188	2.352	2.062	1.878	1.121	0.829
P <sub>2</sub> O <sub>5</sub>	0.21	0.167	0.166	0.131	0.12	0.209	0.141	0.198	0.177	0.579	0.198	0.169	0.185	0.191	0.169
LOI	1.36	1.56	2.14	0.95	1.91	1.1	1.06	0.98	1.02	1.31	0.75	0.97	1.41	1.11	0.89
Ba	548.2	789.8	525.7	416.2	786.8	622.3	509.7	587.4	379.5	706.6	668.1	608.1	520.3	547.5	228
Co	86.6	85.3	96.7	82.4	85.9	90.7	89.4	87.7	86.7	65	19.4	92.8	95.2	73	78.3
Cr	9.2	12.7	45.6	8	32.1	208.6	643	168.9	361.2	74.9	109	219.7	160.1	287.2	528
Ni	na.	na.	1.8	na.	na.	32.9	121	17.7	34.7	19.8	27.8	32	18.7	37.7	67.8
Rb	170.8	139.1	91.1	151.8	100.4	52	79.9	90.6	54.3	129.4	88.7	78.1	90.2	33.1	28.5
Sr	182.3	149.7	260.8	23.9	205.8	461.8	271.8	298.9	303.8	603.4	513.4	306.6	459.6	303.3	191.9
V	15.7	31.8	72.5	10.9	65.6	140.3	157.4	134.4	165.6	183.6	117	111.9	263.7	228.3	230.9
Y	20.2	26.3	40.7	22.9	45.8	24.5	24.7	27.8	24.8	33.5	22.6	21.9	45.3	53.3	45.4
Zn	7.6	12.2	3.9	na.	9.4	78.7	79.6	73	82.5	83.7	84.9	58.2	112.4	144.6	192.3
Zr	147.5	222.1	197.1	113.1	194.6	141.4	108	152.9	98.5	141.2	157.4	146.8	117.5	90.6	77.9
Ce	58.2	98.9	80.1	na.	81.2	57.1	49.1	47.9	53.9	103.4	46.6	na.	85	82.8	71.6
Eu	0.6	0.9	1	na.	0.9	1.5	0.9	1.1	1.1	1.8	1.5	1	1.7	1.7	1.2
La	34.8	44.1	48.6	10.6	42.3	41.9	29.6	27.8	32.3	51.6	52.4	20.1	45.9	39.3	34.7
Nb	8.6	9.5	na.	na.	11.6	na.	na.	na.	na.	21.1	na.	na.	17.3	20.7	21.2
Nd	25.3	42.3	40.8	8.3	34.3	25	22.2	27.3	26.3	49.9	28	22.3	39.3	48.1	29.2
Pb	45.5	18.1	22	4.8	14.4	10.4	17.8	14	13.7	14.9	21.1	15.5	16	9.1	28.5
Sm	5.2	8.5	6	na.	6	4.9	3.3	4.8	4.2	6.9	5.5	3.1	7.4	9.8	5.4
Th	19.9	27	16.3	5.6	26	2.4	8.4	4.6	3.8	9	2.8	3.6	na.	0	5.1
U	na.	na.	na.	na.	na.	na.	na.	na.	na.	na.	2.2	na.	na.	na.	na.
Yb	1.6	2	3.5	2.1	4.1	2.1	2.1	2.4	2.1	3.1	2	1.8	4.3	5.1	4.4
Total	101.79	102.33	102.98	100.18	102.88	101.82	102.48	101.71	102.42	102.13	100.17	103.12	102.45	99.93	102.02
#Mg	0.39	0.39	0.51	0.39	0.45	0.57	0.68	0.54	0.61	0.56	0.52	0.58	0.56	0.51	0.63
#ASI	1.11	1.22	1.07	2.26	1.12	0.88	0.82	0.91	0.80	0.88	0.96	0.91	0.84	0.75	0.63

Table 1. continue

	Kırklareli metagranite								leucocratic gneiss			
Sample	Gk18	Gk100	Gk102	Gk103	Gk104	Gk105	Gk107	Gk124	Gk101	Gk110	Gk112	Gk113
SiO <sub>2</sub>	71.482	70.138	73.032	70.575	72.93	73.934	74.133	70.363	77.88	80.418	77.107	76.272
TiO <sub>2</sub>	0.424	0.475	0.282	0.415	0.36	0.378	0.26	0.535	0.08	0.078	0.055	0.093
Al <sub>2</sub> O <sub>3</sub>	13.872	14.227	13.728	13.989	13.71	14.012	13.326	13.369	13.843	12.337	15.079	14.661
Fe <sub>2</sub> O <sub>3</sub> <sup>tot</sup>	2.653	2.831	2.013	2.807	2.555	2.758	1.958	3.222	0.655	0.406	0.886	1.152
MnO	0.049	0.044	0.05	0.05	0.057	0.056	0.045	0.061	0.011	0.008	0.043	0.037
MgO	0.649	0.824	0.471	0.568	0.562	0.553	0.398	0.905	0.21	0.267	0.232	0.327
CaO	1.537	1.14	1.028	1.455	1.513	1.443	1.181	1.649	0.363	0.581	0.785	0.723
Na <sub>2</sub> O	3.37	4.15	3.942	3.681	3.742	4.015	3.87	3.871	5.294	4.942	5.909	5.289
K <sub>2</sub> O	5.098	5.305	5.085	5.005	4.593	4.681	4.751	4.727	2.879	2.13	1.935	1.993
P <sub>2</sub> O <sub>5</sub>	0.123	0.146	0.089	0.12	0.1	0.113	0.082	0.194	0.147	0.226	0.233	0.261
LOI	0.32	0.65	0.33	0.31	0.31	0.31	0.29	1.67	0.67	0.6	0.58	0.99
Ba	628.7	842.8	391.6	620	416.4	392.3	300	642.6	79.3	454	137.3	293.4
Co	5	100.7	96.3	131.7	139.1	103.2	136.1	93.8	91.3	105.9	1.6	0.5
Cr	4.3	8.9	8.7	8	7.7	7.3	7.4	7.5	4.9	5.9	7.9	6.7
Ni	na.	na.	na.	na.	na.	na.	na.	na.	na.	na.	na.	na.
Rb	197.2	143.4	222.4	196.9	214.7	215.8	235.8	154.7	108.7	65.1	60.2	65.3
Sr	123.9	101.8	78.7	116.4	92	87.5	63.8	112.6	47	130.9	103.6	84.1
V	30.5	33.7	17.8	26.2	26.5	29.6	18.9	33.4	3.2	7.1	1.2	3.7
Y	30.6	36.4	32.4	35.3	33.9	35.9	36.4	33.2	14.6	8.9	8.2	15.4
Zn	43.3	3.6	11.6	7.8	7.6	22.2	na.	18.1	na.	na.	na.	9.6
Zr	211.1	228.9	176.4	208	168.1	203.9	156.6	204.5	90.4	110.2	91.9	105.5
Ce	83.8	124.5	61.1	78	77.6	91.4	68.1	113.4	na.	na.	na.	na.
Eu	0.7	0.8	0.4	0.6	0.5	0.6	0.3	0.7	0.2	0.4	0.4	0.4
La	62.4	52.5	33.2	35.3	37.7	41.9	39.5	52.2	18.1	na.	14.1	12.3
Nb	10.6	na.	12.9	13.9	11.9	13.9	14.7	11.3	9.1	na.	9.1	8.7
Nd	44.8	52.9	33.8	43.2	36	44.4	32.6	53.5	10.8	5	3	4.3
Pb	24	10.3	29.7	28.8	31.6	32.5	32.5	16.7	8.4	27	6	14.5
Sm	7.2	9.2	4.7	5.7	5.7	7.1	5.1	7.4	2.7	2.2	2.5	3.3
Th	19.8	20	17.8	22.4	17.6	29.1	24.4	22.5	5.5	7.5	1.2	6.2
U	na.	na.	na.	na.	na.	na.	na.	na.	na.	1.5	1.8	na.
Yb	2.7	2.9	2.9	3	3	3.1	3.3	2.7	1.3	0.6	0.5	1.2
Total	99.73	100.11	100.17	99.13	100.57	102.39	100.41	100.72	102.08	102.09	102.89	101.86
#Mg	0.32	0.36	0.31	0.28	0.30	0.28	0.29	0.36	0.39	0.56	0.34	0.36
#ASI	1.00	0.97	0.99	0.99	0.99	0.98	0.98	0.92	1.11	1.07	1.14	1.20

Fe<sub>2</sub>O<sub>3</sub><sup>tot</sup> : represent the total iron amount, #Mg: [MgO/(Fe<sub>2</sub>O<sub>3</sub><sup>tot</sup> \*0.9+MgO)], ASI = molecular Al<sub>2</sub>O<sub>3</sub>/(CaO+Na<sub>2</sub>O+K<sub>2</sub>O), na. : not determined

Table 2. Age of biotite-muscovite orthogneisses derived from single grain evaporation method. Errors are two-sigma standard deviations ( $2\sigma$ ).

Sample/Grain	Evaporation temp. C	No. of scans	Mean ratio of $^{207}\text{Pb}/^{206}\text{Pb}$ /error	Age (Ma)	Error (Ma) $\pm$
<b>Gk117</b>					
grain1	1400	110	0.05620 $\pm$ 18	460.3	7.1
grain1	1420	177	0.05652 $\pm$ 18	472.9	6.9
grain2	1380	66	0.05352 $\pm$ 19	350.9	7.9
grain3	1380	110	0.05277 $\pm$ 21	318.9	9.1
grain3	1400	180	0.05372 $\pm$ 14	359.3	5.9
grain4	1380	146	0.055397 $\pm$ 41	428.3	1.7
grain4	1400	36	0.05627 $\pm$ 54	463	21
grain6	1400	148	0.053645 $\pm$ 80	356.2	3.2
grain6	1420	144	0.05725 $\pm$ 11	501.2	4.4
grain7	1380	145	0.05251 $\pm$ 16	307.7	7.1
grain7	1400	105	0.052782 $\pm$ 82	319.4	3.6
grain10	1380	74	0.05259 $\pm$ 19	311.2	8.4
grain10	1400	37	0.05283 $\pm$ 41	321.5	17
grain11	1380	33	0.05249 $\pm$ 30	306.8	13
grain11	1400	111	0.05264 $\pm$ 14	313.3	5
grain11	1420	108	0.052733 $\pm$ 82	317.3	3.6
grain12	1380	145	0.052604 $\pm$ 64	311.8	2.7
grain12	1400	147	0.052681 $\pm$ 85	315.5	3.6
grain13	1380	34	0.05348 $\pm$ 55	349.2	23

Table 3. Ages of hornblende-biotite orthogneisses derived from single grain evaporation method. Errors are two-sigma standard deviations ( $2\sigma$ ).

Sample/Grain	Evaporation temp. C	No. of scans	Mean $^{207}\text{Pb}/^{206}\text{Pb}$ ratio of	Age (Ma)	Error (Ma) $\pm$
<b>Gk35</b>					
grain1	1380	72	0.05378 $\pm$ 19	361.9	7.9
grain2	1380	36	0.05333 $\pm$ 18	342.9	7.7
grain2	1420	249	0.05761 $\pm$ 11	515	4.2
grain2	1440	36	0.06626 $\pm$ 34	814.6	11
grain3	1380	36	0.05280 $\pm$ 54	320.2	23
grain3	1400	143	0.054751 $\pm$ 81	402.5	3.4
grain3	1420	109	0.05626 $\pm$ 12	462.6	4.7
grain4	1420	107	0.055750 $\pm$ 47	442.4	19
grain5	1400	37	0.05361 $\pm$ 42	354.7	17
grain5	1450	70	0.05382 $\pm$ 15	363.5	6.1
grain6	1400	107	0.052756 $\pm$ 78	318.3	3.4
grain7	1390	37	0.05260 $\pm$ 28	311.6	12
grain7	1430	37	0.05473 $\pm$ 34	401.2	14
grain8	1400	36	0.06113 $\pm$ 36	643.8	13
grain9	1400	74	0.05317 $\pm$ 23	336.1	9.1
<b>Gk115</b>					
gr1	1380	145	0.052581 $\pm$ 53	310.8	2.3
gr1	1400	148	0.052573 $\pm$ 47	310.4	2
gr3	1380	144	0.052327 $\pm$ 82	299.7	3.6
gr3	1400	146	0.052324 $\pm$ 43	299.6	1.8
gr4	1380	184	0.052544 $\pm$ 42	309.2	1.8
gr5	1380	74	0.05252 $\pm$ 14	308.1	6.1
gr6	1380	111	0.052668 $\pm$ 86	314.5	3.6
gr6	1400	109	0.052667 $\pm$ 90	314.5	3.9
gr7	1450	141	0.058991 $\pm$ 68	566.8	2.6
gr8	1380	109	0.13429 $\pm$ 28	2154.8	3.7
gr8	1400	72	0.16275 $\pm$ 17	2484.4	1.7
gr9	1420	107	0.05946 $\pm$ 13	584.0	4.8
gr9	1450	109	0.11581 $\pm$ 22	1892.5	3.4
gr10	1400	145	0.052483 $\pm$ 45	306.5	2.0
gr10	1420	73	0.05243 $\pm$ 11	304.2	4.6
gr11	1380	146	0.052661 $\pm$ 33	314.2	1.4
gr11	1400	73	0.05336 $\pm$ 11	344.1	4.8
gr11	1420	36	0.05435 $\pm$ 13	385.6	5.4
gr12	1380	108	0.052694 $\pm$ 61	315.7	2.7
gr12	1400	146	0.052569 $\pm$ 40	310.2	1.8
gr13	1380	142	0.052722 $\pm$ 52	316.9	2.3
gr13	1400	145	0.052668 $\pm$ 66	314.5	3.0
gr13	1420	108	0.052668 $\pm$ 90	314.5	3.9
gr14	1380	144	0.052708 $\pm$ 52	316.3	2.3
gr14	1400	145	0.053413 $\pm$ 65	346.4	2.7
gr14	1420	112	0.05731 $\pm$ 11	503.5	4.2
gr16	1400	74	0.058136 $\pm$ 97	534.9	3.7
gr16	1420	103	0.06044 $\pm$ 14	619.4	4.7

Table 4. U–Pb zircon analytical data of hornblende-biotite orthogneisses (sample Gk 35). All errors are two-sigma standard deviations ( $2\sigma$ ). Measured U–Pb data were calculated ISOPLOT program (Ludwig, 2003) using  $2\sigma$  errors. See text for discussion.

Sample	$^{206}\text{Pb}^*/^{204}\text{Pb}$	U (ppm)	Pb* (ppm)	$^{208}\text{Pb}^*/^{206}\text{Pb}^*$	$^{206}\text{Pb}^*/^{238}\text{U}$	$^{207}\text{Pb}^*/^{235}\text{U}$	$^{207}\text{Pb}^*/^{206}\text{Pb}^*$	Apparent ages (Ma)		
								$^{206}\text{Pb}^*/^{238}\text{U}$	$^{207}\text{Pb}^*/^{235}\text{U}$	$^{207}\text{Pb}^*/^{206}\text{Pb}^*$
<b>Hb-Bt gneiss</b>										
Gk35-1	9212	334	16.7	0.15	0.05021±27	0.3554±27	0.05134±27	308.8	315.8	256.2
Gk35-2	4230	444	27.3	0.10	0.06152±78	0.5589±30	0.06589±79	450.8	384.9	802.9
Gk35-3	484	329	20.4	0.18	0.06234±96	0.4817±40	0.05603±66	399.2	389.8	453.9
Gk35-4	119180	249	13.8	0.08	0.05640±120	0.4970±38	0.06391±153	409.7	353.7	738.6
Gk35-5	2681	364	19.2	0.12	0.05267±58	0.39076±28	0.05380±75	334.9	330.9	362.7

Table 5. Age of Leucocratic gneisses derived from single grain evaporation method. Errors are two-sigma standard deviations ( $2\sigma$ ).

Sample/Grain	Evaporation temperature C	No. of scans	Mean ratio of $^{207}\text{Pb}/^{206}\text{Pb}$ /error	Age (Ma)	Error (Ma)
<b>Gk 39</b>					
grain1	1380	145	0.05349 $\pm$ 39	313.3	10
grain1	1400	108	0.05264 $\pm$ 23	349.6	17
grain1	1420	144	0.05359 $\pm$ 25	353.9	11
grain2	1380	109	0.06125 $\pm$ 41	648	14
grain2	1400	111	0.06747 $\pm$ 24	852.3	7.3
grain2	1420	36	0.07351 $\pm$ 60	1028	16

Table 6. Ages of Kırklareli metagranites derived from single grain evaporation method. Errors are two-sigma standard deviations ( $2\sigma$ ).

Sample/Grain	Evaporation temperature C	No. of Scans	Mean ratio of $^{207}\text{Pb}/^{206}\text{Pb}$ /error	Age (Ma)	Error (Ma)
<b>Gk18</b>					
grain1	1370	144	0.05130 $\pm$ 28	254.3	7.9
grain1	1390	142	0.051272 $\pm$ 44	253.8	2.1
gran2	1380	106	0.05179 $\pm$ 19	276.1	8.2
grain2	1400	107	0.051503 $\pm$ 98	263.4	4.4
grain3	1380	73	0.05179 $\pm$ 15	276.1	6.6
grain4	1380	146	0.0513 $\pm$ 11	254.3	5.1
grain4	1400	142	0.051202 $\pm$ 85	259.9	3.9
grain4	1420	142	0.051494 $\pm$ 99	263	4.4

Fig. 1

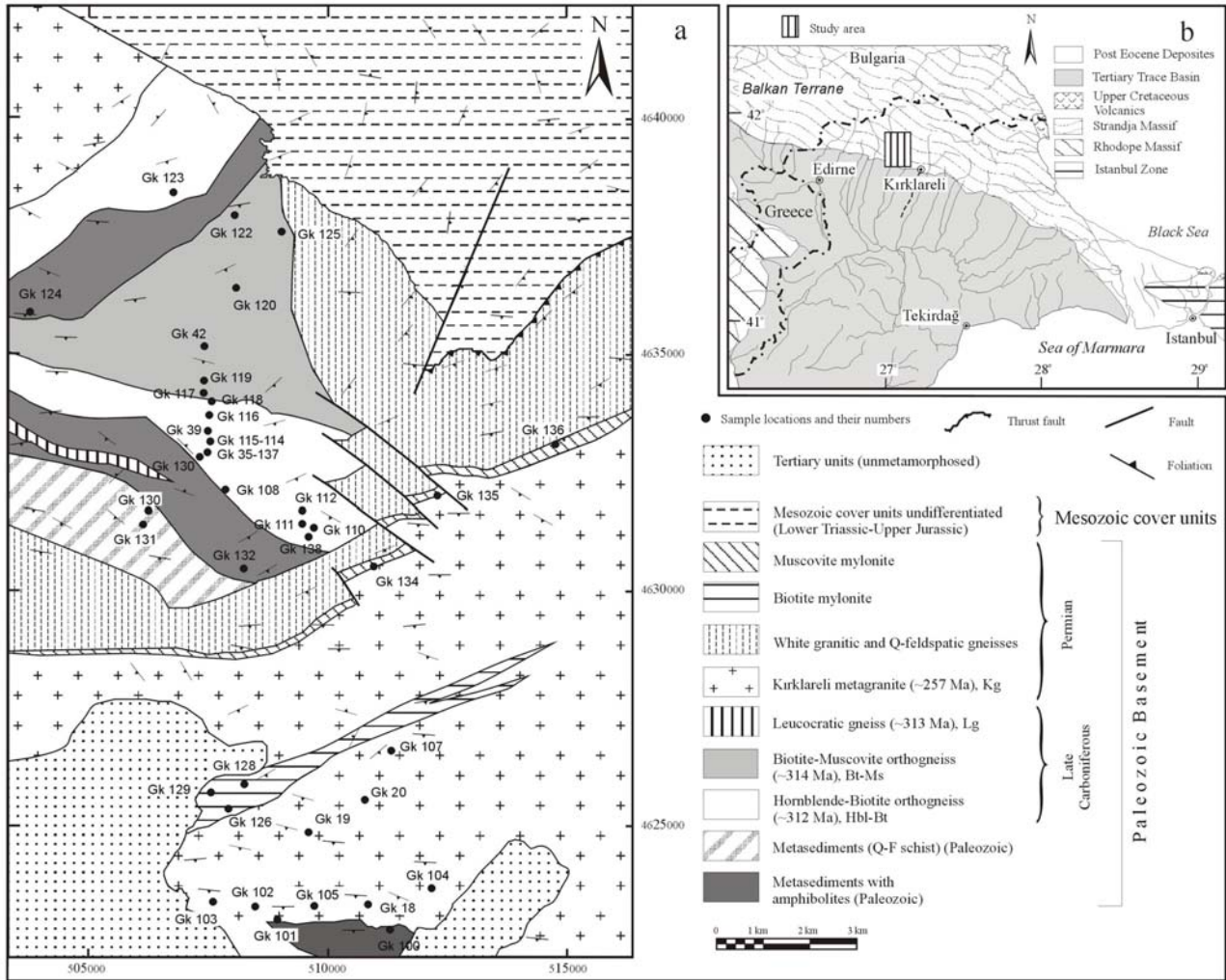


Fig. 2

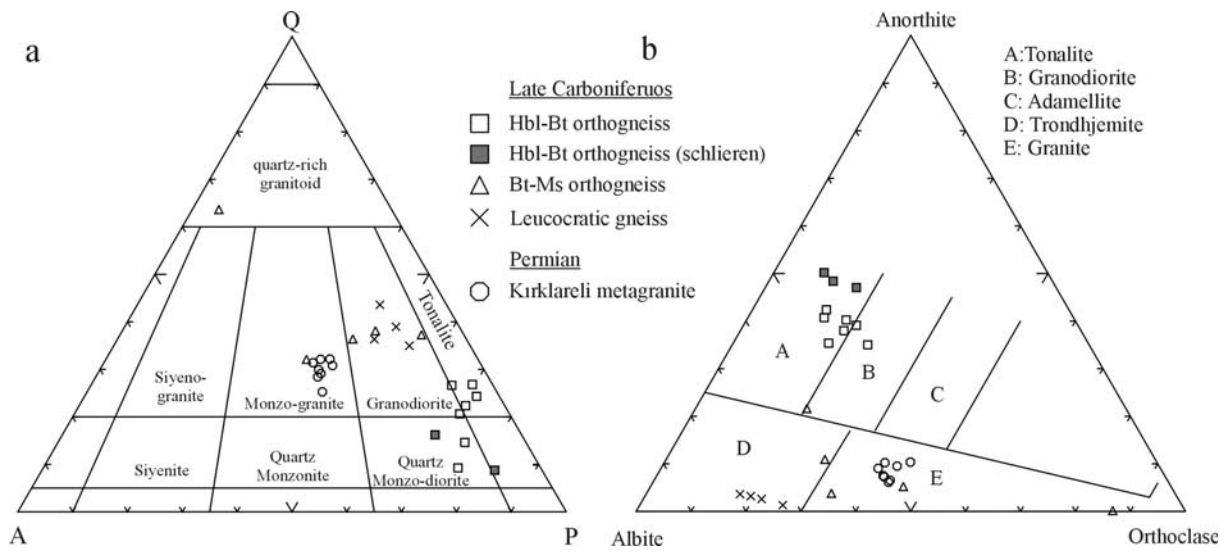




Fig. 3

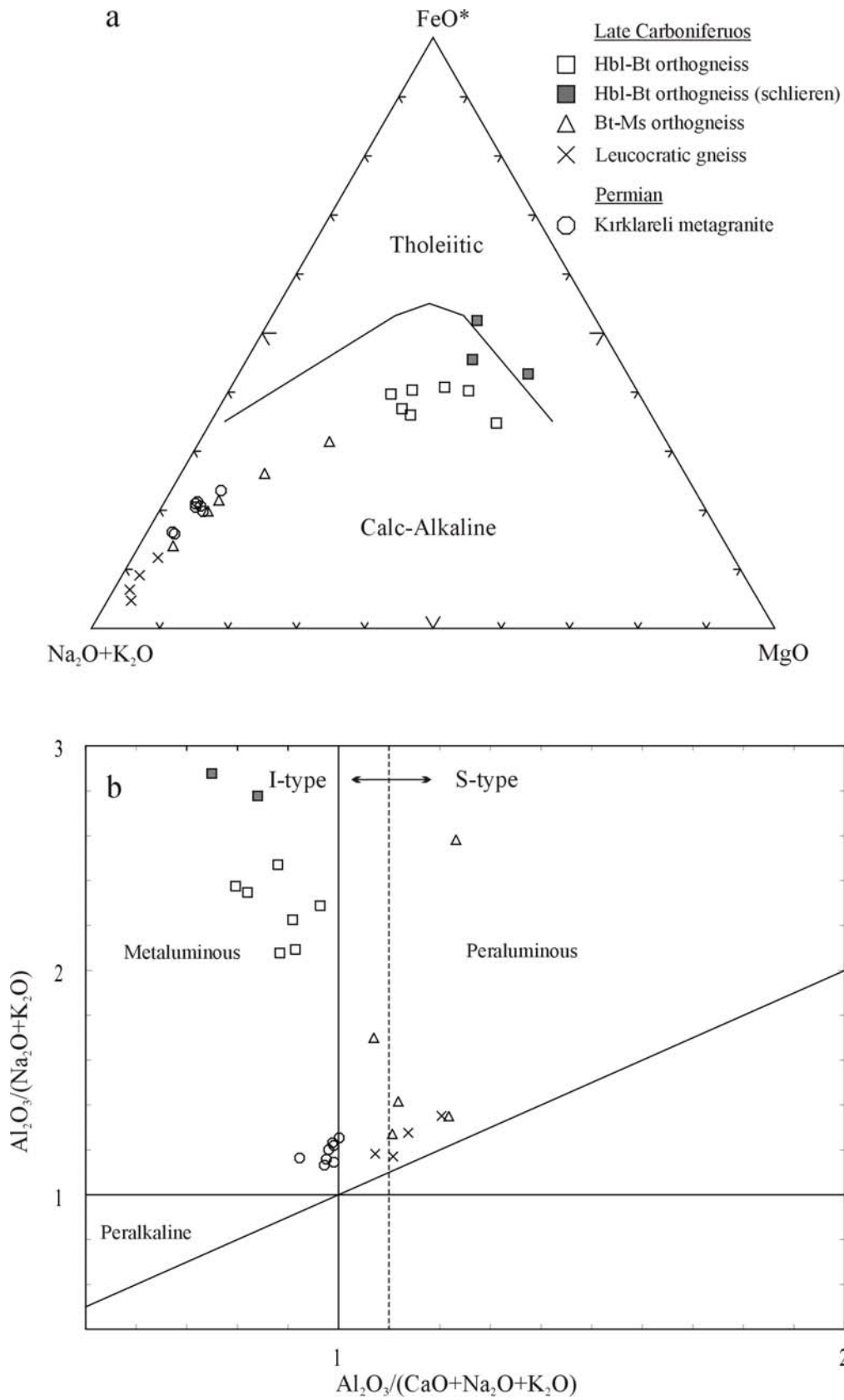


Fig.4

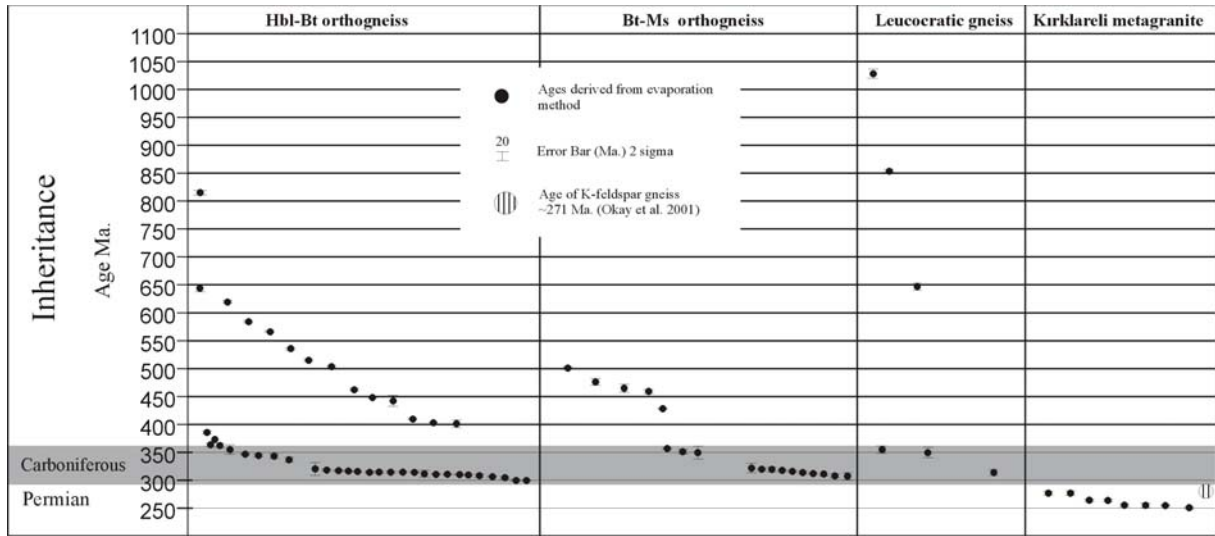


Fig. 5

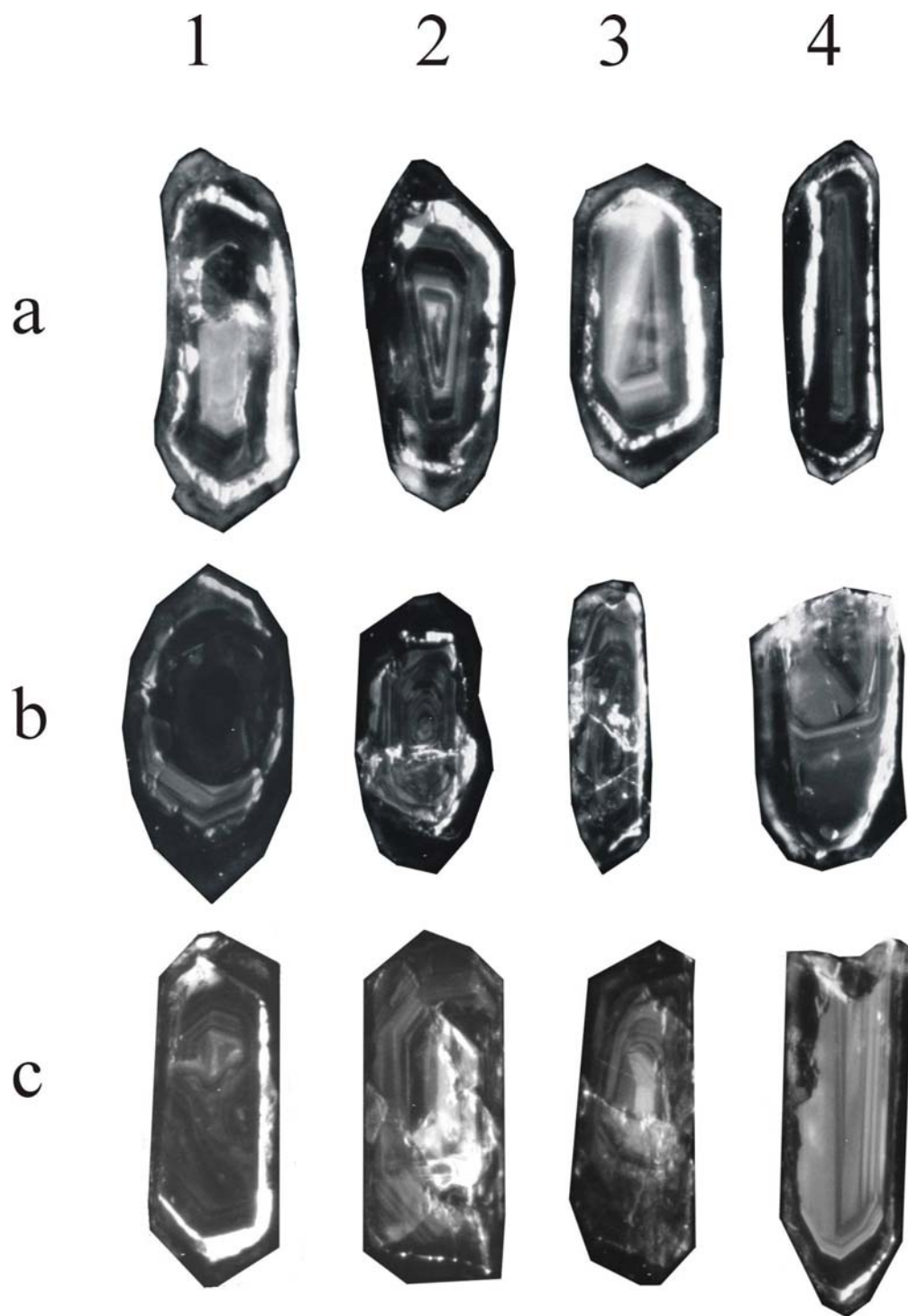
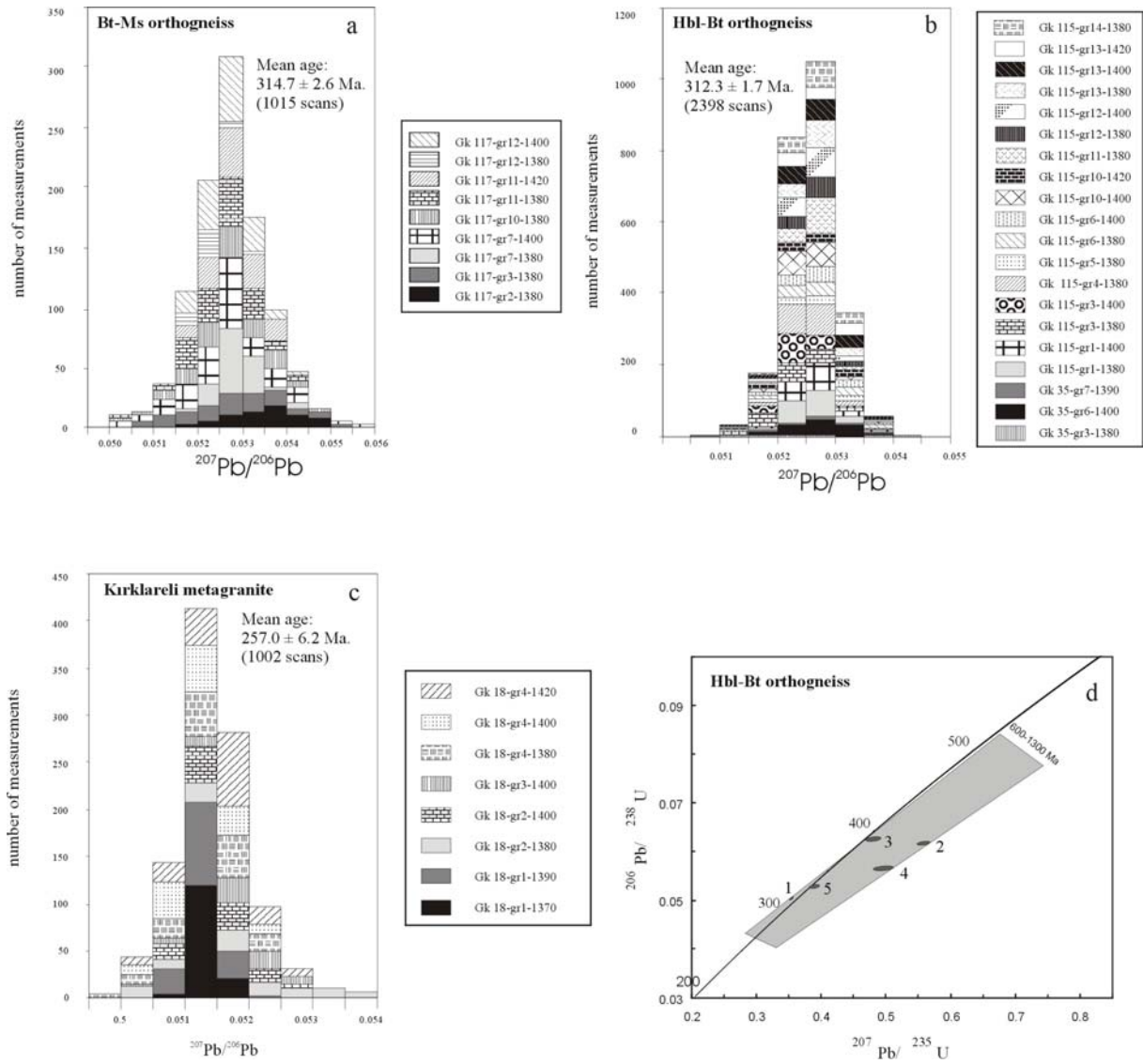


Fig. 6



## **Chapter 2: Paleotectonic position of the Strandja massif, northwest Turkey, and surrounding continental blocks, based on zircon Pb-Pb age studies**

Gürsel Sunal <sup>a,b,\*</sup>, Muharrem Satır <sup>a</sup>, Boris A. Natal'in <sup>b</sup>, Erkan Toraman <sup>c, d</sup>

gsunal@itu.edu.tr; satir@uni-tuebingen.de; natalin@itu.edu.tr; toramane@eas.slu.edu

<sup>a</sup> Universität Tübingen, Institut für Geowissenschaften, Wilhelmstrasse 56, D-72074 Tübingen, Germany

<sup>b</sup> Istanbul Technical University, Department of Geology, TR-34469 Istanbul, Turkey

<sup>c</sup> Department of Earth and Atmospheric Sciences, Saint Louis University, 329 Macelwane Hall 3507 Laclede Ave. St. Louis, MO 63103 USA

<sup>d</sup> ITU Eurasia Institute of Earth Sciences, TR-34469 Istanbul, Turkey

\* Corresponding Author

Published in International Geology Review

Idea:	70%
Problem:	80%
Production of Data:	80%
Evaluation and Interpretation:	70%
Preparation of the manuscript:	70%

## ***Abstract***

Detrital zircon ages from metasedimentary rocks of the Strandja massif (NW Turkey) have been used for revealing its tectonic history, initial position, and some aspects of the Paleozoic motion of this continental block within the Tethyan domain. The age of the metamorphic basement of the massif of NW Turkey has thus far been uncertain. Estimates of the depositional age of metasedimentary rocks range from Precambrian to late Paleozoic, hindering correlation of the massif with other tectonic units. In this study new evaporation Pb-Pb ages of detrital zircons show that biotite schists constituting the central part of the metamorphic basement were deposited later than 430 Ma and prior to 315 Ma. Biotite schists exposed along the southern boundary of the basement were deposited between 300 and 271 Ma.

Episodes of pre-Carboniferous magmatic activity that are inferred from detrital ages cluster around 460-433, 575-525, 700-600, 875-800, 1050-950, 2200-2100, and 2450 Ma. Some of these age ranges are correlative with the ages of late Carboniferous inherited zircons in the orthogneisses (315-300 Ma) of the Strandja massif.

Pan-African or/and Cadomian ages at 575-525 and 700-650Ma respectively, are characteristic of magmatic events in other continental blocks of Turkey (e.g. the Istanbul Zone), as well as in crystalline complexes of surrounding regions, e.g. Crete, the Cyclades massif, the Vardar Zone and the Sredna Gora Zone.

The magmatic history of the source areas of the Strandja detrital zircons prior to the Ordovician is correlative with both the Avalonian and the Armorican tectonic units of Western Europe. Zircon core ages obtained from late Carboniferous orthogneisses in the Strandja massif are correlated with units derived from the North African sector of Gondwana-Land because of the absence of Mesoproterozoic ages. The basement metasediments of the Strandja Massif reveal heterogeneous source areas, which were fed by the North African (Armorica) and the South American (Avalonia) basements. The presence of Mesoproterozoic zircon ages in the metasediments of the Strandja massif indicates the proximity of the Strandja massif to Avalonian (or Baltica) derived units during the late Silurian-Carboniferous interval.

**Keywords:** Strandja Massif; Provenance; Detrital zircon; Single zircon Pb/Pb evaporation ages

## **1. Introduction**

The Strandja Massif covers a third of the Thracian peninsula in NW Turkey (Fig. 1) and forms the eastern continuation of Paleozoic metamorphic rocks of a unit called the ‘Balkan Terrane’ in Bulgaria (Chatalov, 1988; Yanev, 2000; Natal’in et al., 2005a,b; Natal’in, 2006; Sunal et al., 2006) (Fig. 2). The origin of the Strandja Massif is not clear; some researchers interpret this part of the Rhodope-Pontide Fragment (Şengör and Yılmaz, 1981) belt as a part of the Cimmerian microcontinent that rifted from the Gondwana super-continent and collided with Eurasia during the early Mesozoic Cimmerian orogeny (Şengör and Yılmaz, 1981), whereas others claim that the Strandja Massif belonged to the Laurasia margin during the Late Paleozoic and Mesozoic eras (Okay et al., 1996; Okay and Tüysüz 1999; Natal’in et al., 2005a,b; Natal’in, 2006).

Former relationships of continental blocks to ancient continents or supercontinents are generally reconstructed from similarity of ages of magmatic zircons that indicate main episodes of tectonic activity (van der Voo, 1979; Nance and Murphy, 1994; Torsvik, 1998; Unrug, 1997; von Raumer, 1998; Unrug et al., 1999; Murphy et al., 1999; Friedl et al., 2000; Hegner and Kröner, 2000; Matte, 2001; von Raumer et al., 2003; Murphy et al., 2004; Linneman et al., 2004; Samson et al., 2005). In this study, we provide new detrital zircon single grain Pb/Pb ages collected from Paleozoic metasedimentary and magmatic rocks of the Strandja massif in order to determine their sources. Another aspect of this study is to correlate the Strandja Massif with other massifs in its vicinity to establish their possible connections in the geological past.

## **2. Geological framework of the studied area**

The Strandja massif consists of a metamorphic basement that is intruded by late Carboniferous and Permian granitoids and unconformably overlain by a Triassic to Jurassic metasedimentary cover (Aydın, 1974; Aydın, 1982; Çağlayan et al., 1988; Okay et al., 2001; Natal’in et al., 2005; Sunal et al., 2006) (Fig. 1b). Recently, Sunal et al. (2006) showed that the orthogneisses that are intrusive into the metasediments are late Carboniferous in age (between 300-315 Ma). The metasediments intruded by these granitoids (orthogneisses) are located in the central part of the studied area (Natal’in et al., 2005a, b) (Fig. 1a). In the south, biotite schists with amphibolite layers are cut by the early Permian Kırklareli metagranite (Fig. 1a). In the central part, the composition of the Paleozoic metasediments is more

variable: biotite schists, biotite-garnet schists, biotite-muscovite gneisses, and quartzofeldspathic gneisses (Fig. 1a). The metasedimentary units in the basement contain no fossils and thus their age was inferred from regional tectonic correlations. Çağlayan et al. (1988) proposed a Paleozoic age for the basement rocks. Okay et al. (2001) inferred that country rocks of the Kırklareli pluton are late Variscan in age, and Türkecan and Yurtsever (2002) estimated their age as Precambrian.

Besides the late Carboniferous intrusions, the basement of the Strandja Massif is cut by younger plutons of the Kırklareli type. They are monzonitic granites that in places are metamorphosed and deformed (Natal'in et al., 2005 a, b). Aydın (1974 and 1982) reported a  $244 \pm 11$  Ma Rb-Sr whole-rock age of these monzonitic granites while Okay et al. (2001) obtained Permian 278-266 Ma Pb-Pb zircon evaporation ages from them. Samples from the migmatites in the same study yielded  $299 \pm 15$ ,  $276 \pm 12$ ,  $239 \pm 12$ , and  $221 \pm 14$  Ma ages. These younger age determinations were considered as unreliable because of Pb loss and inferred the Triassic age of the sedimentary cover unconformably overlying the metagranites (Okay et al., 2001). Sunal et al. (2006) obtained a  $257 \pm 6.2$  Ma Pb-Pb evaporation age from the Kırklareli metagranite (Fig. 1).

The Kırklareli metagranites also yielded biotite K-Ar ages of 150-149 Ma, Rb-Sr biotite age of 144 Ma (Aydın 1974 and 1982), and Rb-Sr biotite age of  $155 \pm 2$  Ma (Okay et al., 2001). All of these ages were interpreted as the cooling ( $300 \pm 50$  C°) age of regional metamorphism. Rb-Sr muscovite ages are uniformly distributed in the study area and range between 162 to 155 Ma whereas Rb-Sr biotite ages are younger to the north where metamorphic grade decreases to greenschist facies.

### **3. Analytical techniques**

Zircons were extracted from rock samples by standard mineral separation techniques: Wilfley table, heavy liquids, Frantz isodynamic separator. Grains were handpicked under a binocular microscope, then a fraction with grain sizes 63-200  $\mu\text{m}$  was classified according to crystal properties (i.e. euhedral morphology, lack of overgrowth and visible inclusions). Zircons mounted in epoxy resin were polished to expose grain interiors for cathodoluminescence (CL) studies. CL images were obtained using a JEOL JXA-8900RL electron microprobe, using an accelerating voltage of 15 kV and a beam current of 15 nA.

For single-zircon Pb-evaporation, chemically untreated grains were analyzed using a double Re filament configuration as suggested by Kober (1986, 1987). The zircons used for the



evaporation are not the same as those used for CL studies but we rely on the identity of these two groups in our interpretations of ages. Each zircon was embedded in a Re evaporation filament and placed in front of a 1 mm wide Re ionization filament. Each grain was heated first at 1350 °C for 5-10 minute for removal of common (Pb<sup>204</sup>) and radiogenic Pb hosted in less stable phases (e.g. in crystal domains affected by radiation damage) that have low activation energies (Kober, 1986). During repeated evaporation-deposition cycles in 20 °C steps, Pb is deposited on ionization filament for the measurements starting at about 1380 °C (all of the heating steps are unproved). Only high counts, generally 20,000-250,000 per second for <sup>206</sup>Pb, were used for age evaluations. Pb isotopes were dynamically measured in a sequence of 206-207-208-204-206-207 with a secondary electron multiplier. Correction of the common lead contribution to measured <sup>207</sup>Pb/<sup>206</sup>Pb ratios was made according to the two-stage growth model of Stacey and Kramers (1975). Further detailed information on the method is given in Chen et al. (2002), Okay et al. (2001), Siebel et al. (2003), and Sunal et al. (2006). All isotopic ratios were measured in static mode on a Finnigan-MAT 262 multicollector mass spectrometer at the Department of Geochemistry, Tübingen University, Germany.

The age calculations were created using the Isoplot program (Ludwig, 2003). The errors of <sup>207</sup>Pb/<sup>206</sup>Pb ages are given by the 2σ (2 sigma) standard deviation. The <sup>207</sup>Pb/<sup>206</sup>Pb evaporation ages during the course of measurements for Redwitzites granite from the Bohemian massif yielded an average age of 322.8 ± 4.1 Ma, similar to those age ranges reported by Siebel (1994) and Siebel et al. (2003).

## **4. Results**

### *4.1 Description of the samples*

We have analyzed three samples; two from the central region (Gk 33 and Gk 206) and one from the southern (Gk 200) part of the massif (Fig. 1a).

Sample Gk 33 is a medium to fine grained, greenish to gray in color, strongly foliated and lineated biotite schist that was intruded by the late Carboniferous (312.3 ± 1.7 Ma) orthogneisses (Natal'in et al., 2005; Sunal et al., 2006) (Fig. 1a). It consists of quartz (20-25%), K-feldspar (20-25%), plagioclase (10-15%), biotite (10-15%), muscovite (5-10%), epidote (2-5%), calcite (3-5%), minor zircon and opaque minerals. Sample Gk 206 is a medium to fine grained, greenish gray to gray biotite schist that was intruded by the late

Carboniferous biotite-muscovite granitic gneiss (Natal'in et al., 2005; Sunal et al., 2006) (Fig. 1a). It is a biotite schist with quartz (5-10%), plagioclase (35-40%), K-feldspar (10-15%), biotite (15-20%), epidote (20-25%), garnet (2-5%), titanite (1-3%), minor zircon and opaque minerals.

Sample Gk 200 was collected from the southern part of the basement where metasediments with amphibolites are exposed near the contact with the Permian Kırılareli metagranite (Okay et al., 2001; Natal'in et al., 2005; Sunal et al., 2006) (Fig. 1a). It consists of quartz (10-15%), plagioclase (25-30%), K-feldspar (15-20%), biotite (15-20%), muscovite (5-10%), garnet (3-8%), epidote (3-5%), chlorite (3-5%), amphibole (3-5%), minor zircon, titanite, and opaque minerals.

#### *4.2. Zircon populations*

All of the samples contain identical zircon populations which are characterized by different color, size (aspect ratio), crystal quality, transparency, and roundness. The first population is comprised of dark brown, semi-transparent, idiomorphic crystals which have an aspect ratios of 1:2. The second population has light brown color. These are transparent, idiomorphic grains which are either thick or long with an aspect ratio between 1:2 and 1:4. The third population of zircon is colorless. Morphological properties of these zircons are identical with the second group. The second population dominates zircons in all 3 samples, followed by the first and the third populations. Zircons extracted from sample Gk 200 show no or slight roundness. Zircons from the other samples reveal varying degrees of abrasion represented by curved crystal terminations and in some cases perfect roundness (Figs. 3, 4, and 5).

#### *4.3. Zircon internal structures*

##### *4.3.1. Sample Gk 33*

Cathodoluminescence (CL) imaging of sample Gk 33 zircons reveals a variety of internal structures indicating multiple episodes of formation (Fig. 3). Grains belonging to the first type (dark brown ones, grains A to E) show generally oscillatory magmatic zoning surrounding inner rounded cores. These rounded inner cores are most evident in the grains B and E (Fig. 3). Grain C shows an inner idiomorphic and oscillatory zoned xenocrystic core enveloped by a thick, irregular, banded zone that indicates evidence for recrystallization. Traces of these

recrystallization zones are apparent in grain B (bottom left), grain E (bottom right), and grain C (top left) with oscillatory zones truncated by irregular patches.

Similar to the first type of zircons, the second type of zircons (light brown ones: grains F to K) typically show magmatic oscillatory zoning. Grains F, H, J and K have cores composed either of oscillatory (the grains F, H, and J) or homogenous zones (the grain K). Grains G and I are typical magmatic zircons. Grain F reveals an inner part with oscillatory zoning that is truncated and surrounded by an outer part with curved and planar zoning that is bright in CL images. Grain H shows different stages of formation. Its inner part is characterized by oscillatory zoning (black and white zones parallel to the long axis of the zircon) and surrounded by thin, low CL intensity oscillatory zoning. All of these structures are truncated by a gray, homogenous recrystallization zone (right side of the grain). Grain J has an inner part with thinly banded oscillatory zoning surrounded by a dark gray outer part also with oscillatory zoning. The internal part is truncated by the low CL zone on the right side of the zircon (Fig. 3).

The other four grains are represented by colorless zircons (grains L to O). Grains L, N, and O are typical magmatic zircons exhibiting oscillatory zoning. Grain L contains an apparently inherited core. Grain M has a crenulated inner zone truncated by a thick outer structure exhibiting planar zoning. This grain is highly abraded and rounded through sedimentary processes.

Without exception all the grains have an outer, thin, bright CL zone most probably indicating that resorption occurred during the last metamorphic event.

#### 4.3.2. Sample Gk 206

Similar to the sample Gk 33, zircons from the sample Gk 206 reveal a variety of internal structures (Fig. 4). The first 6 grains (A to F) are members of the dark brown zircon population (first type). Grains A and E show typical oscillatory magmatic zoning surrounded by an irregular, bright CL zone representing the recrystallization of the protolith zircon. Grain E is heavily abraded and was probably broken during transportation. Grains B, C, D, and F show homogenous cores (dark gray) that are surrounded by zoned peripheries. These zoned

peripheries are characterized by oscillatory zoning in grains B, D, and F whereas in grain C by weakly developed planar zoning.

Selected light brown zircons are represented by the grains G to K. Grains J and K are typical magmatic zircons with oscillatory zoning and some recrystallization structures (top of grain J). Grains H and I are highly abraded zircons and may have experienced long-distance transport from their source area. In grain H, the oscillatory zoning is truncated by an outermost zone that indicates recrystallization. Grain I has an inner core with oscillatory zoning and is discordantly surrounded by a periphery with planar zoning. Some interesting features can be seen in grain G: The inner part of the grain is a core with low CL (dark) intensity, and this is surrounded and partly truncated by a homogenous, bright CL zone which in turn is overprinted by a weak oscillatory zoning. This thick, low intensity CL oscillatory zone again is truncated by an outer zone with rather high CL intensity.

Colorless zircons (grains L to N) are rounded or sub-rounded. Grain L shows oscillatory magmatic zoning with some irregular recrystallization structures in it (high CL bands on the left and the top of the grain). The inner part of grain M is represented by high CL intensity oscillatory and sector zones truncated and surrounded by an outer rim with planar zoning. Relics of oscillatory zoning are shown in grain N. A recrystallization structure is represented by an homogenous high CL part that truncates and etches early formed oscillatory inner zones.

#### 4.3.3. Sample Gk 200

Selected zircons (Figs. 5, grains A, B, and C) of the honey-colored population show oscillatory magmatic zoning. Sector zoning is also seen in the grain A. Grain B has an unclear and patchy internal structure that is not easy to interpret. Its inner part is surrounded by low CL intensity oscillatory magmatic zones. Planar zoning with rather high CL intensity developed around this oscillatory magmatic zoning. All of the grains have thin bright CL rims.

Light brown zircons (grains D, E, and F) also show oscillatory magmatic zoning and recrystallization rims that truncate the protolith structure. In grain D, the zone of recrystallization cutting earlier oscillatory zones is especially remarkable (grain D, left and

right part). Grain F has an inherited core represented by moderate CL intensity (gray in color) and is surrounded by low CL intensity oscillatory zones (dark zone). This oscillatory zoning structure is overprinted by a recrystallization structure with moderate CL intensity that in places truncates former oscillatory zones (bottom left and right of grain F). A thin outermost bright rim is also typical for this type of zircon.

Grains G, H, and I are members of the colorless population. Grain H is a typical magmatic zircon with oscillatory magmatic zoning and bright CL outer rim similar to the other type of grains of this sample. Grains G and I reveal similar internal structures and both have inherited cores. Grain G consists of a low CL intensity core surrounded by oscillatory magmatic zones whereas grain I has a high CL intensity core represented by sector zoning with dark inclusions (Fig. 5, see SEM image). Both sectors with oscillatory zoning are overprinted by high CL intensity planar zones most probably indicating recrystallization. Bright CL outer rims also developed on both grains (Fig. 5, grains G and I).

#### *4.4. Correlation of zircon ages and zircon populations*

In Figure 6, ages from metasedimentary rocks and zircon core ages in the late Carboniferous orthogneisses are shown separately. Samples Gk33 and Gk 206 reveal different source characteristics (Fig. 6). Ages for sample Gk 200 will be discussed in the following paragraphs.

Ages of 21 zircons at 29 heating steps have been obtained from sample Gk 33 (Table 1). The most abundant age group (31%) is between  $484.2 \pm 4.6$  Ma and  $433.6 \pm 4.8$  (Fig. 6). This age range has been obtained at all heating steps, including the last one (at 1440 Co). Grain 19 gives 470 and 433 Ma at lower and higher temperatures, respectively. Grain 2, however, yields an older age in the first heating step (500 Ma) and a younger age in the second (466 Ma). Three ages in the range between 621 to 612 Ma have been obtained from grains 10 and 13. The complete list of ages and related populations of this sample is given in Table 1 and Figure 6.

Ages of 24 zircons at 35 heating steps were obtained from sample Gk 206 (Table 2). The first population of zircons reveals ages older than 1000 Ma, except grain 9 (685 Ma). The second zircon population shows different age clusters; the first cluster ranges from Ma 495 to 446 Ma similar to Gk 33, whereas the second age cluster ranges between 582 to 525 Ma, this corresponds 64 % of the ages of this population. Only three measurements were made from

the third zircon population and these reveal ages of 998, 931 and 525 Ma (see Table 2 and Fig. 6 for the complete age list).

Unlike those of Gk 33 and Gk 206, zircons of sample Gk 200 reveal younger ages (Table 3, Fig. 6). Ten grains with 20 heating steps were processed. All three of zircon populations gave similar age clusters between 328 to 305 Ma, the age of the late Carboniferous granitoids (orthogneisses) that intruded the basement (Natal'in et al., 2005a, b; Sunal et al., 2006). We also obtained a 236 Ma age from one grain of second population, and 258 Ma from the third one. The second step of the former one gave 314 Ma, which is similar to other ages obtained from this sample. Taking into account the age of Kırklareli metagranite ( $271 \pm 2$  to  $257 \pm 6$  Ma) that cuts these metasediments, these younger ages appear to be unrealistic. We interpret these relatively young ages as a result of Pb loss during the mid Mesozoic metamorphism or mixed ages of the rims developed in this event and the protolith age of the orthogneisses. White rims in the grains of sample Gk 200 (Fig. 5) are much thicker than those of the grains of other samples, as metamorphic grade increases to the south in the study area to amphibolite facies (Natal'in et al., 2005a). Ages of 342 and 336 Ma probably represent core ages. Similar ages are also reported from the late Carboniferous orthogneisses as core ages (Sunal et al., 2006).

The correlation between zircon populations and zircon ages for samples Gk 33 and Gk 206 is shown in Figure 7. With a few exceptions, the dark brown and light brown zircon populations are clustered in different time intervals. Ages of light brown zircons are concentrated between 450 Ma and 1 Ga and between 1.7 and 1.5 Ga. Ages of the dark brown zircons are also concentrated in two intervals: 1.3-1.0 Ga and 2.6-2.0 Ga. Only one younger age  $\sim 685$  Ma has been obtained from the dark brown zircons (Table 2) and one old age ( $\sim 2.7$  Ga, Table 2) from the light brown ones.

The dark brown zircons from the samples Gk 33 and Gk 206 (except 1 grain) show different time intervals of 1.0-1.5 Ma and 2.0-2.7 Ma, respectively (Fig. 7). Interpretation of this result suggests the existence of different sources of these zircons. This inference is supported by the analysis of evaporation temperatures and internal structures. The dark brown zircons from Gk 33 are magmatic in origin because they generally show magmatic oscillatory zoning and few cores (Fig. 3 A to E). In contrast, the dark brown zircons in Gk 206 contain more inherited cores (Fig. 4). Ages obtained at low evaporation temperatures can also be accepted as magmatic ages, but ages obtained at high heating steps are not easy to interpret. These ages may indicate both magmatic and metamorphic events. The latter interpretation is applicable for core structures that do not show any zoning (Fig. 4 A to F).

Ages of light brown and colorless zircons are similar in two samples (Gk 33 and 206). The majority of these ages are distributed between 450 and 1000 Ma, with only 3 exceptions yielding older ages (Tables 1 and 2). Ages ranging between 450-490 Ma and 550-580 Ma should be magmatic in origin because of their usual coherence at different heating steps (e.g. grains 16, 19, 2, and 24 in sample Gk 206).

Some zircons show a large difference in ages at different heating steps. Ages yielded from low heating steps could be interpreted as magmatic since outer rims in all studied zircons generally show oscillatory structure (Fig. 3 F to O and Fig. 4 G to N). However, ages related to high heating steps can also represent metamorphic events. This is especially true for grains having inner unzoned cores that can be interpreted as metamorphic in origin (grains K, L, and M in Fig. 3 and grains F and G in Fig. 4).

#### *4.5. Core and xenocryst ages of late Carboniferous granitoids (orthogneisses)*

Several suites of granitoids intruded the basement at 315-300 Ma (late Carboniferous orthogneisses, Fig. 1a). They are divided into hornblende-biotite, biotite-muscovite, and leucocratic granitic gneisses (Natal'in et al., 2005, Sunal et al., 2006). For the purpose of this study, zircon ages given by Sunal et al. (2006) were carefully analyzed. To avoid mixing, some of the core and xenocryst ages obtained from these orthogneisses have been eliminated. Similar to the detrital zircons, ages from the orthogneisses have considerable variations (Table 4, Fig. 6). Four clusters of ages are established. The first age cluster is between 385 and 340 Ma and is absent in the detrital ages of the metasediments (samples Gk 33 and Gk 206), but present in the detrital zircons of sample Gk 200. The second group is represented by the age range of 428 to 401 Ma and is also absent in the detrital results (the closest age is 433 Ma). The third group ranges between 487 and 442 Ma, and the fourth group is between 535 and 500 Ma. In addition, relatively older ages were obtained; for instance, two grains reveal 584 and 566 Ma and three grains yield 648 and 619 Ma (Table 4).

Sunal et al. (2006) also reported some ID-TIMS, U-Pb ages for 5 fractions containing the three populations of zircons mentioned above. One fraction has a slightly discordant age at 308 Ma. Ages of other fractions could not be defined by a single discordia line in an accepted MSDW value because of a large scatter owing to the presence of inherited cores. Distribution of the core ages could be constrained by drawing different discordia lines representing different fractions with forced regression to the 312 Ma (age of intrusion). Upper intercepts of these discordia lines vary from 1300 to 650 Ma.

## 5. Evaluation of data

To find similarities in the geological evolution of the Strandja Massif and other European massifs, we compiled a database including detrital and inherited zircon ages from previously published papers. Most of these works used different methods for dating (SHRIMP, evaporation, ID-TIMS, SIMS and LA-ICP-MS) that consequently imply different approaches to tectonic interpretations of these ages. Keeping in mind this possibility, we set up some rules for the evaluation of the data:

a) Pb-Pb stepwise evaporation data were included in the database if mean ages are given for magmatic and/or metamorphic events. Detrital or inherited ages listed in the papers are evaluated when the authors discussed their reliability or geological meaning.

b) Ages determined by the ID-TIMS method are accepted when upper or/and lower intercept ages are provided. Only concordant or slightly discordant apparent U238-Pb206 ages for inherited and detrital data younger than 1.0 Ga are included into the compilation. Ages older than 1.0 Ga were added to the database without considering their concordance (Cawood and Nemchin, 2000).

c) SHRIMP, SIMS and LA-ICP-MS data are treated similar to ID-TIMS data.

There are several problems with detrital zircon studies related both to statistical evaluation of data, and determination of their tectonic meaning. Trying to escape falling into methodological traps (e.g. Sircombe and Hazelton, 2004; Nemchin and Cawood, 2005; Andersen, 2005), we rely more on age distributions rather than individual peaks.

The evaporation method has some advantages: a- after separation of zircons no chemical process is needed, which makes the method relatively fast and easy, b- contamination does not occur because no chemical treatment is applied, and c- different heating steps together with CL imaging techniques reveal the history of the zircon. It also has certain disadvantages: a- mixing of different age components, and b- it is not possible to determine the concordance of the Pb/Pb age results without U/Pb data. In order to avoid concordance of the Pb/Pb age results without U/Pb data, ID-TIMS method is used. As it is mentioned in the previous section, no discordia line could be obtained and only a region could be defined that represents core ages.



For the evaluation of data, we first checked the Th/U ratio (derived from the Pb208/Pb206 ratio). Data are taken into consideration only when they have a plateau like distribution. Furthermore we set up two criteria to avoid mixed ages:

1- At least two heating steps during an analysis of the same zircon should give similar ages.

2- Number of coherent ages. For instance, if only one particular age could be obtained from a whole set of analyses, that age was not evaluated (Fig. 8). In addition, the age is evaluated when an individual age obtained in high heating steps (especially the last one) because it represents the most internal part of grain, which hardly mixes with any other age component.

Histograms showing the probability density distribution (PPD) and binned frequency of the evaporation step ages (Figs. 6 and 7) are created using the Age Display program (Sircombe, 2004). The bin width is chosen as 25 Ma and the efficiency value as 75%. The same bin width is also assigned for the compiled data for reliable correlation. If published or compiled histograms have no information about their bin widths, we use them directly without considering their bin widths. Figure 10 shows a binned frequency distribution of the ages as a genetic correlation map like histogram. The genetic map histogram is preferred rather than bar codes due to its convenience for finding out the origin of continents or continental fragments.

## 6. Discussion

### 6.1. Ages of the metasediments in the basement of the Strandja massif

Uncertainties in the age estimations of metasediments in the basement of the Strandja massif ranging from the Precambrian to the late Paleozoic (Aydın, 1974; Aydın 1982; Çağlayan et al., 1988; Okay et al., 2001; Türkecan and Yurtsever, 2002) have been caused by the almost total lack of reliable isotopic age determinations. In this paper we provide some relevant data. In the north, the youngest detrital age recorded in two zircons is ~430 Ma (Figs. 8 and 9). This age is also recorded in the core and xenocrystic zircons extracted from the late Paleozoic orthogneisses (Sunal et al., 2006). A 449 Ma peak is represented by six zircons from the metasedimentary rocks (Figs. 8 and 9). These ages were obtained at high temperatures and repeated heating steps. Similar peaks exist in orthogneisses (Fig. 8 and Table 2 and 3). We infer that 430 Ma can be regarded as the lower age limit (Fig. 9) for the deposition of rocks sampled in the north (samples Gk 206 and Gk 33).

The late Carboniferous orthogneisses (315-300 Ma) crosscutting the metasediments determine the upper age limit for sedimentation (315 Ma). Zircon cores and xenocrysts from

metagranitoids form an obvious peak around 350 Ma (11 zircons). This age interval is very well known in the European Variscides, where it reflects wide-spread magmatism and metamorphism (O'Brien et al., 1990; Kalt et al., 1994; Kröner et al., 1994; Holub et al., 1997; Finger and Roberts, 1997; Bonin, 1998; Schaltegger, 1997; von Raumer, 1998; Altherr et al., 1999; Fernández and Suárez et al., 2000; Kröner et al., 2000; Schaltegger, 2000; Kalt et al., 2000; Klötzli et al., 2001; Romer and Rotzler, 2001, and references therein; Carrigan et al., 2003; Janoušek and Gerdes, 2003; Janoušek et al., 2004; Friedl et al., 2004). This age interval is missing in the metasedimentary rocks of the Strandja massif indicating that 350 Ma old magmatic rocks existed at depth but were not exposed on the surface (Figs. 8 and 9) or sediments deposited prior to 350 Ma. This inference suggests a tool for evaluation of rock ages located at different crustal levels.

The depositional age of the metasediments located in the south of the studied area (Fig. 1a) is relatively easy to interpret. The majority of the detrital zircons have the same ages as the late Carboniferous granitoids (315-300 Ma). They must have been deposited after this magmatic event, and thus the lower limit for sedimentation can be accepted as 300 Ma. These metasediments are cut by the Kırklareli metagranites (271-256 Ma, Okay et al., 2001; Natal'in et al., 2005a, b; Sunal et al., 2006) imposing the upper depositional age limit.

## *6.2. Continental blocks of the surrounding regions*

A number of continental fragments crop out in Turkey and in the neighboring regions of the Balkan Peninsula (Fig. 2). The Strandja massif, the Istanbul Zone, the Menderes massif, and the Kırşehir massif are generally believed to be parts of Gondwana-Land preserving the Pan-African or/and Cadomian orogenic events (Şengör et al., 1984; Şengör and Yılmaz, 1981; Chen et al., 2002; Yiğitbaş et al., 2004; Yanev et al., 2004; Ustaömer et al., 2005). Some researchers suggest that the Strandja massif together with the Istanbul Zone belongs to Laurasia (Okay et al., 1996; Okay and Tüysüz, 1999, Natal'in et al., 2005a, b; Natal'in, 2006). Recently Okay et al. (2006) assigned the Istanbul Zone to the East Avalonia microcontinent, similar to the Pelagonian Zone in Greece (Anders et al., 2005). Yanev (2000) and Yanev et al. (2004) correlated the Istanbul, Balkan, and Bohemian tectonic units with the Saxo-Thuringian Terranes (Eastern Armorican group of terranes) and the Zonguldak and Moesian units with the Rhenohercynian Terranes (Avalonian group of terranes). The latest Neoproterozoic to lower Cambrian metasedimentary rocks of the Menderes-Taurus block was compared with the Angara craton (Kröner and Şengör, 1990). Detrital and inherited zircon ages obtained

from late Paleozoic and Mesozoic rocks in the Cyclades were by contrast correlated with N Africa (Keay and Lister, 2002).

In the European Variscides, two microcontinents of Gondwanian origin have been identified; Avalonia, originally located near S America and NW Africa, in the north, and Armorica, a piece of N Africa, in the south (Van der Voo, 1979; Matte, 1986; Ziegler, 1989; Scotese and McKerrow, 1990; Tait et al., 1997; Torsvik, 1998; Matte 2001). They rifted off Gondwana-Land and collided with Laurasia at different times being separated from each other by the Rheic Ocean. Its closure in part caused the Variscan Orogeny in Europe (Matte, 2001). In Africa, the Archaean and Paleoproterozoic Kalahari, Kongo, and Saharan cratons amalgamated during the Mesoproterozoic, Neoproterozoic, and Cambrian orogens (such as Eburnian, Grenville, Kibaran, Irumide, and Pan-African orogens) (Adelsalam et al., 2002; Johnson et al., 2005). Similar cratonic areas also exist in South America (Rio de la Plata and Amazonian cratons, Silva et al., 2005). These cratonic nuclei are surrounded by mobile orogenic belts. The Grenville (Sunsas belt) and Pan-African (Brasiliano) orogenies are also recorded in South America (Silva et al., 2005). Unlike Africa, South America has a long record of Mesoproterozoic orogenesis such as the Rodonia-Juruena and Rio-Negro (Linneman et al., 2004 and references therein). Baltica is very similar to South America in terms of time distribution of orogenic events. The Grenville orogeny, which dominates Baltica and the Pan-African orogeny are not recorded in this continent. However, in the similar period of Pan-African events, the Timanian orogeny occurred in Baltica (Cocks and Torsvik, 2005). Unlike South America, Baltica has anorogenic Rapakivi plutons in the Mesoproterozoic interval.

Continental blocks derived from north Africa and Armorica, typically lack Mesoproterozoic ages, whereas the Avalonian units have a strong signal at this time interval (Nance and Murphy, 1994; Linneman et al., 2004; Samson et al., 2005). The Archean ages are widespread in the Armorican type units but this interval is represented by a gap in Avalonian units (Avalonia minimum zone) (Murphy, 1994; Linneman et al., 2004; Nance and Samson et al., 2005).

Laurasia-derived tectonic units can be distinguished from Gondwanian ones by the gap in the Neoproterozoic between 600 and 900 Ma – the Baltican Gap (Fig. 10). Another time gap occurs in the late Archean-Paleoproterozoic interval. However, a similar gap (Avalonia minimum, Samson et al., 2005) is known in South America and the Avalonian tectonic units in Europe (Fig. 10).

In the following section, we discuss the correlation of the Anatolian and the Aegean region massifs or zones, their relations with the European Variscides and their possible provenance regions using the zircon age compilation.

### *6.3. Comparison of the units*

The Cyclades and the Strandja massif show an almost identical pattern of zircon age distributions (Fig. 10). In both of them, the Ordovician peak is present. In nearby tectonic units (e.g. Menderes, Pelagonia and Kırşehir) this peak is absent (Keay and Lister, 2002). The Ordovician peak is known in the Sredna Gora-Balkan Zone (Titorenkova et al., 2003; Malinov et al., 2004; Peytcheva et al., 2004; von Quadt and Peytcheva, 2004; Carrigan et al., 2005) that is the continuation of the Strandja massif (Natal'in et al., 2005a, b; Natal'in, 2006). These ages are obtained from late Paleozoic to Early Mesozoic, syn- to post-Variscan rocks. Figure 7 shows the differences between zircon ages obtained from magmatic and metasedimentary rocks in the Strandja massif. Zircon ages from magmatic rocks have a distribution pattern that is similar to the Menderes massif. The detrital ages overlap the Mesoproterozoic gaps presented in the Menderes massif (Figs. 6, 8, and 10). The similar Mesoproterozoic gap exists in metagranitoids exposed in the Cyclades although ages of this time interval are found in Mesozoic sediments (Keay and Lister, 2002).

It is believed that the Menderes and the Kırşehir massifs in Central Anatolia were rifted from N Africa and attached to Laurasia during Jurassic-Paleocene time (Özgül, 1984; Şengör, 1979; Şengör and Yılmaz, 1981). This interpretation is supported by the recently discovered absence of the Mesoproterozoic ages in these massifs (e.g. Keay and Lister, 2002; Gessner et al., 2004) (Fig. 9). Avigad et al. (2003) has cast doubt on the absence of the Mesoproterozoic ages in North Africa. Studying Cambrian siliciclastic rocks, they found Mesoproterozoic ages (0.9-1.1 Ga) and interpreted them as the evidence of the Kibaran Orogeny. Similar zircon ages were reported in the Kırşehir, Menderes and Cyclades Massifs (Kröner and Şengör, 1990; Loos and Reischmann, 1999; Keay and Lister, 2002; Whitney et al., 2003). In addition, Nd model ages from the Aegean and Anatolian crust yield a cluster around 1 Ga (Pe Piper and Piper, 2001). As a result, in the following correlations we will use a narrowed Proterozoic gap for north Africa-derived units in accord with recent discoveries.

The presence of Mesoproterozoic ages in detrital zircons from Paleozoic or Mesozoic sedimentary rocks reported around the Aegean region and the Anatolia may indicate a mixing of different sources that appeared later in the geological history of these tectonic units. The

Cyclades are a good example for this case. We infer that the Menderes and the Kırşehir massifs show North African affinity although with a considerable gap between 2 and 2.5 Ga in the Kırşehir massif (for data source see Whitney et al., 2003) which is more similar with the situation on the Angaran craton in Siberia than with Gondwana-Land (Fig. 10).

The Pelagonian and the Sredna-Gora zones have the same age gaps in the Precambrian. However, the limited number of ages obtained from the Pelagonian Zone makes this comparison tentative. The zircon age distributions in the Sredna-Gora- Balkan, Strandja, and the Cyclades are very similar; all of them have Ordovician ages, but the 1.5 to 1.0 Ga interval is not present in the Sredna-Gora-Balkan Zone (Fig. 10).

Age distributions of magmatic pre-Ordovician rocks in the Saxothuringian Zone and the Sudetes in Europe reveal similarities with the Strandja massif and the Cyclades (Fig. 10). All of the ages belonging to the Saxothuringian Zone and the Sudetes were obtained from pre-Ordovician magmatic rocks and therefore they unequivocally indicate events occurring in the crust, and the problem of source mixing (Strandja, Cyclades) is eliminated. An example of source mixing was provided for the Armorican quartzite by Fernandez-Suarez et al. (2002) (Fig. 10). According to their model, the Armorican quartzite (early-middle Ordovician) was fed by both northwest Iberia (Amazonian source) and southwest Iberia (north African source). The Istanbul zone has a more or less continuous record that starts in the mid-Paleoproterozoic and ends in the late Cambrian (Fig. 10). Its zircon age distribution has no equivalent around the Aegean region and Anatolia. This zone might be correlated with the Rhenohercynian Zone (Eckergneiss complex), which is believed to be part of eastern Avalonia that had been derived mainly from north of south America (Amazonia) (Geisler et al., 2005 and references therein). The Paleozoic succession of the Istanbul Zone has been correlated with the Scythian platform of the Southern Urals in Russia (Okay et al., 1994). Recent studies have revealed close connections between the Scythian platform, Moesia, and the Istanbul Zone with the tectonic zones in northern Europe. Kalvado et al. (2003) reaffirmed that the Istanbul and the Rhenohercynian Zones can be counterparts, considering their paleobiogeographic data and the Variscan history as originally shown by Paekelmann (1925, 1932).

Comparisons of these two units (the Eckergneiss complex (Rhenohercynian Zone), and the Istanbul Zone) reveal some similarities and dissimilarities. Both of them have Mesoproterozoic ages (Fig. 10). However, no ages predating the middle Paleoproterozoic are known from either of these units. The Eckergneiss complex has a gap during the Cambrian but the Istanbul Zone does not. In some respects, the Istanbul zone and the Eckergneiss

complex can be compared both with South America and Baltica in terms of age distributions. The presence of magmatic activity around 1.5 Ga is typical for Baltica-derived units.

As was seen in the previous correlations, sometimes it is not easy to distinguish the original position of microcontinents using known criteria such as the Mesoproterozoic gap in N Africa or the presence of the Cadomian or Pan-African ages. In addition, the nature of the host rocks containing the zircons is important. The presence and the kind of zircons in sedimentary rocks strongly depend on mechanisms of lateral transport. Thus, they may be derived from widely separated sources and give mixed ages. Inherited zircons in magmatic rocks are more dependant on vertical ascent of magma. Hence they better record the history of the continental crust through which they ascend.

Instead of gaps, 'minimum zones' (Samson et al., 2005) can be used for correlations. In this study, we propose a criterion for the distinction between Baltica- and Gondwana-Land-derived continental blocks. Blocks of Gondwanian origin (mainly east Gondwana-Land) are characterized by a minimum zone of ages between 1.4 to 1.65 Ga. In Baltica, the same time span is well represented by zircon ages and geologically known magmatic and metamorphic events (Fig. 10). With few exceptions, such as the Sudetes and the Menderes Massif, all units derived from east Gondwana-Land have this minimum zone (e.g. the Strandja, the Cyclades, the Kırşehir massif, the Sredna-Gora-Balkan, the Pelagonia Zone, Iberia, the Cadomia, the Armorican Massif, Tepla Barrandian, and Saxo Thuringian zones, Fig. 10). In the Menderes massif, only two ages (evaporation ages) out of 82 measurements were reported around 1.5 Ga (Loos and Reischmann, 1999; Gessner et al., 2004). In Baltica, ages around 1.5 Ga, charnockitic rocks in Poland (Dörr et al., 2002; Gawęda et al., 2005), Rapakivi granite-gabbro-anorthosite in Lithuania (Rämö and Haapala, 1996; Motuza, 2005), similar granitoids in Sweden (Persson, 1999) and in Russia (Amelin et al., 1997) have been reported.

## **7. Conclusions**

Metasedimentary rocks constituting the basement of the Strandja massif developed in two different intervals; Silurian- Carboniferous (430-315 Ma) and Permo-Carboniferous (300-271 Ma), respectively.

Continental blocks and tectonic zones located around the Aegean region show clear N-NE African affinity, except the Istanbul Zone. Gondwanian affinity for the Kırşehir massif is also a plausible interpretation (Özgül, 1984).

The geologic history and age distribution of the Istanbul Zone show a great similarity with the Rhenohercynian zone of northern Europe, which is a part of the East Avalonian microcontinent.

Close similarities have been recognized in the pre-Mesozoic history of the Strandja and the Cyclades. Both have garnet-bearing Paleozoic metasediments and Variscan granitoids which are similar in ages and age distributions.

The difference between core ages in the late Paleozoic orthogneisses and the detrital age spectrum of the Strandja massif can be interpreted as follows: Africa-derived Precambrian basement of the Strandja massif that had not been exposed in the region arrived into the proximity of Amazonia- or Baltica-derived tectonic units. The Paleozoic (430-315 Ma) sedimentary rocks present a record of these mixed sources.

## 8. Acknowledgements

This study was supported by TÜBİTAK (The Scientific and Technical Research Council of Turkey, Project no: YDABCAG 101Y010) and resulted from the cooperative study between Istanbul Technical University, Turkey and University of Tübingen, Germany. It is also a part of the IGCP-480 project. G. Bartholomä for the mineral separations is gratefully acknowledged. We wish to thank Dr. W. Siebel and E. Reitter for help in isotopic measurements. We warmly thank Dr. T.T.B. Nguyen from Vietnam for help in mineral separation and isotopic measurements. We sincerely thank Y. Dilek, D. Whitney, S. Özeren and Z. Çakır for improving the English of the text and their critical and constructive comments and M. Kibaroğlu for the CL study. Thanks are also due to A.M.C. Şengör (associate editor) for his invaluable critics and constructive comments on the text.

## 9. References

- Abdelsalam M.G., Liégeois, J.P., Stern, R.J., 2002. The Saharan Metacraton. *Journal of African Earth Sciences* 34, 119-136.
- Aftalion, M., Bibikova, E.V., Bowes, D.R., Hopgood, A.M., Perchuk, L.L., 1991. Timing of early Proterozoic collisional and extensional events in the granulite–gneiss–charnokite–granite complex, Lake Baikal, USSR: A U–Pb, Rb–Sr and Sm–Nd isotopic study. *J. Geol.* 99, 851–862.

- Altherr, R., Henes-Klaiber, U., Hegner, E., Satir, M., Langer, C., 1999. Plutonism in the Variscan Odenwald (Germany): from subduction to collision. *Int. Journ. Earth Sciences* 88, 422–443.
- Amelin, Y.A., Larin, A.M., Tucker, R.D., 1997. Chronology of multiphase emplacement of the Salmi rapakivi granite-anorthosite complex, Baltic Shield: implications for magmatic evolution. *Contrib. Mineral. Petrol.* 127, 353-368.
- Anders, B., Reischmann, T., Kostopoulos, D., U. Poller, U., 2005. The oldest rocks of Greece: first evidence for a Precambrian terrane within the Pelagonian Zone. *Geol. Mag.* 142 (5), 1–18.
- Andersen, T., 2005. Detrital zircons as tracers of sedimentary provenance: limiting conditions from statistics and numerical simulation. *Chemical Geology* 216, 249–270.
- Atanasova-Vladimirova, S., Mavrudchiev, B., von Quadt, A., Peytcheva, I., Georgiev, S., 2004. Petrology and Geochemistry of lamprophyric dykes in the Vitosha pluton. Bulgarian Geological Society, Annual Scientific Conference, Geology, December, 16-17, pp. 100-102.
- Avigad, D., Kolodner, K., McWilliams, M., Persing, H., Weissbrod, D., 2003. Origin of northern Gondwana Cambrian sandstone revealed by detrital zircon SHRIMP dating. *Geological Society of America* 31 (3), 227–230.
- Aydın, Y., 1974. Etude petrographique et geochimique de la partie centrale du Massif d'Istranca (Turquie), Thesis, University of Nancy, no Ac 10415, 164 pp.
- Aydın, Y., 1982. Geology of the Yıldız (Istranca) Mountains. Thesis, Istanbul Technical University, İstanbul, 1982, 106 pp.
- Bagiński, B., Krzemińska, E., 2005. Various kinds of charnockitic rocks from NE Poland. *Pol. Tow. Mineral. Prace Spec.* 26, 13-17.



- Bonin, B., 1998. Orogenic to non-Orogenic magmatic events: overview of the late Variscan magmatic evolution of the Alpine belt. *Turkish Journal of Earth Sciences* 7, 133-143.
- Boyanov, I., Ruseva, M., Toprakchieva, V., Dimitrova, E., 1990. Lithostratigraphy of the Mesozoic rocks from the Eastern Rhodopes, *Geol. Balc.* 20, 3-28.
- Çağlayan, A.M., Şengün, M., Yurtsever, A., 1988. Main Fault systems shaping the Istranca Massif, Turkey, *J. Pure Appl. Sci. Ser. A Geosci.* 21, 145-154.
- Carrigan, C.W., Mukasa, S.B., Haydoutov, I., Kolcheva, K., 2005. Age of Variscan magmatism from the Bulgarian sector of the orogen. *Lithos* 82, 125-147.
- Carrigan, C.W., Mukasa, S.B., Haydoutov, I., Kolcheva, K., 2003. Ion microprobe U-Pb zircon ages of pre-Alpine rocks in the Balkan, Sredna Gora, and Rhodope terranes of Bulgaria: Constraints on Neoproterozoic and Variscan tectonic evolution. *J. Czech Geol. Soc.* 48, 32-33.
- Cawood, P.A., Nemchin, A.A., 2000. Provenance record of a rift basin: U/Pb ages of detrital zircons from the Perth Basin, Western Australia. *Sedimentary Geology* 134, 209-234.
- Chatalov, G., 1988. Recent developments in the geology of the Strandja Zone in Bulgaria. *Bull. Tech. Univ. Istanbul* 41, 433-466.
- Chen, F., Siebel, W., Satır, M., Terzioğlu, N., Saka K., 2002. Late Proterozoic continental accretion in the north-western Turkey: evidence from zircon U–Pb and Pb–Pb dating and Nd–Sr isotopes. *Int. J. Earth Sci.* 91, 469-481.
- Cocks, L.R.M., Torsvik, T.H., 2005. Baltica from the late Precambrian to mid-Palaeozoic times: The gain and loss of a terrane's identity. *Earth-Science Reviews* 72, 39-66.
- Compston, W., Sambridge, M.S., Reinfrank, R.F., Moczydłowska, M., Vidal G., Claesson, S. 1995. Numerical ages of volcanic rocks and the earliest faunal zone within the late Precambrian of East Poland. *J. Geol. Soc. Am. Bull.* 152 (4), 599 -611.

- Dannat, C., 1997. Geochemistry, geochronology and Nd–Sr isotopy of granitoid core gneisses of the Menderes Massif, southwest Turkey. PhD thesis, Johannes Gutenberg University, Mainz, 120 pp.
- Dörr, W., Belka, Z., Marheine, D., Schastok, J., Valverde-Vaquero, P., Wiszniewska, J. 2002. U-Pb and Ar-Ar geochronology of anorogenic granite magmatism of the Mazury complex NE Poland. *Precambrian Res.* 119, 101-120.
- Drost, K., Linnemann, U., Fatka, O., Kraft, P., Gehmlich, M., Tonk, C., Marek, J., 2003. Neoproterozoic - early palaeozoic geotectonic history of a Gondwana-derived terrane in Central Europe (Tepla -Barrandian, Bohemian Massif). 99th Annual Meeting Geological Society of America, April 1–3, Puerto Vallarta, Mexico (Abstracts).
- Fernández-Suárez, J., Dunning, G.R., Jenner, G.A., Gutiérrez-Alonso, G., 2000. Variscan collisional magmatism and deformation in NW Iberia: constraints from U–Pb geochronology of granitoids. *J. Geol. Soc. Lond.* 157, 565-576.
- Fernández-Suárez, J., Gutiérrez-Alonso, G., Jeffries, T.E., 2002. The importance of along-margin terrane transport in northern Gondwana: insights from detrital zircon parentage in Neoproterozoic rocks from Iberia and Brittany, *Earth and Planetary Science Letters* 204, 75-88.
- Finger, F., Roberts, M.P., 1997. Haunschmid B., Schermaier A., Steyrer H.P., Variscan granitoids of central Europe: their typology, potential sources and tectonothermal relations. *Mineral. Petrol.* 61. 67-96.
- Franke, W., 1989. Tectonostratigraphic units in the Variscan belt of Central Europe. *Geol Soc. Am. Spec. Pap.* 230, 67-90.
- Friedl, G., Finger, F., Paquette, J.L., von Quadt, A., McNaughton, N.J., Fletcher, I.R., 2004. Pre-Variscan geological events in the Austrian part of the Bohemian Massif deduced from U–Pb zircon ages, *Int. J. Earth Sci. (Geol Rundsch)* 93, 802–823.

- Friedl, G., Finger, F., McNaughton, N.J., Fletcher, I.R., 2000. Deducing the ancestry of terranes: SHRIMP evidence for South America- derived Gondwana fragments in central Europe. *Geology* 8, 1035-1038.
- Gawęda, A., Wiszniewska, J., Dörr, W., 2005. Polystage mafic plutonism within Amcg Mazury Complex -the Sejny IG-1 Borehole, NE Poland , *Mineralogical Society of Poland, Special Papers*, 26, 36-39.
- Gebauer, D., Williams, I.S., Compston, W., Grünfelder, M., 1989. The development of Central European continental crust since the Early Archaean based on conventional and ion-microprobe dating of up to 3.84 b.y. old detrital zircons. *Tectonophysics* 157, 81–96.
- Geisler, T., Vinx, R., Martin-Gombojav, N., Pidgeon, R.T., 2005. Ion microprobe (SHRIMP) dating of detrital zircon grains from quartzites of the Eckergneiss Complex, Harz Mountains (Germany): implications for the provenance and the geological history, *Int. J. Earth Sci. (Geol Rundsch)* 94, 369-384.
- Gessner, K., Piazzolo, S., Güngör, T., Ring, U., Kröner, A., Passchier, C.W. 2001. Tectonic significance of deformation patterns in granitoid rocks of the Menderes nappes, Anatolide belt, southwest Turkey. *International Journal of Earth Sciences*, 89, 766–780.
- Gessner, K., Collins, A.S., Ring, U., Güngör, T. 2004. Structural and thermal history of poly-orogenic basement: U–Pb geochronology of granitoid rocks in the southern Menderes Massif, Western Turkey. *Journal of the Geological Society, London* 161, 93–101.
- Hegner, E., Kröner, A., 2000. Review of Nd isotopic data and xenocrystic and detrital zircon ages from the pre-variscan basement in the eastern Bohemian Massif: speculations on 780 palinspastic reconstructions. *Geol. Soc. Lond Spec. Publ.* 179, 113-129.

- Hetzel, R., Reischmann, T., 1996. Intrusion age of Pan-African augen gneisses in the southern Menderes Massif and the age of cooling after Alpine ductile extensional deformation. *Geological Magazine* 133, 565–572.
- Hetzel, R., Romer, R.L., Candan, O., Passchier, C.W., 1998. Geology of the Bozdag area, central Menderes massif, SW Turkey: Pan-African basement and Alpine deformation. *Geologische Rundschau* 87, 394–406.
- Holub, F.V., Cocherie, A., Rossi, P., 1997. Radiometric dating of granitic rocks from the Central Bohemian Plutonic Complex (Czech Republic): constraints on the chronology of the thermal and tectonic events along the Moldanubian-Barrandian boundary. *C. R. Acad Sci. Paris Earth Planet Sci.* 325, 19-26.
- Janoušek, V., Gerdes, A., 2003. Timing the magmatic activity within the Central Bohemian Pluton, Czech Republic: conventional UPb ages for the Sázava and Tábora intrusions and their geotectonic significance. *J. Czech Geol. Soc.* 48, 70-71.
- Janoušek, V., Braithwaite, C.J.R., Bowes, D.R., Gerdes, A., 2004. Magma-mixing in the genesis of Hercynian calc-alkaline granitoids: an integrated petrographic and geochemical study of the Sázava intrusion, Central Bohemian Pluton, Czech Republic, *Lithos* 78, 67-99.
- Johnson, S.P., Rivers, T., De Waele, B., 2005. A review of the Mesoproterozoic to early Palaeozoic magmatic and tectonothermal history of south–central Africa: implications for Rodinia and Gondwana. *Journal of the Geological Society, London* 162, 433-450.
- Kalt, A., Corfu, F., Wijbrans, J.R., 2000. Time calibration of a P–T path from a Variscan high-temperature low-pressure metamorphic complex (Bayerischer Wald, Germany), and the detection of inherited monazite. *Contrib. Mineral. Petrol.* 138, 143–163.
- Kalt, A., Hanel, M., Schleicher, H., Kramm, U., 1994. Petrology and geochronology of eclogites from the Variscan Schwarzwald (F.R.G.). *Contrib. Mineral. Petrol.* 115, 287–302.

- Kalvoda, J., Leichmann, J., Bábek, O., Melichar, R., 2003. Brunovistulian Terrane (Central Europe) and Istanbul Zone (NW Turkey): Late Proterozoic and Paleozoic tectonostratigraphic development and paleogeography. *Geologica Carpathica* 54 (3), 1-14.
- Keay, S., Lister, G., 2002. African provenance for the metasediments and metaigneous rocks of the Cyclades, Aegean Sea, Greece, *Geological Society of America* 30 (3), 235-238.
- Khudoley, A.K., Rainbird, R.H., Stern, R.A., Kropachev, A.P., Heaman, L.M., Zanin, A.M., Podkovyrov, V.N., Belova, V.N. and Sukhorukov, V.I., 2001. Sedimentary evolution of the Riphean-Vendian basin of southeastern Siberia. *Precambrian Res.* 111, 129-163.
- Klimas, K., Fanning, M., Madej, S., Kryza, R., Oberc-Dziedzic, T., 2003. Morphology and SHRIMP study of zircons from the Light Stachów Gneisses (Lipowe Hills, Fore-Sudetic block): petrological implications, *Mineralogical Society of Poland, Special Papers* 23, 81-83.
- Klötzli, U.S., Koller, F., Scharbert, S., Höck, V., 2001. Cadomian lower-crustal contributions to Variscan granite petrogenesis (South Bohemian pluton, Austria): Constraints from zircon typology and geochronology, whole-rock, and feldspar Pb-Sr isotope systematics. *J. Petrol.* 42, 1621-1642.
- Kober, B., 1987. Single-zircon evaporation combined with Pb<sup>+</sup> emitter-bedding for <sup>207</sup>Pb/<sup>206</sup>Pb-age investigations using thermal ion mass spectrometry, and implications to zirconology. *Contrib. Mineral. Petrol.* 96, 63-71.
- Kober, B., 1986. Whole-grain evaporation for <sup>207</sup>Pb/<sup>206</sup>Pb age investigations on single zircons using a double-filament thermal ion source. *Contrib. Mineral. Petrol.* 93, 481-490.
- Koralay, O.E., Dora, O.Ö., Chen, F., Satır, M., Candan, O., 2004. Geochemistry and geochronology of orthogneisses in the Derbent (Alaşehir) area, eastern part of the Ödemiş-Kiraz submassif, Menderes Massif: Pan-African magmatic activity, *Turkish J. Earth Sci.* 13, 37-61.

- Kröner, A., Şengör, A.M.C., 1990. Archean and Proterozoic ancestry in late Precambrian to early Paleozoic crustal elements of southern Turkey as revealed by single-zircon dating. *Geology* 18, 1186-1190.
- Kröner, A., Hegner, E., Hammer, J., Haase, G., Bielicki, K.H., Krauss, M., Eidam, J., 1994. Geochronology and Nd-Sr systematics of Lusatian granitoids: significance for the evolution of the Variscan orogen in east-central Europe. *Geol. Rundsch. (Int. J. Earth Sci.)* 83, 357-376.
- Kröner, A., Willner, A.P., 1998. Time of formation and peak of Variscan HP-HT metamorphism of quartz-feldspar rocks in the central Erzgebirge, Saxony, Germany. *Contrib. Mineral. Petrol.* 132, 1-20
- Kröner, A., Wendt, I., Liew, T.C., Compston, W., Todt, W., Fiala, J., Vankova, V., Vanek, J., 1988, U-Pb zircon and Sm-Nd model ages of high-grade Moldanubian metasediments, Bohemian Massif, Czechoslovakia. *Contrib. Mineral. Petrol.* 99, 257-266.
- Kröner, A., Jaeckel, P., Hegener, E., Olpetal, O., 2001. Single zircon ages and whole-rock Nd isotopic systematics of early Palaeozoic granitoid gneisses from the Czech and Polish Sudetes (Jizerské hory, Krkonose Mountains and Orlice-Sneznik Complex). *Int. J. Earth Sci. (Geol Rundsch)* 90, 217-233.
- Kröner, A., P.J., Nemchin, A.A., Pidgeon, R.T., 2000. Zircon ages for highpressure granulites from South Bohemia, Czech Republic, and their connection to the Carboniferous high temperature processes. *Contrib. Mineral. Petrol.* 138, 127-142.
- Linnemann, U., McNaughton, N.J., Romer, R.L., Gehmlich, M., Drost, K. and Tonk, C., 2004. West African provenance for Saxo-Thuringia (Bohemian Massif): did Armorica ever leave pre-Pangean Gondwana? U/Pb- SHRIMP zircon evidence and Nd-isotopic record. *Int. J. Earth Sci.* 93, 683-705.

- Loos, S., Reischmann, T., 1999. The evolution of the southern Menderes Massif in SW Turkey as revealed by zircon dating. *Journal of the Geological Society, London* 156, 1021-1030
- Ludwig, K.R., 2003. *Isoplot 3.0, A Geochronological Toolkit for Microsoft Excel*, Berkeley Geochronology Center Special Publication No. 4.
- Malinov, O., von Quadt, A., Peytcheva, I., Aladjov, T., Aladjov, A., Naydenova, S., Djambazov, S., 2004. The Klissura granite in the western – Questions and answers from new field and isotope studies, Bulgarian Geological Society, Annual Scientific Conference, *Geology*, December, 16-17.
- Matte, P., 1986. Tectonics and plate tectonics model for the Variscan belt of Europe. *Tectonophysics* 126, 329-374.
- Matte, P., 2001. The Variscan collage and orogeny (480–290 Ma) and the tectonic definition of the Armorica microplate: a review. *Terra Nova* 13, 122-128
- Mazur, S., Turniak, K., Bröcker, M., 2004. Neoproterozoic and Cambro-Ordovician magmatism in the Variscan Kłodzko Metamorphic Complex (West Sudetes, Poland): new insights from U/Pb zircon dating. *Int. J. Earth Sci.* 93, 758-772.
- Morgan, J.W., Stein, H.J., Hannah, J.L., Markey, R.J., Wiszniewska, J., 2000. Re-Os study of Fe-Ti-V oxide and Fe-Cu-Ni sulfide deposits, Suwalki Anorthosite Massif, Northeast Poland. *Miner. Deposita* 35, 391-401.
- Motuza, G., 2005. Structure and formation of the crystalline crust in Lithuania, *Mineralogical Society of Poland, Special Papers* 26, 69-79.
- Murphy, J.B., Keppie, J.D., Dostal, J., Nance, R.D., 1999. Neoproterozoic-Early Paleozoic evolution of Avalonia, in Ramos, V.S., and Keppie, J.D., eds., *Laurentia- Gondwana Connections before Pangea*: Boulder, Colorado, Geological Society of America Special Paper 336, 253-266.

- Murphy, J.B., Pisarevsky, S.A., Nance, R.D., Keppie, J.D., 2004. Neoproterozoic—Early Paleozoic evolution of peri-Gondwanan terranes: implications for Laurentia-Gondwana connections, *Int. J. Earth Sci. (Geol Rundsch)* 93, 659-682.
- Muszyński, A., Machowiak, K., Kryza, R., Armstrong, R., 2002. SHRIMP U-Pb zircon geochronology of the Late-Variscan Żeleźniak Rhyolite intrusion, Polish Sudetes – preliminary results, *Mineralogical Society of Poland, Special Papers* 20, 156-158.
- Nance, R.D., Murphy, J.B., 1994. Contrasting basement isotopic signatures and the palinspastic restoration of peripheral orogens: Example from the Neoproterozoic Avalonian-Cadomian belt. *Geology* 22, 617–620
- Natal'in, B. A., Satır, M., Sunal, G., Toraman, E., 2005a. Structural and metamorphic evolution of the Strandja massif. Project No: 101Y010: The Scientific and Technical Research Council of Turkey, Ankara, (Unpublished).
- Natal'in, B., Sunal, G., and Toraman, E., 2005b. The Strandja arc: anatomy of collision after long-lived arc parallel tectonic transport, in: E.V. Sklyarov, (Ed), *Structural and Tectonic Correlation across the Central Asia Orogenic Collage: North-Eastern Segment*. Guidebook and abstract volume of the Siberian Workshop IGCP-480, IEC SB RAS, Irkutsk, pp. 240-245.
- Natal'in, B., 2006, Paleozoic evolution of the northern margin of Paleo-Tethys, in Tomurhuu, D., Natal'in, B., Ariunchimeg, Y., Khishigsuren, S., and Erdenesaikhan, G., eds., *Second International Workshop and Field Excursions for IGCP Project-480. Structural and Tectonic correlation across the Central Asian Orogenic Collage: Implications for Continental Growth and Intracontinental Deformation. Abstracts and Excursion Guidebook*: Ulaanbaatar, Institute of Geology and Mineral Resources, Mongolian Academy of Sciences, p. 33-36.
- Nemchin, A.A., Cawood, P.A., 2005. Discordance of the U-Pb system in detrital zircons: Implication for provenance studies of sedimentary rocks, *Sedimentary Geology* 182, 143-162.



- O'Brien, P.J., Carswell, D.A., Gebauer, D., 1990. Eclogite formation and distribution in the European Variscides. In: Carswell, D.A. (Ed.), *Eclogite Facies Rocks*, Blackie, Glasgow, pp. 204-224.
- O'Brien, P. J., Carswell, D. A., 1993. Tectonometamorphic evolution of the Bohemian Massif: evidence from high pressure metamorphic rocks. *Geologische Rundschau* 82, 531–555.
- O'Brien, P. J., Kröner, A., Jaeckel, P., Hegner, E., Żelaźniewicz, A., Kryza, R., 1997. Petrological and isotopic studies on Palaeozoic high-pressure granulites, Góry Sowie Mts, Polish Sudetes. *Journal of Petrology* 38, 433–456.
- Okay, A.I., Satır, M., Tüysüz, O., Akyüz, S., Fukun, C., 2001. The tectonics of the Strandja Massif: late-Variscan and mid-Mesozoic deformation and metamorphism in the Northern Aegean. *Int. J. Earth Sciences* 90, 217-233.
- Okay, A.I., Tüysüz, O., 1999. Tethyan sutures of northern Turkey. In: Durand, B., Jolivet, L., Horvath, F. and Seranne, M. (Eds.), *The Mediterranean Basins: Tertiary Extension within the Alpine Orogen*. Geological Society, London, Special Publication 156, 475-515.
- Okay, A.I., Satır, M., Maluski, H., Siyako, M., Monie, P., Metzger, R., Akyüz, S., 1996. Paleo- and Neo-Tethyan events in northwestern Turkey: Geologic and geochronological constraints. In: Yin, A. & Harrison, M. (Eds.), *The Tectonic Evolution of Asia*. Cambridge University Press 420-441.
- Okay, A.I., Şengör, A.M.C., Görür, N., 1994. Kinematic history of the opening of the Black Sea and its effect on the surrounding regions. *Geology* 22, 267-270.
- Okay, A.I., Satır, M., Siebel, S., 2006. Pre-Alpide Palaeozoic and Mesozoic orogenic events in the Eastern Mediterranean region, Geological Society, London, *Memoirs* 32, 389-405.

- Özgül, N., 1984. Stratigraphy and tectonic evolution of the Central Taurides. International Symposium on the Geology of the Taurus Belt, O.Tekeli ve M.C.Göncüoğlu (eds), 77-90.
- Paeckelmann, W., 1925. Beiträge zur Kenntnis des Devons am Bosphorus, insbesondere in Bithynien. Abh. Preuss. Geol. L.Ä.N.F., 98.
- Paeckelmann, W., 1938. Neue Beiträge zur Kenntnis der Geologie, Paläontologie und Petrographie der Umgegend von Konstantinopel. Abh. Preuss. Geol. L.-A., N. F. 186
- Piper, G., Piper, D.J.W., 2001. Late Cenozoic, post-collisional Aegean igneous rocks: Nd, Pb and Sr isotopic constraints on petrogenetic and tectonic models, Geological Magazine 138(6), 653-668.
- Persson, A.I., 1999. Absolute (U-Pb) and relative age determinations of intrusive rocks in the Ragunda rapakivi complex, central Sweden. Precambrian Research 95, 109–127.
- Peytcheva, I., von Quadt, A., Ovtcharova, M., Handler, R., Neubauer, F., Salnikova, E., Kostitsyn, Y., Sarov, S., Kolcheva, K., 2004. Metagranitoids from the eastern part of the Central Rhodopean Dome (Bulgaria): U–Pb, Rb–Sr and  $^{40}\text{Ar}/^{39}\text{Ar}$  timing of emplacement and exhumation and isotope-geochemical features, Mineralogy and Petrology 82, 1-32.
- Rainbird, R.H., Stern, R.A., Khudoley, A.K., Kropachev, A.P., Heaman, L.M., Sukhorukov, V.I., 1998. U-Pb geochronology of Riphean sandstone and gabbro from southeast Siberia and its bearing on the Laurentia-Siberia connection: Earth and Planetary Science Letters 164, 409–420.
- Rämö, O.T., Haapala, I., 1996. Rapakivi granite magmatism: a global review with emphasis on petrogenesis. In: Deaiffe, D. (Ed.), Petrology and geochemistry of magmatic suites of rocks in continental and oceanic crusts. A volume dedicated to Professor Jean Michot. Université Libre de Bruxelles, Royal Museum of Central Africa (Tervuren). 177-200.

- Ring, U., Gessner, K., Güngör, T., Passchier, C.W., 1999. The Menderes Massif of western Turkey and the Cycladic Massif in the Aegean-do they really correlate? *Journal of the Geological Society, London* 156, 3-6.
- Ring, U., Collins, A.S., 2005. U–Pb SIMS dating of synkinematic granites: timing of core-complex formation in the northern Anatolide belt of western Turkey, *Journal of the Geological Society, London* 162, 289-298.
- Romer, R.L., Rötzler, J., 2001. P-T-t evaluation of ultrahigh-Temperature granulites from the Saxon Granulite Massif, Germany. Part II: Geochronology. *Journal of Petrology* 42, 2015-2032.
- Salnikova, E.B., Sergeev, S.A., Kotov, A.B., Yakovleva, S.Z., Steiger, R.H., Reznitskiy, L.Z., Vasil'ev, E.P., 1998. U-Pb dating of granulite metamorphism in the Sludyansky complex, Eastern Siberia, *Gondwana Research, Vol. 1, No 2*, 195-205.
- Samson, S.D., D'lemos, R.D., Miller, B.V., Hamilton, M.A., 2005. Neoproterozoic palaeogeography of the Cadomia and Avalon terranes: constraints from detrital zircon U–Pb ages. *Journal of the Geological Society, London* 162, 65-71.
- Schaltegger, U., 1997. Magma pulses in the Central Variscan Belt: episodic melt generation and emplacement during lithospheric thinning. *Terra Nova* 9, 242-245.
- Schaltegger, U., 2000. U-Pb geochronology of the Southern Black Forest Batholith (Central Variscan Belt): timing of exhumation and granite emplacement. *Int. J. Earth Sci.* 88, 814-828.
- Scotese, C.R., McKerrow, W.S., 1990. Revised world maps and introduction. In: *Palaeozoic Palaeogeography and Bio- geography*. In: McKerrow, W.S. and Scotese, C.R. (Eds). *Mem. Geol. Soc. London*, 12, 1-21.
- Şengör, A. M. C., 1979. The North Anatolian transform fault: its age, offset and tectonic significance. *Journal of the Geological Society, London* 136, 269-282.

- Şengör A.M.C., Yılmaz Y., 1981. Tethyan evolution of Turkey: A plate tectonic approach. *Tectonophysics* 75, 181-241.
- Şengör, A.M.C., Yılmaz, Y., Sungurlu O., 1984. Tectonics of the Mediterranean Cimmerides: Nature and evolution of the western termination of Paleo-Tethys. In: Dixon, J.E. and Robinson, A.H.F. (Eds.), *The geological evolution of the Eastern Mediterranean*. Geological Society of London Special Publication 17, 77-112.
- Siebel, W., Chen, F., Satır, M., 2003. Late-Variscan magmatism revisited: new implications from Pb-evaporation zircon ages on the emplacement of redwitzites and granites in NE Bavaria, *International Journal of Earth Sciences* 92, 36-53.
- Siebel, W., 1994. Inferences about magma mixing and thermal events from isotopic variations in redwitzites near the KTB site. *KTB Rep* 94(3), 157-164.
- Silva, da L.C., McNaughton, N.J., Armstrong, R., Hartmann, L.A., Fletcher, I.R., 2005. The neoproterozoic Mantiqueira Province and its African connections: a zircon-based U–Pb geochronologic subdivision for the Brasiliano/Pan-African systems of orogens *Precambrian Research* 136, 203-240.
- Sircombe, K.N., 2004. AGEDISPLAY: an EXCEL workbook to evaluate and display univariate geochronological data using binned frequency histograms and probability density distributions. *Computers and Geosciences* 30 (1), 21-31.
- Sircombe, K. N., Hazelton, M. L., 2004. Comparison of detrital age distributions by kernel functional estimation: *Sedimentary Geology* 171, 91-111.
- Söllner, F., Nelson, D., Miller, H., 1997. Provenance deposition and age of gneiss units from the KTB drill hole (Germany): evidence from SHRIMP and conventional U–Pb zircon age determinations. *Geol. Rundschau* 86 (Suppl), 235–250.
- Stacey J.S., Kramers J.D., 1975. Approximation of terrestrial lead isotope evolution by a two stage model. *Earth Planet. Sci. Lett.* 26, 207-221.

- Strnad, L. and Mihaljevic, M., 2005. Sedimentary provenance of Mid-Devonian clastic sediments in the Tepla'-Barrandian Unit (Bohemian Massif): U-Pb and Pb-Pb geochronology of detrital zircons by laser ablation ICP-MS, *Mineralogy and Petrology* 84, 47-68.
- Sultan, M., Tucker, R.D., El Alfy, Z., Attia, R., 1994. U-Pb (zircon) ages for the gneissic terrane west of Nile, southern Egypt. *Geol. Rundschau* 83, 514-522.
- Sunal, G., Natal'in, B.A., Satir, M., Toraman, E., 2006. Paleozoic magmatic events in the Strandja Massif, NW Turkey, *Geodinamica Acta* 19 (5), 281-298.
- Tait, J.A., Bachtadse, V., Franke, W., Soffel, H.C., 1997. Geodynamic evolution of the European Variscan fold belt: paleomagnetic and geological constraints. *Geol. Rndsch.* 86, 585-598.
- Teixeira, W., Tassinari, C.C.G., Cordani, U.G., Kawashita, K., 1989. A review of the geochronology of the Amazonian Craton: tectonic implications. *Precamb Res.* 42, 213-227.
- Tichomirowa, M., Berger, H.J., Koch, E.A., Belyatski, B.V., Götze, J., Kempe, U., Nasdala, L., Schaltegger, U., 2001. Zircon ages of high-grade gneisses in the Eastern Erzgebirge (Central European Variscides) – constraints on origin of the rocks and Precambrian to Ordovician magmatic events in the Variscan foldbelt. *Lithos* 56, 303-332.
- Titorenkova, R., Macheva, L., Zidarov, N., von Quadt, A., Pejtcheva, I., 2003. Metagranites from SW Bulgaria as a part of the Neoproterozoic to early Paleozoic system in Europe: new insight from zircon typology, U-Pb Isotope data and Hf-tracing, *Geophysical Research, Abstracts* vol. 5, 08963.
- Torsvik, T.H., 1998. Palaeozoic palaeogeography: a North Atlantic viewpoint. *Geol. Soc. Sweden (G.F.F.)* 120, 109-118.

- Turniak, K., Mazur, S., Bröcker, M., 2002. Timing of Pre-Variscan magmatism in the Kłodzko metamorphic complex (Central Sudetes, Poland): first insights from conventional U/Pb zircon dating, *Mineralogical Society of Poland – Special Papers* 20, 214-217.
- Türkecan, A., Yurtsever, A., 2002. Geological map of Turkey. Istanbul. General Directorate of Mineral Research and Exploration, Ankara.
- Unrug, R., 1997. Rodinia to Gondwana: The Geodynamic Map of Gondwana Supercontinent Assembly. *GSA Today* 7, 1-6.
- Unrug, R., Haranczyk, C. and Chocyk- Jaminska, M., 1999. Easternmost Avalonian and Armorican-Caledonian terranes of Central Europe and Caledonian-Variscan evolution of the polydeformed Krakow mobile belt: geological constraints. *Tectonophysics* 302, 133-157.
- Ustaömer, P.A., Mundil, R., Renne, P.R., 2005. U/Pb and Pb/Pb zircon ages for arc-related intrusions of the Bolu Massif (W Pontides, NW Turkey): evidence for Late Precambrian (Cadomian) age, *Terra Nova* 17, 215-223.
- Van der Voo, R., 1979. Paleozoic assembly of Pangea: a new plate tectonic model for the Taconic, Caledonian and Hercynian orogenies. *EOS, Trans. Am. geophys. Un.*, 60, 241.
- Vernikovsky, V.A., Vernikovskaya, A.E., Salnikova E.B., Kotov, A.B., Kovach, V.P. 2003. Neoproterozoic accretion-collisional events on the western margin of the Siberian Craton: New geological and geochronological evidence from the Yenisey Ridge, *Tectonophysics* 375 (1-4), 147-168.
- von Quadt, A., Peytcheva, I., 2004. Magmatic evolution of the Cretaceous rocks within the panagyurishte district (Central Srednegerie, Bulgaria) based on U-Pb and Hf-zircon, Nd and Sr whole rock data. *Bulgarian Geological Society, Annual Scientific Conference, Geology, December, 16-17, pp. 60-62.*

- von Raumer J.F., 1998. The Palaeozoic evolution in the Alps: from Gondwana to Pangea, *Geol. Rundsch* 87, 407–435.
- von Raumer, J.F., Stampfli, G.M. and Bussy, F., 2003. Gondwana-derived microcontinents – the constituents of the Variscan and Alpine collisional orogens. *Tectonophysics* 365, 7-22.
- Whitney, D.L., Teyssiera, C., Fayona, A.K., Hamilton, M.A., Heizler, M., 2003. Tectonic controls on metamorphism, partial melting, and intrusion: timing and duration of regional metamorphism and magmatism in the Niğde Massif, Turkey, *Tectonophysics* 376, 37-60.
- Wiszniewska, J., 2002. Wiek i geneza rud Fe-Ti-V i skał towarzyszących w suwalskim masywie anortozytowym (północno-wschodnia Polska). *Biul. PIG* 401, 1-96.
- Wiszniewska, J., Claesson, S., Stein, H., Vander Auwera, J., Duchesne, J.C., 2002: The north-eastern Polish anorthosite massifs: petrological, geochemical and isotopic evidence for a crustal derivation. *Terra Nova* 14, 451-460.
- Wiszniewska, J., Krzeminska, E., 2005. Precambrian crystalline basement of northeastern Poland – new approach, *Mineralogical Society of Poland – Special Papers* 26, 97-104.
- Wiszniewska, J., Krzemińska, E., Williams, I., 2004. Metavolcanic rocks from Łomża, NE Poland: geochemistry, age and geotectonic interpretation, *Mineralogical Society of Poland – Special Papers* 24, 397-400.
- Yanev, S., 2000. Palaeozoic terrans of the Balkan Peninsula in the framework of Pangea assembly, *Palaeogeography, Palaeoclimatology, Palaeoecology* 161, 151-177.
- Yanev, S., Göncüoğlu, M.C., Boncheva, I., Gedik, I., Lakova, I., Maliakov, Y., Özgül, N., Sachanski, V., Sağlam, G., Timur, E., 2004. Correlation of the Paleozoic terranes in Bulgaria and NW Turkey: preliminary results. 5th International Symposium on Eastern Mediterranean Geology Thessaloniki, Greece, April, 14-20, pp. 5-12.

Yiğitbaş, E., Kerrich, R., Yılmaz, Y., Elmas, A., Qianli, X. 2004. Characteristics and Geochemistry of Precambrian Ophiolites from the Western Pontides, Turkey: Following the Missing Chain of the Precambrian South European Suture Zone to the East. *Precambrian Research* 132 (1-2), 179-206.

Ziegler, P., 1989. *Evolution of Laurussia. — A Study in Late Palaeozoic Plate Tectonics* Kluwer, Dordrecht, 102 pp.



## Figure captions

Figure 1. a- Simplified geological map of the study area (modified after Natal'in et al., 2005 and Sunal et al., 2006), b- Map showing the main tectonic divisions and the position of the Strandja Massif in the Marmara region.

Figure 2. Main tectonic divisions of Europe and the Aegean region compiled after Franke (1989), Boyanov et al. (1990), Okay et al. (1994), Okay et al. (1996), Ring et al. (1999) and Carrigan et al. (2005). AM; Armorican massif, BM; Bohemian massif, BZ; Balkan Zone, CYC; Cyclades, HZ; Harz Mountains (Eckergneiss complex), IASZ; Izmir-Ankara suture Zone, IAZ; Internal Alpine Zones, IZ; Istanbul Zone, KM; Kırşehir massif, MM; Menderes massif, MP; Moezia Platform, MS; Morova-Silesia Zone, NWIB; NW Iberia, PZ; Pelagonia Zone, RM; Rhodope massif, SG; Sredna-Gora Zone, SMM; Serbo-Makedonian massif, SJ; Strandja massif, SWIB; SW Iberia, SZ; Sakarya Zone, TB; Tepla-Barrandian Zone, TESZ; Trans European suture Zone, VZ; Vardar Zone.

Figure 3. CL and secondary-electron images of selected grains of sample Gk 33 (see text for explanations).

Figure 4. CL and secondary-electron images of selected grains of sample Gk 206 (see text for explanations).

Figure 5. CL and secondary-electron images of selected grains of sample Gk 200 (see text for explanations).

Figure 6. Graph of ages of samples (Gk33, Gk 206, Gk 200) and cores in late Carboniferous orthogneisses.

Figure 7. Comparison of ages obtained from detrital zircon populations extracted from samples Gk 33 and Gk 206.

Figure 8. Probability density distribution histograms of the ages obtained from the study area.

Figure 9. Probability density distribution histogram of the ages younger than 700 Ma. Bar shows deposition interval of metasediments of the basement units (see text for discussion).

Figure 10. Age distributions (genetic maps) of selected Europe, surrounding Aegean region massifs (Zones), and main cratonic areas. 1- West African Craton (Nance and Murphy, 1994 and Söllner et al., 1997), 2- NE African Craton (Sultan et al., 1994 and Avigad et al., 2003), 3- Baltica-East European Craton (Compston et al., 1995; Morgan et al., 2000; Dörr et al., 2002; Wiszniewska et al., 2002; Wiszniewska, 2002; Wiszniewska et al., 2004; Bagiński and Krzemińska, 2005; Gawęda, et al., 2005 and the references therein; Wiszniewska and Krzemińska, 2005 and the references therein; Strnad and Mihaljevic, 2005 and references therein), 4- South America Craton (Amazonian Craton) (Teixeira et al., 1989), 5 - Siberia and Angara (Rainbird et al., 1998; Salnikova et al., 1998; Aftalion et al., 1991; Khudoley et al., 2001; Vernikovskiy et al., 2003), 6- NW Iberia ( Fernandez-Suarez et al., 2002 and the references therein), 7- Cadomia ( Fernandez-Suarez et al., 2002 and the references therein), 8- SW Iberia ( Fernandez-Suarez et al., 2002 and the references therein), 9- Armorican Quartzite ( Fernandez-Suarez et al., 2002 and the references therein), 10- Tepla-Barrandian Zone (Bohemia Massif) (Drost et al., 2003; Strnad and Mihaljevic, 2005), 11- Erbenburg-Vchenstrass Zone (Bohemia Massif) (Söllner et al., 1997), 12- Saxothuringian Zone (Bohemia Massif) ( Kröner and Willner, 1998; Tichomirowa et al., 2001; Linneman et al., 2004), 13- Moldanubian Zone (Bohemia Massif) (Gebauer et al., 1989; Kröner et al., 1988; Friedl et al., 2004), 14- Sudetes (Bohemia Massif) (O'Brien et al., 1993; O'Brien et al., 1997; Kröner et al., 2001; Muszyński et al., 2002; Turniak et al., 2002; Klimas et al., 2003; Mazur et al., 2004; Turniak et al., 2005), 15- Moravia-Silesia (Bohemia Massif) (Friedl et al., 2004), 16- Eckergneiss Complex (Harz Mountains, Rhenohercynian Zone) (Geisler et al., 2005), 17- Istanbul Zone (Chen et al., 2002; Ustaömer et al., 2005), 18- Eastern Pelagonia Zone (Anders et al., 2005), 19- Menderes Massif (Kröner and Şengör, 1990; Hetzel and Reischmann, 1996; Dannat, 1997; Hetzel et al., 1998; Loos and Reischmann, 1999; Gessner et al., 2001; Gessner et al., 2004; Koralay et al., 2004; Ring and Collins, 2005), 20- Sredna Gora and Balkan Zone (Titorenkova et al., 2003; Peytcheva et al., 2004; von Quadt and Peytcheva, 2004; Atanasova et al., 2004; Carrigan et al., 2005), 21- Cyclades (Keay and Lister, 2002), 22- Strandja Massif (this study), 23- Kırşehir Massif (Whitney et al., 2003). AVMZ: Avalonia Minimum zone, ARMZ: Armorica Minimum Zone.

Table 1. Age results of the sample Gk 33

Grain No	Zircon description	Evaporation Temp.C <sup>o</sup>	No. of scans	Mean ratio of Pb <sup>207</sup> /Pb <sup>206</sup> /error	Age (Ma)	Error (Ma)±
1	lb, lg, tr, id	1400	37	0,05662 ±51	476,8	20
2	lb, thc, tr, id	1370	147	0,05722 ±80	500,3	3,1
2		1400	288	0,05635 ±78	466,2	3,1
3	db, thc, tr, id, rdt	1360	34	0,07273 ±13	1006,4	3,4
3		1420	219	0,07499 ±98	1068,3	2,6
4	lb, lg, tr, id	1420	109	0,05660 ±14	476	5,5
5	lb, lg, tr, id	1440	144	0,05628 ±10	463,5	2,4
6	lb, thc, tr, id	1380	36	0,05639 ±12	467,8	4,7
7	lb, thc, tr, id	1440	75	0,05629 ±98	464,1	3,8
8	clrs, thc, tr, id	1380	217	0,06710 ±22	840,9	6,7
9	lb, thc, tr, id, rdt	1440	181	0,05912 ±12	571,5	4,6
10	lb, thc, tr, id, rdt	1450	149	0,06041 ±14	618,3	5,2
11	lb, lg, tr, id	1440	141	0,05723 ±11	500,4	4,4
12	lb, thc, tr, id, rdt	1380	36	0,06246 ±42	689,9	14
13	lb, lg, tr, id	1390	183	0,06023 ±39	612	1,4
13		1400	72	0,06049 ±16	621,1	5,6
14	db, thc, tr, id	1410	38	0,06896 ±89	897,5	27
14		1420	36	0,06945 ±46	912,1	14
14		1430	257	0,07817 ±10	1151,2	2,6
15	lb, lg, tr, id	1440	71	0,05681 ±12	484,2	4,6
16	db, thc, tr, id	1420	36	0,08314 ±32	1272,5	16
16		1450	73	0,08318 ±23	1273,4	5,4
17	lb, thc, tr, id, rdt	1420	145	0,09514 ±18	1530,8	3,6
18	lb, lg, tr, id	1420	108	0,06524 ±19	782,1	6,1
19	lb, thc, tr, id	1380	144	0,05553 ±12	433,6	4,8
19		1420	142	0,05647 ±11	470,9	4,3
20	db, thc, tr, id	1400	107	0,07761 ±13	1136,9	3,3
21	lb, thc, tr, id, rdt	1400	38	0,06569 ±35	796,5	11,2
21		1420	146	0,10414 ±86	1699,2	1,5

lb: light brown, db: dark brown, clrs: colorless, lg: long, thc: thick, tr: transparent, str: slightly-transparent, id: idiomorphic, rdt: rounded terminations

Table 2. Age results of the sample Gk 206. Abbreviations are the same as Table 1.

Grain No	Zircon description	Evaporation Temp.C°	No. of scans	Mean ratio of Pb <sup>207</sup> /Pb <sup>206</sup> /error	Age (Ma)	Error (Ma)±
1	db, thc, str, id	1380	73	0,13259 ±60	2132,5	7,9
1		1400	138	0,15375 ±23	2388,1	2,5
2	lb, thc, tr, rdt	1400	73	0,05667 ±30	478,7	11,7
3	lb, lg, str, id	1400	110	0,05851 ±82	549,0	3,1
3		1420	147	0,05806 ±82	532,3	3,1
4	clrs, lg, tr, rtd	1400	35	0,07011 ±21	931,6	6,1
4		1420	71	0,07245 ±36	998,6	10,1
5	clrs, thc, tr, id	1400	72	0,05790 ±21	526,0	8,0
6	lb, thc, tr, id	1420	70	0,06269 ±21	697,7	7,1
7	lb, thc, tr, rtd	1420	37	0,06128 ±42	649,1	14,7
8	lb, lg, tr, id	1420	110	0,05789 ±15	525,6	5,7
9	lb, lg, str, rtd	1400	37	0,05585 ±40	446,4	15,9
9		1420	73	0,05895 ±24	565,2	8,9
10	db, thc, str, id	1400	110	0,08322 ±16	1274,4	3,7
10		1420	138	0,14224 ±12	2254,7	1,5
11	lb, thc, tr, id	1420	36	0,06477 ±27	766,9	8,8
12	lb, thc, tr, rtd	1400	73	0,05711 ±25	495,8	9,6
12		1420	102	0,05891 ±25	563,8	9,2
13	lb, thc, tr, id	1400	144	0,05793 ±94	527,2	3,6
13		1420	110	0,05943 ±13	582,9	4,7
14	lb, thc, str, id	1420	146	0,05594 ±66	450,3	2,6
14		1440	74	0,05592 ±16	449,2	6,4
15	db, thc, str, id	1420	71	0,12317 ±37	2002,6	5,3
16	lb, thc, tr, id	1380	143	0,05899 ±42	567,1	1,5
16		1400	106	0,05921 ±52	574,8	1,9
16		1420	73	0,05856 ±31	550,8	11,6
17	db, thc, str, id	1420	144	0,06233 ±47	685,8	1,6
18	lb, thc, str, id	1400	110	0,05789 ±89	525,8	3,4
18		1420	215	0,05831 ±66	541,5	2,5
19	db, thc, str, id	1380	36	0,13030 ±46	2102,0	6,2
19		1400	73	0,16028 ±43	2458,6	4,5
19		1420	109	0,17384 ±19	2595,0	1,8
20	lb, lg, tr, id	1420	109	0,18595 ±20	2706,7	1,8
21	lb, thc, tr, id	1400	106	0,05912 ±16	571,5	5,9
21		1420	108	0,05897 ±69	566,2	2,5

Table 3. Age results of the sample Gk 200. Abbreviations are the same as Table 1.

Grain No	Zircon description	Evaporation Temp.C <sup>o</sup>	No. of scans	Mean ratio of Pb <sup>207</sup> /Pb <sup>206</sup> /error	Age (Ma)	Error (Ma)±	
1	clrs, lg, tr, id	1420	35	0,05250 ±29	307,2	12,6	
2	db, thc, str, rdt	1400	36	0,05332 ±25	342,4	10,6	
3	lb, lg, str, id	1380	144	0,05090 ±15	236,3	6,8	led loss
3		1420	144	0,05265 ±87	314,0	3,8	
4	lb, lg, str, id	1380	106	0,05268 ±10	315,0	4,3	
4		1400	71	0,05248 ±17	306,4	7,4	
4		1420	36	0,05293 ±28	325,8	12,0	
5	db, thc, str, rdt	1380	71	0,05277 ±22	318,9	9,5	
5		1400	147	0,05302 ±14	329,7	6,0	
5		1420	107	0,05294 ±18	326,2	7,7	
6	lb, lg, tr, id	1380	147	0,05272 ±12	316,8	5,2	
6		1400	118	0,05249 ±77	307,2	3,3	
6		1420	107	0,05246 ±57	305,5	2,5	
7	clrs, lg, tr, id	1400	108	0,05140 ±65	258,8	29,1	led loss
8	lb, lg, tr, id	1400	36	0,05255 ±46	309,4	19,9	
8		1420	73	0,05300 ±22	328,8	9,4	
9	db, lg, str, id, rdt	1380	145	0,05266 ±74	314,6	3,2	
9		1400	110	0,05276 ±72	318,5	3,1	
10	lb, lg, tr, id	1400	144	0,05248 ±20	306,4	8,7	
10		1420	73	0,05284 ±12	321,9	5,2	

Table 4. Core and xenosryt ages obtained from late Carboniferous granite gnisses (data after Sunal et al., 2006).

Biotite-muscovite gneiss		Hornblende-Biotie gneiss		leucocratic gneiss	
Age (Ma)	Error (Ma)±	Age (Ma)	Error (Ma)±	Age (Ma)	Error (Ma)±
343,7	5	361,9	7,9	349,6	17
349,2	23	342,9	7,7	353,9	11
350,9	7,9	344,1	4,8	648	14
356,2	3,2	346,4	2,7	852,3	7,3
359,9	4,9	354,7	17	1028	16
428,3	1,7	363,5	6,1		
444,8	3,8	385,6	5,4		
460,3	7,1	401,2	14		
463	21	402,5	3,4		
466,2	14	410,5	2,7		
472,9	6,9	442,4	19		
477,2	12	448,4	2,7		
487,3	12	462,6	4,7		
501,2	4,4	503,5	4,2		
516,9	8,6	515	4,2		
		534,9	3,7		
		566,8	2,6		
		584,0	4,8		
		619,4	4,7		
		643,8	13		
		814,6	11		
		1801,4	4,9		
		1892,5	3,4		
		2154,8	3,7		
		2484,4	1,7		

Fig. 1

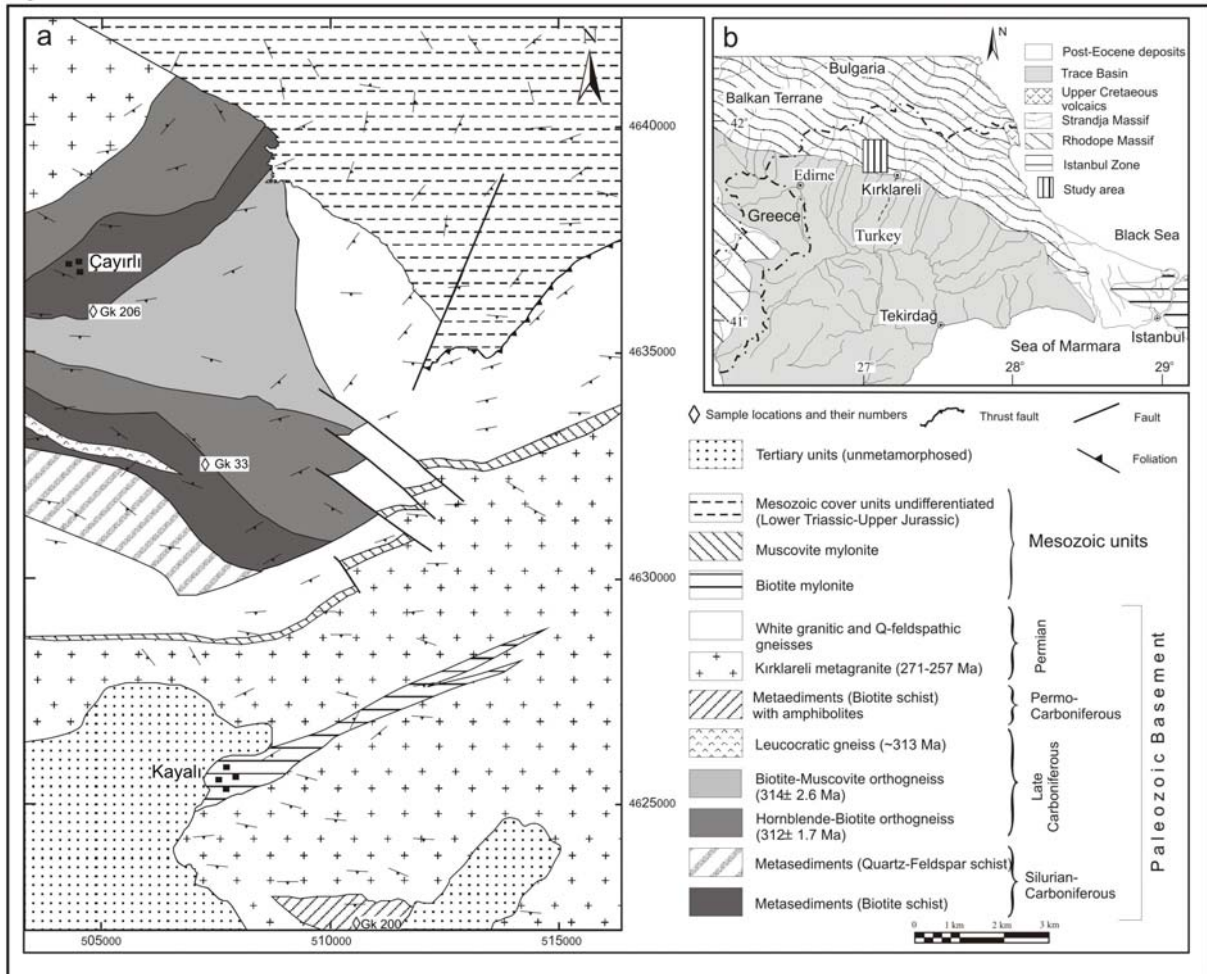


Fig. 2

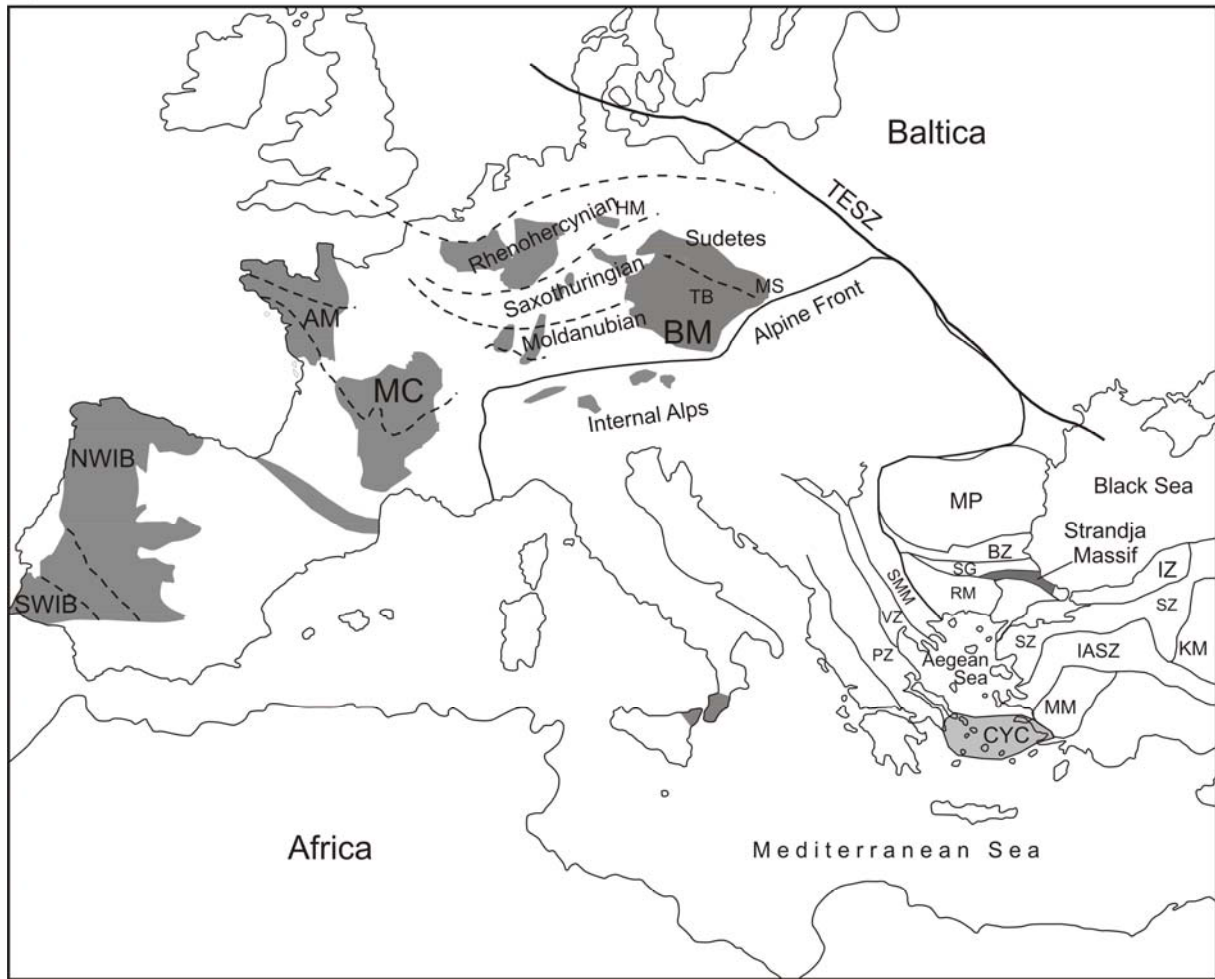




Fig. 3

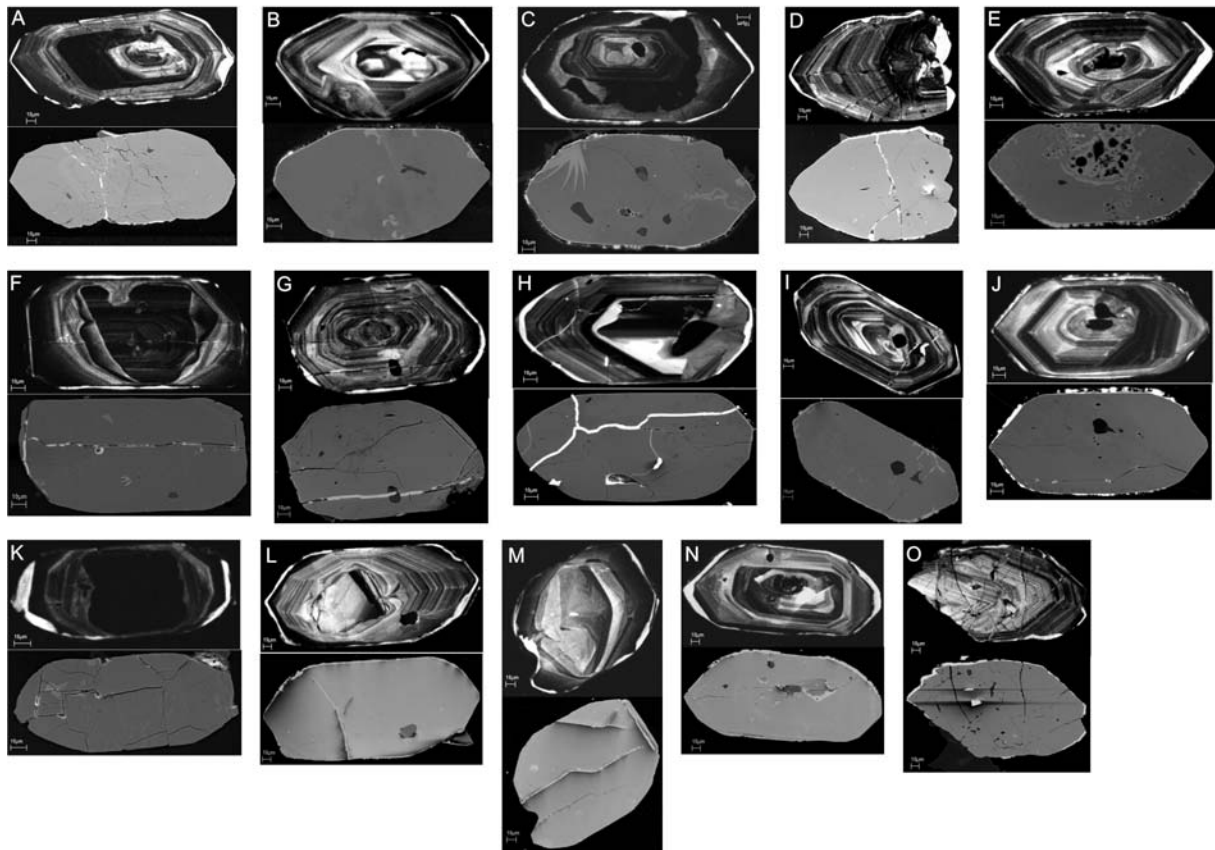


Fig. 4

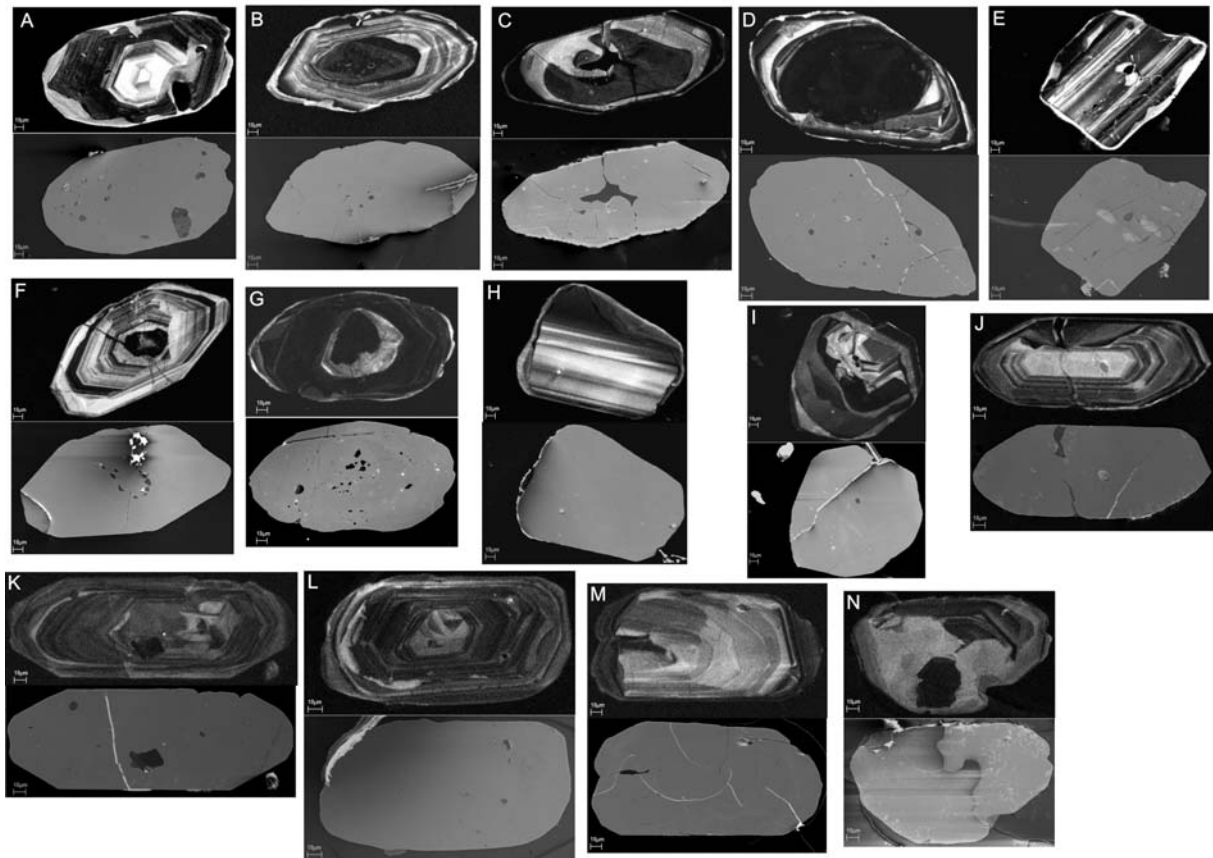


Fig. 5

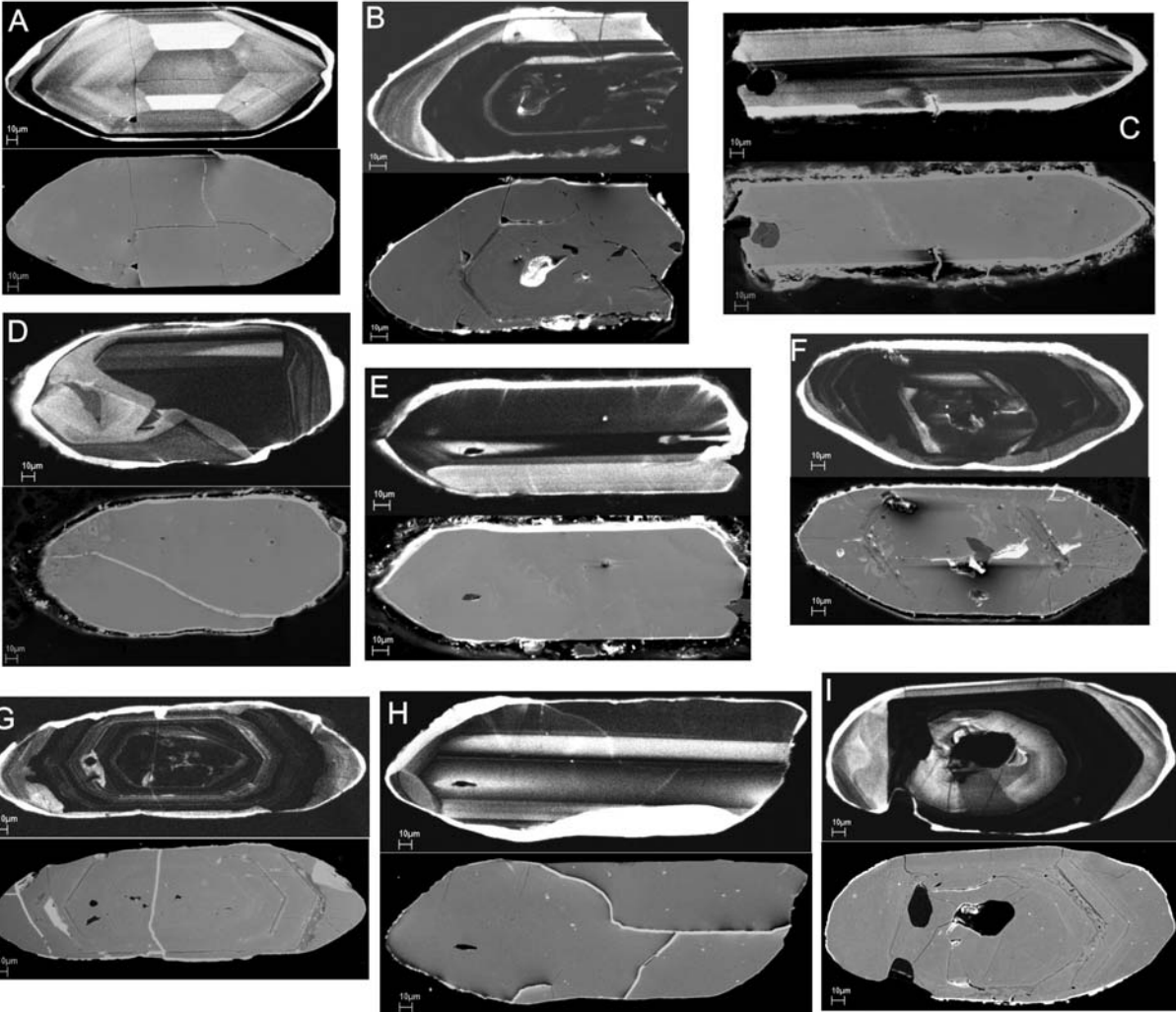


Fig. 6

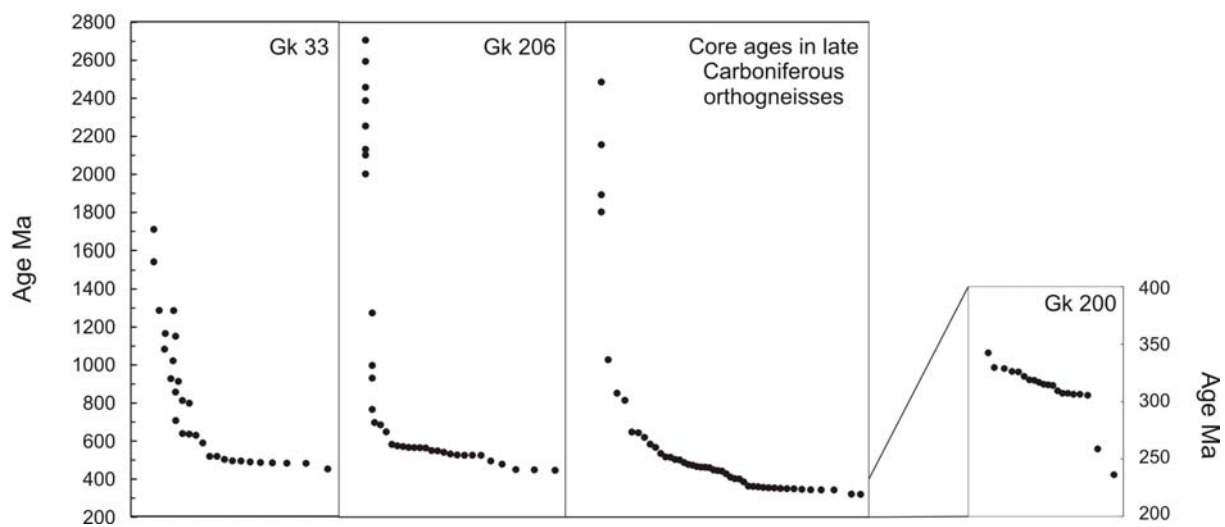


Fig. 7

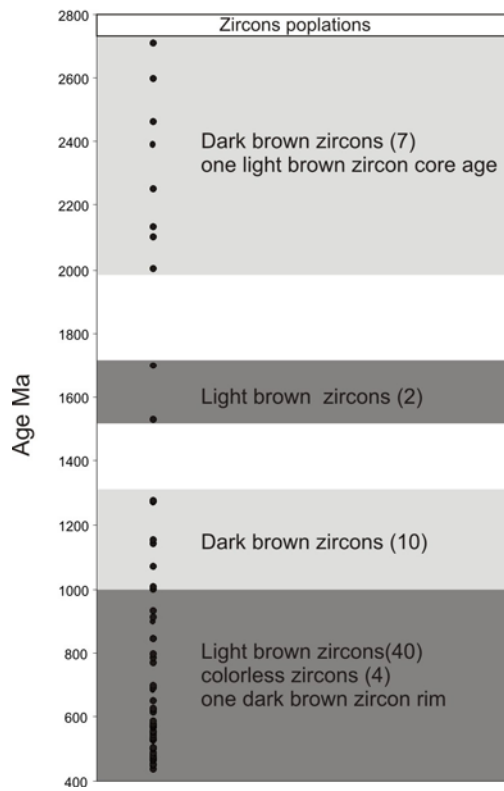


Fig. 8

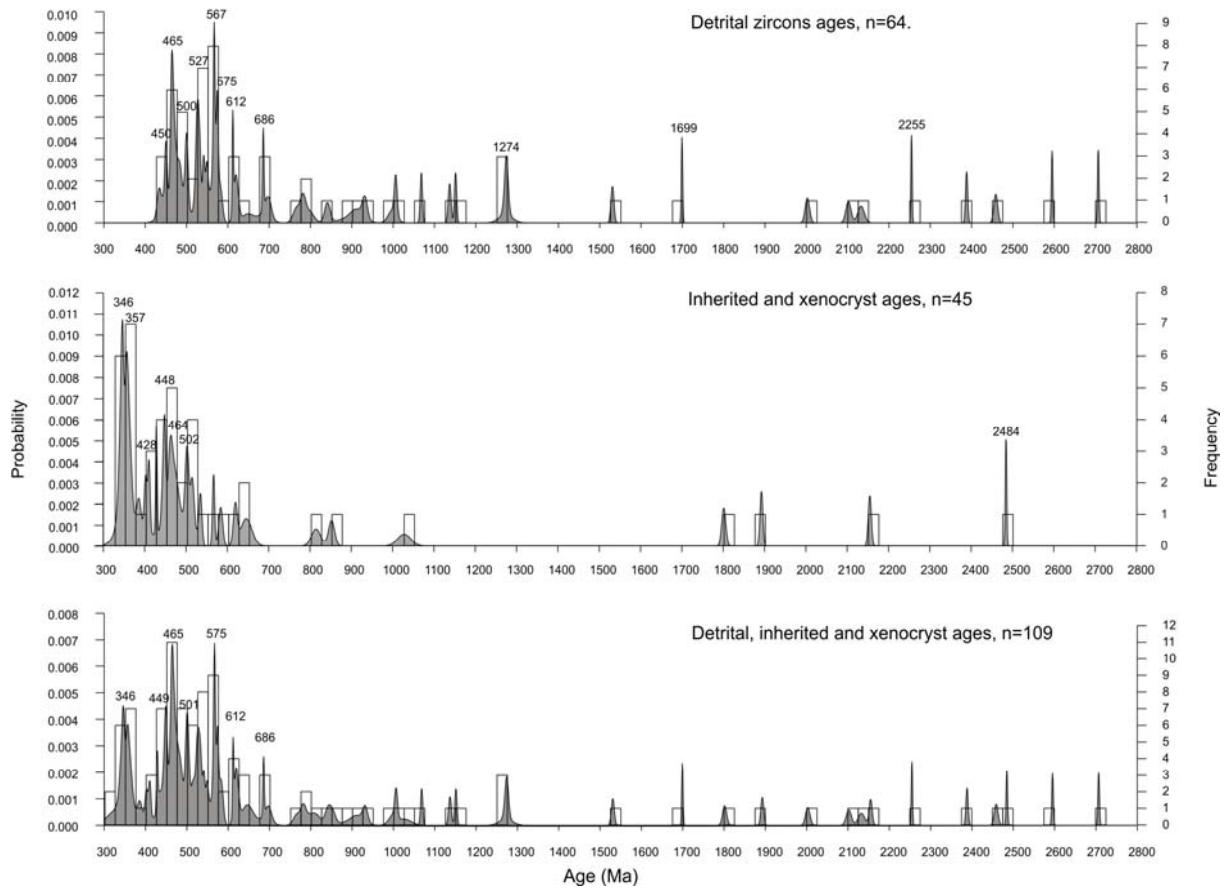
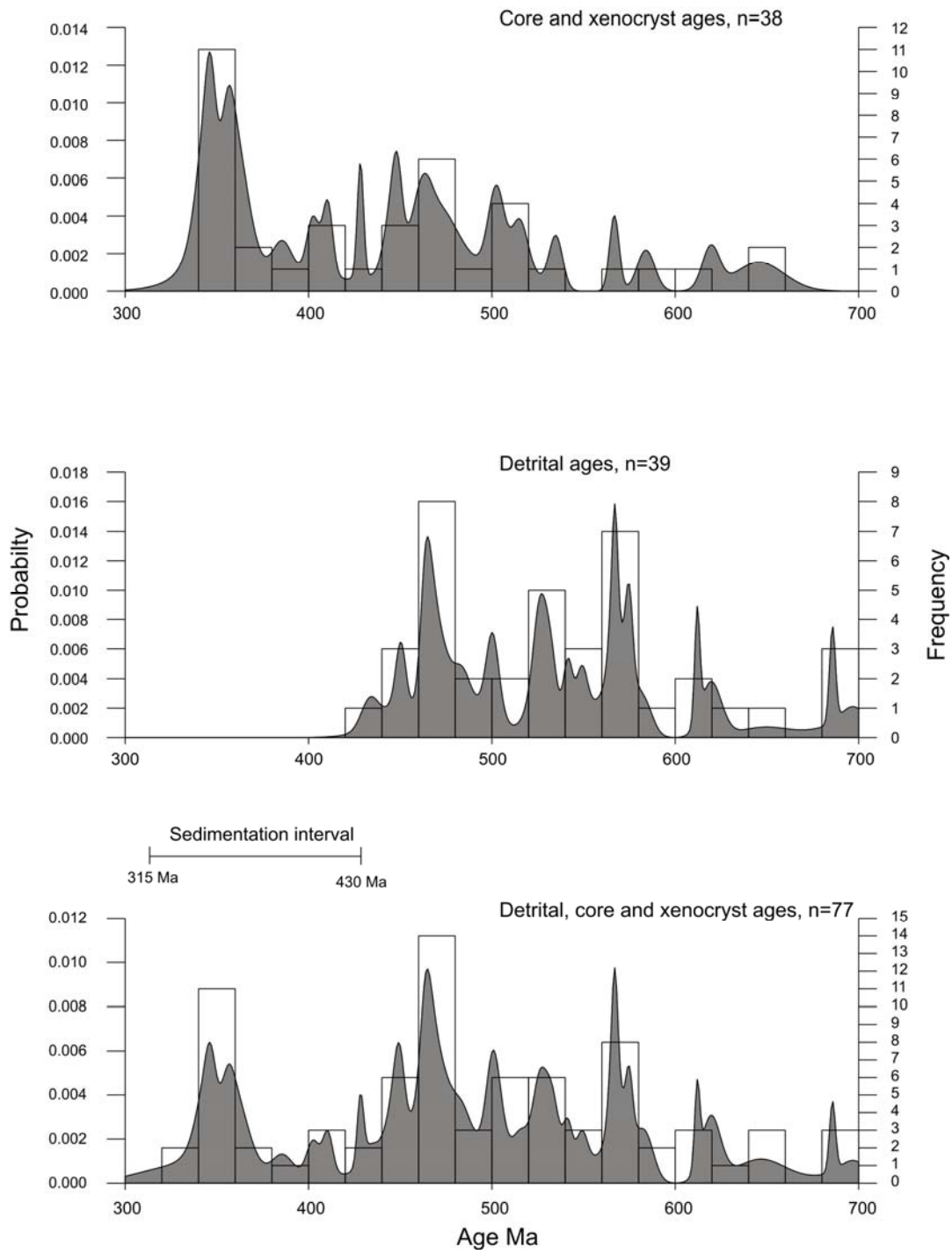
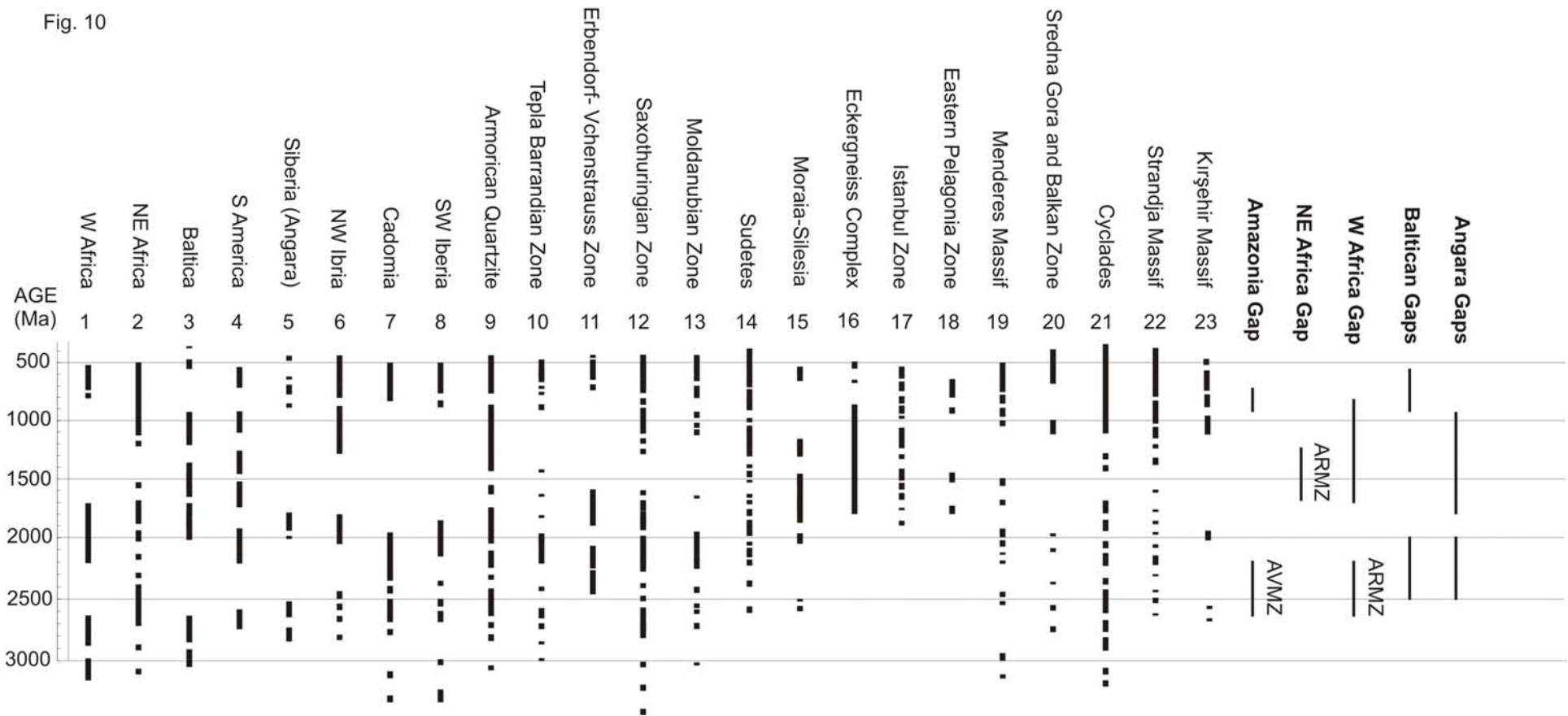


Fig. 9







### **Chapter 3: Diachronous metamorphism and exhumation in a contractional orogen: the Strandja Massif, NW Turkey**

G. Sunal\*<sup>ab</sup>, M. Satır<sup>a</sup>, B. A. Natal'in<sup>b</sup>, G. Topuz<sup>c</sup>, O. Vonderschmidt<sup>a</sup>

<sup>a</sup>Universität Tübingen, Institut für Geowissenschaften, Wilhelmstrasse 56, D-72074 Tübingen, Germany

<sup>b</sup>İstanbul Teknik Üniversitesi, Jeoloji Mühendisliği Bölümü, TR-34469 Maslak, Istanbul, Turkey

<sup>c</sup>İstanbul Teknik Üniversitesi, Avrasya Yerbilimleri Enstitüsü, TR-34469 Maslak, Istanbul, Turkey

\* Corresponding Author

Submitted to the Journal of Geology on 11<sup>th</sup> November 2008

Idea:	50%
Problem:	50%
Production of Data:	40%
Evaluation and Interpretation:	60%
Preparation of the manuscript:	50%

## **Abstract**

The southern part of the Strandja Massif, northern Thrace, Turkey, comprises a basement of various gneisses, micaschists and rare amphibolite, and a cover of metaconglomerate and metasandstone, separated from each other by a pre-metamorphic unconformity. Metamorphic grade decreases from the epidote-amphibolite facies in the south to the albite-epidote amphibolite/greenschist-facies transition in the north. Estimated  $P$ - $T$  conditions are 485-530 °C and 0.60-0.80 GPa in the epidote-amphibolite facies domain, and ~450-500 °C in transitional domain. Rb-Sr muscovite ages decrease systematically northwards from 162 to 142 Ma, and are extraordinarily old (279-296 Ma) in the northernmost part. The Rb-Sr biotite ages also decrease systematically from 153 Ma in the south to 134 in the north. These age values in conjunction with the attained temperatures suggest that both the metamorphism and exhumation occurred diachronously, and Rb-Sr muscovite ages were not reset during the metamorphism in the northernmost part. Structural features such as (i) consistent south-dipping foliation and southwest to southeast-plunging stretching lineation, (ii) top to north shear sense, and (iii) north-vergent ductile shear zones and brittle thrusts suggest a north-vergent compressional deformation coupled with exhumation. We tentatively ascribe this diachronous metamorphism and following exhumation to the northward propagation of a thrust slice. The compressional events in the Strandja Massif were most probably related to the coeval north-vergent subduction/collision system in the southerly lying Rhodope Massif.

**Key-words:**  $P$ - $T$  estimates, Rb-Sr dating, diachronous metamorphism and cooling, compressional exhumation, Strandja Massif, Turkey

## **Introduction**

Exhumation of metamorphic areas requires a vertical movement of deeply buried rock assemblages, which at least to a certain extent is associated with the removal of the overburden (e.g. England and Molnar 1990). Tectonic processes and erosion present two not mutually exclusive end-members of the exhumation. Among the tectonic processes, extension (e.g. normal faulting, detachments and ductile thinning) is frequently regarded as the main process, which accommodates main vertical displacement of the deeply buried material (Ring et al. 1999 and the references therein). Compression in form of thrusting and large-scale folding usually gives rise to crustal thickening. In compressional systems, focused denudation (erosion) and mid-crustal channel flow represent the main agents of exhumation (e.g. Godin et al. 2006). Determination of the exhumation mechanism entails a combination of detailed regional structural, petrological and geochronological data.

In this paper we present new structural, petrological and geochronological data on the metamorphic evolution of the Strandja Massif, NW Turkey. Our results indicate that the metamorphism and following exhumation in the Strandja Massif occurred diachronously in response to a north-vergent compressional deformation, starting in the south and progressing to the north systematically.

## **Geological Setting & Field Relations**

The Strandja Massif is a NW-SE trending metamorphic belt, ~300 km long and ~100 km wide, unconformably overlain by either unmetamorphosed Upper Cretaceous volcanic and volcano-clastic rocks to the north or by an Eocene-Oligocene sequence of limestone, sandstone and shale to the south (Fig. 1). To date, three tectonostratigraphic units are differentiated in the Strandja Massif: (i) a Paleozoic basement comprising micaschist and various types of orthogneiss and amphibolite (Aydın 1974 & 1982; Okay et al. 2001; Natal'in et al. 2005 a and b; Sunal et al. 2006, 2008) (ii) a lower to middle Triassic to middle Jurassic

cover sequence (Chatalov 1991; Toraman 2002) consisting of metaconglomerate, metasandstone, phyllite, calc-phyllite and marble (Okay et al. 2001; Hagdorn and Gönçüoğlu 2007) and (iii) an allochthonous unit of Triassic metasedimentary and metavolcanic rocks which was thrust onto the former two units (e.g. Chatalov 1991; Gerdjikov 2005).

The Strandja Massif underwent greenschist- to lower amphibolite metamorphism during the Late Jurassic (Aydm 1982; Okay et al. 2001; Lilov et al. 2004; Natal'in et al. 2005 a and b). Furthermore, the Paleozoic basement rock association of the Strandja Massif was involved in a pre-Triassic regional metamorphic event, which is deduced from (i) a discordance between the internal foliation of metagranite clasts and that of the matrix of the basal metaconglomerate of the cover sequence (Toraman 2002; Gerdjikov 2005; Natal'in et al. 2005 a and b), (ii) the presence of two distinct foliations in pre-Permian orthogneisses (Natal'in et al. 2005 a and b), and (iii) the presence of a migmatitic gneiss with a Pb-Pb zircon evaporation age of  $285 \pm 13$  Ma (Okay et al. 2001). The metamorphic grade of the older pre-Triassic metamorphism is not constrained.

We studied a 15 km by 20 km area on the southern margin of the Strandja Massif where the pre-Triassic basement and the Triassic cover sequence, are exposed (figs. 1 and 2). The pre-Triassic basement is represented by various types of strongly- to weakly foliated metagranites, orthogneisses, micaschists and amphibolites, while the Triassic cover sequence consist of a metasedimentary series starting with metaconglomerates and passing into metasandstones.

The metagranites and orthogneisses comprise the Kirklareli metagranite, leucocratic metagranite, hornblende-biotite orthogneiss, biotite-muscovite orthogneiss and leucocratic orthogneiss. Intrusive contacts and up to 2 m. thick mafic microgranular enclaves are still recognizable in the Kirklareli metagranite and hornblende-biotite orthogneiss. The Kirklareli metagranite is pinkish grey and displays an augen gneiss structure defined by K-feldspar and

locally plagioclase porphyroclasts in a relatively fine-grained matrix. The leucocratic metagranite differs from the Kırklareli metagranite by its leucocratic and fine-grained nature. The hornblende-biotite orthogneiss is greenish dark grey and has an equigranular texture. The biotite-muscovite orthogneiss has a fine-grained equigranular texture. The leucocratic orthogneiss occurs as 0.5 to 25 m-thick dikes in the hornblende-biotite, biotite-muscovite and biotite schists. The Pb-Pb evaporation ages of relict igneous zircons yielded ages ranging from 315 to 256 Ma, testifying the presence of the Late Carboniferous to Permian magmatic activity in the Strandja Massif (Okay et al. 2001; Natal'in et al. 2005 a and b ; Sunal et al. 2006).

The micaschists are of two types: Type-1 is represented by garnet biotite schists, type-2 by biotite schists. Type-1 is exposed in the middle part of the study area and is of sedimentary origin as testified by detrital zircons with Pb-Pb evaporation ages of 460 to 2700 Ma (Sunal et al. 2008). Type-2 is associated with the well-foliated amphibolites and exposed in the southernmost part of the study area (fig. 2).

The metaconglomerate of the cover sequence comprises stretched and elongated gravels of orthogneiss and quartzite, ranging from 1 to 30 cm in size in a well-foliated matrix. Some orthogneiss clasts in the metaconglomerate contain an old foliation which is discordant to the matrix foliation, suggesting derivation from a pre-Triassic metamorphic domain (Toraman 2002; Gerdjikov 2005; Natal'in et al. 2005 a and b). The metasandstones are characterized by a fine grain size ( $\varnothing \sim 1$  mm) and a greenish color. Bedding and cross-bedding are locally recognizable.

The foliation generally strikes in an E-W direction, dipping at 20-60° to the south, and commonly crosscuts the lithological boundaries (fig. 2) (Natal'in et al. 2005 a). However, local bending of the foliation occurs due to folding. The stretching lineation dips on average to the south at 10 to 60°. The orthogneisses are dissected by two mylonite zones: One is

approximately 400 m-thick and 5-km-long, and is represented by biotite mylonites in the Kırklareli metagranite (fig. 2). The second one is represented by ~100 m thick and ~15 km long muscovite mylonite and defines the northern lithological boundary of the Kırklareli metagranite (fig. 2; Natal'in et al. 2005a). Kinematic criteria such as oblique foliation, mantled porphyroclasts and (S-C) structures consistently indicate top to the north shear sense. Moreover, east of the study area, a large thrust slice consisting of basement orthogneisses was mapped lying along a shear zone with north-south lineation over the Triassic cover rocks (Okay et al. 2001; Natal'in et al. 2005a, b), which indicates that the shear zone in the region studied is also of contractional nature. North-vergent deformation has also been described from the other parts of the Strandja Massif (Çağlayan et al. 1988; Okay et al. 2001; Gerdjikov 2005).

### **Analytical Techniques**

Mineral analyses were performed at Heidelberg University using a CAMECA SX-51 microprobe equipped with five wavelength-dispersive spectrometers and an additional Si-Li detector (Oxford Instruments). Operating conditions were 15 kV accelerating voltage and 20 nA beam current. Counting times were usually 10 s except for Mg, Ca, Al (20 s) and Ti (30 s) in spinel. Beam diameter was usually ~1  $\mu\text{m}$  except for feldspar analyses which were performed with a defocused beam (5–10  $\mu\text{m}$ ). Raw data were corrected for matrix effects with the help of the PAP algorithm (Pouchou and Pichoir 1984, 1985) implemented by CAMECA. Synthetic and natural standards were used for calibration before each measurement session. Detection limits are generally on the order of 0.1 wt% of the element under consideration.

Mineral separation (biotite, muscovite) were carried out using conventional techniques including crushing, sieving, magnetic separator and heavy liquids. Rb-Sr isotopic analyses were performed with a FINNIGAN MAT-262 multicollector mass spectrometer in Tübingen. Rb and Sr contents of whole rocks were determined by XRF, using lithium borate fusion discs

with an accuracy better than 2%. Rb and Sr concentrations of mineral separates were determined by isotopic dilution. Sr and light rare-earth elements were isolated on quartz columns by conventional ion exchange chromatography with a 5 ml resin bed of Bio Rad AG 50W-X12, 200–400 mesh. Sr was loaded with a Ta-HF activator on preconditioned W filaments and was measured in single-filament mode. Analyses of 28 separate loads of the NBS987 Sr standard yielded  $^{87}\text{Sr}/^{86}\text{Sr}$  ratio of  $0.710259 \pm 0.000012$ . Total procedural blanks were  $<200$  pg for Sr was loaded with a Si-gel onto a pre-conditioned Re filament and measured at  $\sim 1,300$  °C in single-filament mode. Age determinations are based on  $^{87}\text{Rb}$  decay constant of  $1.42 \times 10^{-11}$  /yr (Steiger and Jäger 1977). Fractionation was corrected by normalizing the  $^{86}\text{Sr}/^{88}\text{Sr}$  ratios to 0.1194. The input errors for age computations are 1% ( $2\sigma$ ) for  $^{87}\text{Rb}/^{86}\text{Sr}$  ratios and 0.003% ( $2\sigma$ ) for  $^{87}\text{Sr}/^{86}\text{Sr}$  ratios. Rb–Sr age calculations were performed using the Isoplot 3.0 program produced by Ludwig (2003).

### **Petrography & Mineral Compositions**

Estimated modal abundances of the investigated samples are summarized in Table 1 and mineral compositions are listed in Tables 2-5, and are shown in figs. 4-5.

The *Kırklareli metagranite* consists of muscovite, biotite, microperthitic microcline, plagioclase, quartz, and accessory epidote, zircon, apatite, titanite and magnetite. Foliation is defined by the parallel elongation of biotite and muscovite. Both microperthitic microcline ( $X_{\text{Or}} \sim 0.94-0.98$ ) and plagioclase ( $\text{An}_{2-35}$ ) locally form porphyroclasts, representing mostly igneous relics (figs. 3c-d and 4a). Myrmekites are common. Muscovites display Si contents of 3.20-3.40 cations pro 11-oxygens (fig. 4c).  $X_{\text{Mg}}$  values of biotites show a large scatter from 0.47 to 0.70 (fig. 4b; Table 3). Epidotes are characterized by  $\text{Fe}^{3+}/(\text{Fe}^{3+}+\text{Al})$  of 0.20-0.31 (fig. 4d).

*Amphibolites* are usually well-foliated, and comprise hornblende, biotite ( $X_{Mg} \sim 0.52-0.57$ ), plagioclase ( $An_{23-34}$ ), chlorite ( $X_{Mg} \sim 0.55-0.62$ ), epidote and variable amounts of quartz. Some of the plagioclase grains contain relic cores with  $An_{13-14}$ , coinciding with the peristerite gap. With increase in the amount of quartz they grade into amphibole-bearing biotite gneisses. Rutile, apatite, titanite and ilmenite form accessory phases. Epidote occurs both as inclusion in hornblende and as discrete grains in the matrix, and displays  $X_{Fe3}$  values of 0.17-0.27 (fig. 4d). Hornblendes are characterized by tschermakitic compositions with  $X_{Mg}$  of 0.48-0.62 (fig. 5; Table 5), are compositionally zoned (fig. 4a), whereby Si, Mg and Ca decrease, and Al, Fe and Na increase towards the rim (Table 5).

*Garnet-biotite schists* (Type-1) include biotite, plagioclase ( $An_{22-39}$ ), epidote, quartz, garnet and accessory zircon, ilmenite and apatite. Modal abundance of epidote is variable (Table 1). Garnet occurs as small sub- to idioblastic grains with very few or no inclusions (50-300  $\mu m$ ; fig. 3b). They show a compositional range  $Alm_{57-74}Pyp_{6-11}Grs_{22-3}Sps_{24-12}$  (Table 4). All the garnet grains in the sample 206 have a Fe-Mg-rich core and a Ca-rich and Fe-Mg-poor overgrowth, separated from each other by a compositional jump (fig. 6). Mn in both domains increases rimwards. This compositional feature is characteristic of diffusion-controlled zoning. Similar compositional jumps in garnets were ascribed either to polymetamorphism (e.g. Jeřábek et al. 2008) or fractionation and different garnet-forming reactions during the metamorphic cycle (e.g. Konrad-Schmolke et al. 2008). Both garnet domains are inclusion-free, hindering any inference on the associated mineral phases during the growth of each garnet domain. Epidote is characterized by  $X_{Fe3+}$  values of 0.14-0.26, and some have REE-richer cores (up to 5 wt %). Ilmenite occurs both as inclusions in garnet and as discrete grains in the matrix, and in both cases display elevated MnO contents (2 and 3 wt%).

*Metasandstone* comprises muscovite-phengite, quartz, albite ( $An_{0-2}$ ), calcite, K-feldspar ( $X_{Or} \sim 0.95-0.96$ ), biotite ( $X_{Mg} \sim 0.72-0.74$ ;  $Ti \sim 0.12-0.16$  c.p.f.u.) and accessory apatite, zircon



and titanite. Albite displays multiple twinning and locally forms large grains. Large grains of muscovite form bent and kinked crystals, and are relict detritic grains (fig. 3e), displaying Si contents of 3.0-3.15 cations pro 11-oxygens. However, finer-grained muscovites are represented by phengites (Si= 3.25-3.45 cations pro 11-oxygens), defining the foliation, and locally have relic muscovite cores (figs. 3e and f).

### **Metamorphic Conditions**

On the basis of the arguments outlined above, it was suggested that portions of the basement sequence were subjected to a pre-Triassic metamorphism during the early Permian (Okay et al. 2001; Natal'in et al. 2005a). Apart from the relict igneous phases in the Kirklareli metagranite and garnet with core and overgrowth domains separated by a compositional jump in garnet-biotite schist, we did not observe any obvious distinct mineral assemblages in the basement sequence which can be clearly ascribed to former pre-Triassic metamorphism. Hence the P-T conditions derived from the documented mineral assemblages refer to the latest metamorphism.

### *Metamorphic facies*

The metamorphic mineral assemblages in the amphibolites and orthogneisses (pre-Triassic basement) are characterized by the stable coexistence of “plagioclase (An<sub>17-35</sub>) + epidote ± hornblende ± quartz”, suggestive of epidote-amphibolite-facies conditions (e.g. Miyashiro 1993, p. 280-287). In these rock types, the metamorphic plagioclases are represented by An<sub>17-35</sub>, suggesting that the metamorphic conditions exceeded the peristerite gap (Laird 1982; Maruyama et al. 1982). However, the metasandstone sample GK304 (Triassic cover) comprises the mineral assemblage “biotite + muscovite + K-feldspar + albite + quartz + calcite”, suggesting that the peristerite gap was not crossed. The sample NK86-2 from the

basement contains both albite ( $An_{0-4}$ ) and oligoclase ( $An_{\geq 16}$ ), and should be regarded as transitional over the peristerite gap. This mineral assemblage “biotite + muscovite + K-feldspar + albite + quartz + calcite” can occur in the greenschist or albite-epidote amphibolite facies, a transitional facies between greenschist- and epidote-amphibolite-facies (e.g. Maruyama et al. 1983; Topuz et al. 2004). These features suggest that the metamorphic grade decrease northwards. However, absence of metabasic lithologies in the northern part hampers any deduction on whether the northern part is of greenschist-facies or albite-epidote-amphibolite facies. Northward decrease of metamorphic grade and consistent south-dipping foliation suggest an inverse metamorphic field gradient.

#### *P-T Estimates*

In general, the mineral assemblages documented are not very suitable to place “tight” constraints on the *P-T* conditions. However, some constraints on the *P-T* conditions could be placed from the mineral assemblages in the garnet-biotite schist (sample 206) and amphibolite (samples 200 & 203). Metamorphic temperatures are estimated by garnet-biotite and hornblende-plagioclase thermometry, metamorphic pressures by garnet-biotite-plagioclase-quartz barometry. Compositions of the matrix biotites and garnet rims are used, because the garnet core domains are not in equilibrium with the matrix assemblages, and we do not have any constraint on the mineral assemblage present during the growth of garnet cores. Garnet-biotite thermometry according to the formulation of Ferry and Spear (1978) together with the garnet solution model after Berman (1990) yields 485-530 °C, the garnet-biotite-plagioclase-quartz barometry after Hoisch (1991 and 1992) gives 0.6-0.8 GPa (fig. 7). Hornblende-plagioclase thermometry after Spear (1980 and 1981) for the compositions of the adjacent hornblende-plagioclase compositions consistently yields temperatures of 520-540 °C, what is in agreement with the garnet-biotite temperatures (fig. 8).

The metasediments (e.g. sample GK304) contain a high-variance mineral assemblage “biotite + muscovite + K-feldspar + albite + quartz + calcite”. The P-T conditions for the northernmost domain are poorly defined. Based on the presence of un-crossed nature of peristerite gap and presence of biotite, we tentatively infer that the metamorphic temperatures were slightly lower (~450 °C). Newly formed white micas (phengites) have Si contents between 3.25 and 3.45 cations pro 11-oxygens, corresponding to pressures of 0.5-0.7 GPa at the assumed temperature of 450 °C (Massonne and Schreyer 1987).

To summarize, the P-T conditions are ~485-540 °C and 0.6-0.8 GPa in the south, and slightly lower in the northern part.

### **Geochronology**

To constrain the timing and cooling of low to medium-grade metamorphism, Rb-Sr biotite and muscovite-whole rock dating were performed on 21 samples distributed over the whole area (fig. 2). Analytical data are listed in Table 7. Pb-Pb zircon evaporation data on the orthogneisses on the same rock types revealed that their igneous protoliths were formed between 315 and 256 Ma (Okay et al. 2001; Natal'in et al. 2005 a; Sunal et al. 2006); and the micaschists contain detrital zircons with age intervals of 430-2700 Ma (garnet-biotite schist) and 300-350 Ma (biotite schist). CL images revealed the presence of small metamorphic overgrowths on the zircons which however could not be dated by Pb-Pb evaporation method (Sunal et al. 2008). On the other hand, the Rb-Sr systematics on biotite and muscovite should refer to the latest metamorphic event in the Strandja Massif.

The Rb-Sr biotite ages range from ~153 Ma in the south to ~134 Ma in the north (fig. 9). Likewise, muscovite ages decrease northwards, from 157-162 to 144-149 Ma. However, the muscovites from the northernmost low-grade portion yielded considerably older age values between 279 and 295 Ma. Given the small uncertainties in the age values (up to 3 Ma, 2 $\sigma$ )

and identical grain size (125-180  $\mu\text{m}$ ) of the dated fractions, we regard these differences to be geologically significant.

Closure temperatures of muscovite and biotite for Sr-diffusion are estimated to be around  $500 \pm 50$  and  $300 \pm 50$   $^{\circ}\text{C}$ , respectively (Purdy and Jäger 1976; Cliff 1985; Blankenburg et al. 1989). The southern part of the area was subjected to temperatures of 485-530 $^{\circ}\text{C}$ , and the northernmost part to  $\sim 450$   $^{\circ}\text{C}$ . Hence the muscovite ages should be regarded as the age of the medium grade metamorphism. The unusually old muscovite ages, 279-296 Ma, should be interpreted as mixed ages (igneous and latest metamorphism), because the dated samples contains both relict igneous muscovite and metamorphic phengite, and the metamorphic temperatures attained ( $\sim 450$   $^{\circ}\text{C}$ ) were near the lower limit of the closure temperature of muscovite for Sr diffusion. The distribution of biotite ages suggests that the southern part cooled 20 Ma before the northern part. The difference between age values of muscovite and biotite in the same rocks is in the order of 7 to 9 Ma, resulting in the cooling rates of 22-29  $^{\circ}\text{C}/\text{Ma}$ .

To summarize, both the metamorphism and cooling in this part of the Strandja Massif were diachronous, starting in the south and progressing to the north. These Rb-Sr mica ages (apart from those of unusually old “mixed” ones) are indistinguishable from the previously published scarce K-Ar biotite and Rb-Sr biotite ages (Aydın 1974, 1982; Okay et al. 2001; Lilov and Maliakov 2001; Lilov et al. 2004).

## **Discussion**

As described above, the basement sequence comprises various types of orthogneisses which intruded into metasedimentary rocks, whereas middle to late Triassic metaclastic cover sequences are of epiclastic nature. Both the basement and cover sequences are devoid of any oceanic crustal lithologies. On the basis of the overall absence of the oceanic crustal

assemblages and high-pressure metamorphism, we infer that these rock assemblages in this part of the Strandja Massif were not involved in any subduction process. However, an allochthonous Triassic sequence which was described by Chatalov (1991) and not observed in the studied part of the Strandja Massif, comprise greenschist-facies phyllite and metabasite. This unit was formerly interpreted as accretionary complex (e.g. Şengör et al. 1984).

Both the metamorphism and subsequent cooling display significant diachronism, suggesting that the burial and exhumation are asymmetric, and the tectonic event controlling the metamorphism and cooling/exhumation propagated northward between the late Jurassic and early Cretaceous. The present separation (15-20 km) and age difference (~20 Ma) between the northern and southern parts suggest an average cooling propagation rate of 0.75-1 km/Ma. Diachronous cooling was described from different tectonic settings such as compressional (e.g. Boyle et al. 1994; Dallmeyer et al. 1997; Crowley & Parrish 1999; Gray et al. 2006; Tricart et al. 2007; Jeřábek et al. 2008), extensional (e.g. Holm & Dokka 1993; Bertrand et al. 2001) and transpressional segments of strike-slip systems (Morillon et al. 2000; Koons et al. 2003). All these tectonic regimes have the asymmetry in common. In case of the Strandja Massif, compression led to overturned folding and thrusting, deduced from (i) the occurrence of the cover sequence beneath the basement (fig. 9, Okay et al., 2001), (ii) an inverse metamorphic gradient, and (iii) top-to-the north ductile shear zones (Natal'in et al. 2005 a and b).

During the metamorphism the Strandja Massif was buried to depths of 22-29 km. The oldest non-metamorphic rocks unconformably resting on the Strandja Massif are represented by earliest Late Cretaceous sandstones (Cenomanian, ~95 Ma, Okay et al. 2001; Türkecan and Yurtsever 2002) on the northern flank and Eocene-Oligocene sequence of limestone, sandstone and shale on the southern flank (Çağlayan et al 1998). This suggests that at least parts of the Strandja Massif were at the Earth's surface earlier than 95 Ma. Compression

generally results in crustal thickening. Mid- to lower crustal channel flow of the partially molten rocks and extrusion which is suggested to be a significant exhumation agent in the Himalayas (Godin et al. 2006; Jessup et al. 2006; Searle et al. 2008) are ruled out in case of the Strandja Massif. No partially molten domain in form of late Jurassic-early Cretaceous migmatites is described so far. We therefore think that the exhumation mechanism was probably erosion. During the early Cretaceous, a nearly E-W trending depositional trough (basin) was present on the Balkan, Mosean and parts of the Srednogora zone (Minkowska et al. 2002; fig. 1). The southern margin of this basin is represented mainly by up to 4000 m thick flysch-type coarse siliciclastics, while the northern margin is made up of a considerably wider shallow water carbonate platform. This suggests significant clastic input from the south, namely from the Strandja and parts of Rhodopes.

The Rhodopes, Circum-Rhodop Belt and small metamorphic domains in southern Thrace and Biga Peninsula are located to the south of the Strandja Massif (fig. 1). In contrast to the Strandja Massif, these metamorphic domains have locally rock assemblages that suggest involvement in accretion and subduction events (e.g. Okay & Satir 2000; Mposkos and Krohe 2006; Bonev et al. 2006; Turpaud 2006; Bauer et al. 2007; Topuz et al. 2008). The timing of the high-P/T metamorphism in southern Thrace and the Biga Peninsula is late Cretaceous (Okay & Satir 2000; Topuz et al. 2008). Recent geochronological data consistently suggest the timing of high to ultrahigh-pressure metamorphism in the Rhodopes occurred at  $\geq 160$  Ma (e.g. Mposkos and Krohe 2006; Bauer et al. 2007), indicative of coeval nature of subduction in the Rhodopes and metamorphism in the Strandja Massif. The compressional deformation in the Strandja Massif was probably related to the subduction and accretion events in the Rhodopes. However, the relationship between the Strandja and Rhodope Massifs is not known during the late Jurassic to early Cretaceous interval. In the Bulgaria, a pronounced right-lateral strike-slip fault, the Maritsa fault (MFZ, fig. 1), with an

offset of over 100 km occurs between these two metamorphic domains (Burg et al. 1996; Ivanov 2000). The elongation of the Maritsa fault into Turkey is concealed in the Miocene-Pliocene sedimentary rocks of the Thrace basin (c.f. Perinçek 1991; Yaltrak et al. 2002).

## **Conclusions**

The southern part of the Strandja Massif, NW Turkey, comprises a basement of various orthogneisses, micaschists and amphibolites, and an epiclastic cover of metaconglomerate and metasandstone. Both sequences underwent a transitional greenschist to epidote amphibolite-facies metamorphism during late Jurassic to early Cretaceous. This metamorphism and subsequent cooling occurred diachronously in a compressional regime, starting in the south and progressing to the north. The compressional regime probably resulted from thrusting and overturned folding, and was ultimately related to the coeval subduction and collision events in the southerly Rhodope Massif.

## **Acknowledgements**

This paper forms a part of the PhD thesis of G. Sunal at the university of Tübingen. Field work and travel expenses are funded by ITU Research fond (#11-07-128) and IGCP-480 project. Helps of G. Bartholomä during mineral separation, W. Siebel and E. Reitter during isotopic measurements are gratefully appreciated. Early drafts of the manuscript were reviewed by A.I. Okay, P. Bons and W. Siebel which led to considerable improvement of the ideas. We thank R. Altherr for friendly access to electron microprobe facility in Heidelberg.

## **References**

Aydın, Y. 1974. Etude petrographique et geochemique de la partie centrale du Massif d'Istranca (Turquie), PhD Thesis, University of Nancy.

- Aydın, Y. 1982. Geology of the Yıldız (Istranca) Mountains. Habilitation thesis, Istanbul Technical University, İstanbul. 106 pp.
- Baker, A. J. 1990. Introduction to metamorphic textures and microstructures. Blackie, New York, 162 pp.
- Bauer, C.; Rubatto, D.; Krenn, K.; Proyer, A.; Hoinkes, G. 2007. A zircon study from the Rhodope Metamorphic Complex, N-Greece: time record of a multistage evolution. *Lithos*. 99:207-228.
- Berman, R. G. 1990. Mixing properties of Ca-Mg-Fe-Mn garnets. *Am Mineral*. 75: 328-344.
- Bertrand, G.; Rangin, C.; Maluski, H.; Bellon, H. 2001. Diachronous cooling along the Mogok Metamorphic Belt (Shan Scarp, Myanmar): the trace of the northward migration of the Indian syntaxis. *J. Southeast Asian Earth Sci.* 1: 649–659.
- Blanckenburg, F. von; Villa I. M.; Baur, H.; Morteani, G.; Steiger R. H. 1989. Time calibration of a PT-path from the Western Tauern Window, Eastern Alps: the problem of closure temperatures. *Contrib Mineral Petrol*. 101: 1–11.
- Bonev, N.; Marchev, P.; Singer, B. 2006.  $^{40}\text{Ar}/^{39}\text{Ar}$  geochronology constraints on the Middle Tertiary basement extensional exhumation, and its relation to ore-forming and magmatic processes in the eastern Rhodope (Bulgaria). *Geodinamica Acta*. 19: 267-282.
- Boyle, A. P.; Burton, K. W.; Westhead, R. K. 1994. Diachronous burial and exhumation of a single tectonic unit during collision orogenesis (Sulitjelma, central Scandinavian Caledonides). *Geology*. 22: 1043-1046.
- Burg, J. P.; Ricou, L. E.; Ivanov, Z.; Godfriaux, I.; Dimov, D., and Klain, L. 1996. Syn-metamorphic nappe complex in the Rhodope Massif: Structure and kinematics. *Terra Nova*. 8: 6-15.



- Chatalov, A. G. 1991. Triassic in Bulgaria- a review, in Special issue on tectonics, In: JF Dewey (ed). Bull. of the Tech. Uni. of Istanbul. 44 (1-2): 103-135.
- Cliff, R. A. 1985. Isotopic dating in metamorphic belts. J Geol Soc Lond. 142: 97–110.
- Çağlayan, A. M.; Şengün, M., and Yurtsever, A. 1988. Main Fault systems shaping the Istranca Massif, Turkey: Journal of Pure and Applied Science, Series A, Geosciences. 21: 145–154.
- Crowley, J. L.; Parrish, R. R. 1999. U-Pb isotopic constraints on diachronous metamorphism in the northern Monashee complex, southern Canadian Cordillera. Journal of Metamorphic Geology. 17: 483-502
- Dallmeyer, R. D.; Martínez Catalán, J. R.; Arenas, R.; Gil Ibarguchi, J.I.; Gutiérrez Alonso, G.; Farias, P.; Bastida, F.; Aller, J. 1997. Diachronous Variscan tectonothermal activity in the NW Iberian Massif: Evidence from  $^{40}\text{Ar}/^{39}\text{Ar}$  dating of regional fabrics. Tectonophysics. 277: 307-337.
- England, P. C.; Molnar, P. 1990. Surface uplift, uplift of rocks, and exhumation of rocks. Geology. 18: 1173-1177.
- Ferry, J. M., and Spear, F. S. 1978. Experimental calibration of the partitioning of Fe and Mg between biotite and garnet. Contr. Mineral. Petrol. 66: 113-117.
- Gerdjikov, I. 2005. Alpine metamorphism and granitoid magmatism in the Strandja zone: new data from the Sakar unit, SE Bulgaria. Turkish J. Earth Sci. 14: 167-183.
- Godin, L.; Grujic, D.; Law, R. D.; Searle, M. P. 2006. Channel Flow, Ductile Extrusion, and Exhumation in Continental Collision Zones. Geol. Soc., Lond. Sp. Pub. 268: 269-292.
- Gray, D. R.; Foster, D. A.; Goscombec, B.; Passchier, C. W.; Trouwe, R. A. J. 2006.  $^{40}\text{Ar}/^{39}\text{Ar}$  thermochronology of the Pan-African Damara Orogen, Namibia, with implications for tectonothermal and geodynamic evolution. Precambrian Research. 150: 49–72.

- Hagdorn, H., and Göncüoğlu, M. C. 2007. Early-Middle Triassic echinoderm remains from the Istranca Massif, Turkey. *N. Jb. Geol. Paläont. Abh.* 246/2: 235–245.
- Hoisch, T. D. 1991. Equilibria within the mineral assemblage  $\text{anz} + \text{muscovite} + \text{biotite} + \text{garnet} + \text{plagioclase}$ , and implications for the mixing properties of octahedrally-coordinated cations in muscovite and biotite. *Contributions to Mineralogy and Petrology.* 108: 43-54.
- Hoisch, T. D. 1992. Thermodynamic properties of muscovite and biotite: inferences from natural compositions. *Trends in Mineralogy.* 1: 107-115.
- Holm, D.K., and Dokka, R.K. 1993. Interpretation and tectonic implications of cooling histories - an example from the Black Mountains, Death-Valley extended terrane, California. *Earth and Planetary Science Letters.* 116 (1-4): 63-80.
- Ivanov, Z. 2000. Tectonic position, structure and tectonic evolution of Rhodope massif. Guide to excursion ABCDGEODE 2000 Workshop, Borovets, Bulgaria, 1-6.
- Jeřábek, P.; Faryad, W. S.; Schulmann, K.; Lexa, O.; Tajčmanová, L. 2008. Alpine burial and heterogeneous exhumation of Variscan crust in the west Carpathians: insight from thermodynamic and argon diffusion modeling. *Journal of Geological Society, London.* 165: 479-498.
- Jessup, M. J.; Law, R. D.; Searle, M. P., & Hubbard, M. S. 2006. Structural evolution and vorticity of flow during extrusion and exhumation of the Greater Himalayan Slab, Mount Everest Massif, Tibet/Nepal: implications for orogen-scale flow partitioning. *In: Law, R. D.; Searle, M. P., & Godin, L. Eds. Channel Flow, Ductile Extrusion and Exhumation in Continental Collision Zones.* Geological Society, London, Special Publication. 268: 379–413.

- Konrad-Schmolke, M.; O'Brien, P. J.; de Capitani, C.; Carswell, D. A. 2008. Garnet growth at high- and ultra-high pressure conditions and the effect of element fractionation on mineral modes and composition. *Lithos.* 103: 309-332.
- Koons, P. O.; Norris, R. J.; Craw, D.; Cooper, A. F. 2003. Influence of exhumation on the structural evolution of transpressional plate boundaries: An example from the Southern Alps, New Zealand. *Geology.* 31: 3–6.
- Krogh, E. J.; Oh C. W.; Liou, J. G. 1994. Polyphase and anticlockwise P-T evolution for Franciscan eclogites and blueschists from Jenner, California, USA. *J Metamorph Geol.* 12:121–134.
- Laird, J. 1982. Amphiboles in metamorphosed basaltic rocks. In *Amphiboles. MSA Reviews in Mineralogy.* 9B: 113-158.
- Lilov, P. ; Maliakov, Y. 2001. Données de géochronologie isotopique sur les métadiabases du Strandja. *C.R. Acad. Bulg. Sci.* 54 (7): 67-70.
- Lilov, P.; Maliakov, Y.; Balogh, K. 2004. K-Ar dating of metamorphic rocks from Strandja massif, SE Bulgaria. *Bulgarian Academy of Sciences, Geochemistry, Mineralogy and Petrology.* 41: 107-120.
- Ludwig, K. R. 2003. *Isoplot 3.0, a geochronological toolkit for Microsoft Excel*, Berkeley Geochronology Center, Special Publication. No. 4.
- Maruyama, S.; Liou, J. G.; Suzuki, K. 1982. The peristerite gap in low-grade metamorphic rocks. *Contrib Mineral Petrol.* 81: 268-276.
- Maruyama, S.; Suzuki, K.; Liou, J. G. 1983. Greenschist-amphibolite transition equilibria at low pressures. *J Petrol.* 24: 583-604.
- Massonne, H. J.; Schreyer, W. 1987. Phengite geobarometry based on the limiting assemblage with K-feldspar, phlogopite, and quartz. *Contrib. Mineral. Petrol.* 96: 212-224.

- Minkovska, V.; Peybernès, B, Nikolov.; T. 2002. Palaeogeography and geodynamic evolution of the Balkanides and Moesian 'microplate' (Bulgaria) during the earliest Cretaceous. *Cretaceous Research*. 23: 37-48.
- Miyashiro, A. 1993. *Metamorphic Petrology*, UCL Press, 404 pp.
- Morillon, A. C.; Féraud, G.; Sosson, M.; Ruffet, G.; Crevola, G.; Lerouge, G. 2000. Diachronous cooling on both sides of a major strike slip fault in the Variscan Maures Massif (south-east France), as deduced from a detailed  $^{40}\text{Ar}/^{39}\text{Ar}$  study. *Tectonophysics*. 321: 103-126.
- Mposkos, E.; Krohe, A. 2006. Pressure–temperature–deformation paths of closely associated ultra-high-pressure (diamond-bearing) crustal and mantle rocks of the Kimi complex: implications for the tectonic history of the Rhodope Mountains, northern Greece. *Can. J. Earth Sci.* 43(12): 1755–1776.
- Natal'in, B. A.; Satır, M.; Sunal, G., and Toraman, E. 2005a. Structural and metamorphic evolution of the Strandja massif. Project No: 101Y010: Ankara, Turkey, Report, Scientific and Technical Research Council of Turkey.
- Natal'in, B. A.; Sunal, G.; Toraman, E. 2005b. The Strandja arc: anatomy of collision after long-lived arc parallel tectonic transport, *In*: Sklyarov, E. V. ed. *Structural and Tectonic Correlation across the Central Asia Orogenic Collage: North-Eastern Segment*. Guidebook and abstract volume of the Siberian Workshop IGCP-480, IEC SB RAS, Irkutsk, pp 240-245.
- Okay, A. I, and Satır, M. 2000. Upper Cretaceous eclogite facies metamorphic rocks from the Biga Peninsula, northwest Turkey. *Turkish Journal of Earth Sciences*. 9: 47-56.
- Okay, A. I.; Satır, M.; Tüysüz, O.; Akyüz, S.; Chen, F. 2001. The tectonics of the Strandja Massif: late-Variscan and mid-Mesozoic deformation and metamorphism in the Northern Aegean. *Int. J. Earth Sciences*. 90: 217-233.

- Perinçek, D. 1991. Possible strand of the North Anatolian Fault in the Thrace basin, Turkey—an interpretation. *American Association of Petroleum Geologists, Bulletin*. 57: 241–257.
- Pouchou, J. L.; Pichoir, F. 1984. A new model for quantitative analyses. I. Application to the analysis of homogeneous samples. *La Recherche Aérospatiale*. 3: 13–38.
- Pouchou, J.L.; Pichoir, F. 1985. “PAP” (f-r-Z) correction procedure for improved quantitative microanalysis. *In: Armstrong, J. T. ed. Microbeam analysis*. San Francisco Press. pp 104–106.
- Purdy, J. W, and Jäger, E. 1976. K-Ar ages on rock forming minerals from the Central Alps. *Mem Ins Geol Mineral Univ Padova*. 30: 1–30.
- Ring, U.; Brandon, M. T.; Willett, S. D.; Lister, G. S. 1999. Exhumation processes. *In: Ring, U.; Brandon, M. T, Lister, G. S., and Willett, S. D. eds. Exhumation Processes: Normal Faulting, Ductile Flow and Erosion*. Geological Society, London, Special Publications. 154: 1-27.
- Schumacher, J. C. 1997. The estimation of ferric iron in electron microprobe analyses of amphiboles. *Eur. J. Mineral*. 9:643–651.
- Searle, M. P.; Law R. D.; Godin, L.; Larson, K. P.; Streule, M. J.; Cottle, J. M., and Jessup, M. J. 2008. Defining the Himalayan Main Central Thrust in Nepal. *Journal of the Geological Society*. 165 (2): 523-534.
- Şengör, A. M. C.; Yılmaz., Y.; Sungurlu, O. 1984. Tectonics of the Mediterranean Cimmerides: nature and evolution of the western termination of Paleo-Tethys. *In: Dixon, J. E., and Robinson, A. H. F. eds. The geological evolution of the Eastern Mediterranean*. Geological Society of London Special Publication. 17:77-112.
- Spear, F. S. 1980. NaSi=CaAl exchange equilibrium between plagioclase and amphibole. An empirical model. *Contrib Mineral Petrol*. 72: 33-41.

- Spear, F. S. 1981. Amphibole-plagioclase equilibria: an empirical model for the relation albite + tremolite = edenite + 4 quartz. *Contrib Mineral Petrol.* 77: 355-364.
- Steiger, R. H, and Jäger, E. 1977. Subcommittee on geochronology: Convention on the use of decay constants in geo- and cosmochemistry. *Earth and Planetary Science Letters.* 36: 359-362.
- Sunal, G.; Natal'in, B. A.; Satır, M.; Toraman, E. 2006. Paleozoic magmatic events in the Strandja Massif, NW Turkey. *Geodinamica Acta.* 19 (5): 281-298.
- Sunal, G.; Satır, M.; Natal'in, B. A.; Toraman, E. 2008. Paleotectonic position of the Strandja Massif and surrounding continental blocks based on zircon Pb-Pb age studies. *International Geology Review.* 50 (5): 519–545.
- Topuz, G.; Altherr, R.; Satır, M.; Schwarz, W.H. 2004. Low-grade metamorphic rocks from the Pular complex, NE Turkey: implications for the pre-Permian evolution of the Eastern Pontides. *International Journal of Earth Sciences.* 93: 72-91.
- Topuz, G.; Okay, A. I.; Altherr, R.; Satır M.; Schwarz, W. H. 2008. Late Cretaceous blueschist-facies metamorphism in the southeastern Thrace (NW Turkey) and its regional implications. *Journal of Metamorphic Geology.* inpress.
- Toraman, E. 2002. Istranca masifinin Erikler-Elmacık köyleri civarındaki mesozoik yaşlı kayalarındaki deformasyonların yapısal ve kinematik analizi. Master thesis, İstanbul Teknik Üniversitesi, Avrasya Yer Bilimleri Enstitüsü, İstanbul. 58 p.
- Tricart, P.; Van der Beek, P.; Schwartz, S.; Labrin, E. 2007. Diachronous late-stage exhumation across the western Alpine arc: constraints from apatite fission-track thermochronology between the Pelvoux and Dora-Maira Massifs. *Journal of the Geological Society.* 164 (1): 163-174.

- Turpaud, P. 2006. Characterization of igneous terranes by zircon dating: implications for the UHP relicts occurrences and suture identification in the Central Rhodope, Northern Greece. PhD Thesis, Johannes-Gutenberg Universität, Mainz, 108 pp.
- Türkecan, A., and Yurtsever, A. 2002. Geological map of Turkey. Istanbul: Ankara, Turkey, General Directorate of Mineral Research and Exploration.
- Vonderschmidt, O. 2004. Rb/Sr-Datierungen an Kristallingesteinen des Strandja Massives, NW-Türkei und die geologische Position innerhalb der Pontiden. Diplomarbeit am Institut für Geowissenschaften der Eberhard Karls Universität, Tübingen, 108 pp.
- Yaltrak, C.; Sakıncı, M.; Aksu, A. E.; Hiscott, R. N.; Galeb, B.; Ulgen, U. B. 2002. Late Pleistocene uplift history along the southwestern Marmara Sea determined from raised coastal deposits and global sea-level variations. *Marine Geology*. 190: 283-305.

## Figure captions

**Figure 1.** Main tectonic units of the northern Aegean, the Balkanides and NW Turkey (modified after Okay and Satır 2000). IAES: Izmir-Ankara-Erzincan suture, NAF: North Anatolian Fault, MFZ: Maritsa Fault, WCFZ: West Crimean Fault.

**Figure 2.** Geological map of the study area. For location see Fig. 1.

**Figure 3.** Photomicrographs illustrating microtextural features of micaschists, orthogneisses, amphibolites and metasediments. (a) a large hornblende grain with inclusions of plagioclase, quartz and epidote in amphibolite (sample GK203). (b) an idioblastic garnet grain in a matrix consisting of plagioclase, biotite, quartz and epidote (sample GK206) (c) and (d) Relict feldspar grains with myrmekites in biotite-muscovite orthogneiss (Kırklareli metagranite, sample NK86-2). (e) Relict large muscovite grain is bent and finer grained phengites overgrow the muscovite grain. Note that the finer-grained phengites define the foliation and the relict muscovite is bent (sample GK304). (f) Some fine-grained phengite-rich white micas have relict cores of muscovite. Back-scattered electron image

**Figure 4.** Compositional variations of plagioclase from the basement orthogneisses and schists (Ep amphibolites), and the cover schists (greenschists), **b-** Chemical variation of biotites from the basement orthogneisses and schists (Ep amphibolites), and the cover schists (greenschists), **c-** Variation of (Fe+Mg) vs Si in K-white micas from the basement orthogneisses and schists (Ep amphibolites), and the cover schists (greenschists), **d-** Epidote compositions (X<sub>Fe3</sub>) from the basement orthogneisses and schists (Ep amphibolites), and the cover schists (greenschists).

**Figure 5** Amphibole compositions of the basement amphibolites (samples Nk-11.1 and Gk203).



**Figure 6. a-** Ca, Fe, Mg, and Mn chemical imaging of the garnets from the basement schists (sample Gk206). Note that line with arrow indicate chemical profile. **b-** Compositional profile across garnet grain from the basement schists.

**Figure 7.** P–T estimates deduced for the basement units from sample Gk206 and the cover units from sample GK304. Actinolite- hornblende transition according to Baker (1990). Approximate boundaries between metamorphic facies are shown as dotted lines: GS greenschist facies; LBS lawsonite-blueschist facies; EBS epidote blue-schist facies; EA epidote-amphibolite facies; AM amphibolite facies (Krogh et al. 1994 and references therein); Si isopleths for phengites (dashed lines) are from Massonne and Schreyer (1987).

**Figure 8.** Temperature estimates of the basement amphibolites (Spear 1980 and 1981).

**Figure 9.** Distribution of Rb-Sr biotite and muscovite ages in the study area and alignment of them on a roughly S-N directed cross-section.

Table 1. Mineral assemblages of orthogneisses, amphibolites, biotite schists and muscovite schists

Sample	Bt	Qtz	Pl	Kfs	Phe	Ep	Hbl	Grt	Chl	Ap	Zr	Ttn	Ilm	Rt	Cal
Basement orthogneisses															
NK11	++	++	++	++	-	+	-	-	-	o	o	o	-	-	-
NK2	++	++	++ <sup>1</sup>	++	+	+	-	-	-	o	o	-	-	-	-
NK31	+	++	++	++	+	+	-	-	o	o	o	-	o	-	-
NK86.2	o	++	++ <sup>1</sup>	++	+	+	-	-	o	o	o	o	o	-	-
amphibolites															
NK11.1	++	+	++	-	-	+	+	-	+	o	o	o	o	-	o
GK203	++	+	++	-	-	+	++	-	+	o	o	-	o	o	o
biotite schists															
GK200	++	+	++	-	+	++	-	-	+	o	o	o	-	-	-
GK206	++	++	+	++	-	+	-	+	+	o	o	-	o	-	-
Cover schists															
GK304	+	++	++ <sup>2</sup>	++	++ <sup>3</sup>	-	-	-	+	o	o	o	-	-	o

++ major constituent; + minor constituent; o accessory phase; - not observed; <sup>1</sup> relict albite; <sup>2</sup> only albite; <sup>3</sup> relict muscovite

Table2. Selected representative analyses of epidote minerals from basement amphibolites, orthogneisses, and schists.

	Basement Gneisses						Basement Amphibolites				Basement Schists			
	NK11		NK31		NK86-2		NK 11-1		GK203		GK200		GK206	
SiO <sub>2</sub>	37,74	37,77	36,04	36,21	38,08	37,66	38,53	38,08	36,02	35,44	38,09	37,94	37,17	38,29
TiO <sub>2</sub>	0,15	0,08	0,11	0,07	0,10	0,12	0,12	0,10	0,06	0,09	0,12	0,27	0,20	0,25
Al <sub>2</sub> O <sub>3</sub>	25,16	25,02	21,66	21,55	24,69	24,03	26,35	25,38	23,65	22,91	26,31	27,47	24,16	26,59
Cr <sub>2</sub> O <sub>3</sub>	0,02	0,00	0,02	0,07	0,00	0,00	0,01	0,00	0,03	0,00	0,09	0,03	0,09	0,05
FeO	10,77	10,29	13,28	13,20	10,33	11,42	8,81	10,72	9,90	10,23	9,04	7,63	9,98	7,88
MnO	0,41	0,34	0,30	0,23	0,37	0,42	0,31	0,30	0,26	0,17	0,31	0,19	0,21	0,26
MgO	0,04	0,03	0,08	0,11	0,00	0,00	0,08	0,00	0,27	0,43	0,03	0,09	0,01	0,01
CaO	22,72	23,19	21,43	21,42	22,68	22,73	23,23	22,57	20,26	19,39	23,48	23,29	22,36	23,14
Na <sub>2</sub> O	0,02	0,00	0,00	0,01	0,00	0,00	0,00	0,00	0,03	0,03	0,01	0,03	0,01	0,04
K <sub>2</sub> O	0,00	0,00	0,02	0,00	0,02	0,03	0,00	0,05	0,00	0,02	0,02	0,00	0,00	0,02
Total	97,03	96,70	92,93	92,88	96,25	96,41	97,44	97,20	90,48	88,69	97,49	96,92	94,18	96,52
Cation occupation on the basis of 12.5 oxygens														
Si	2,98	2,99	2,99	3,01	3,02	3,00	3,01	2,99	3,03	3,04	2,98	2,97	3,01	3,01
Ti	0,01	0,00	0,01	0,00	0,01	0,01	0,01	0,01	0,00	0,01	0,01	0,02	0,01	0,01
Al	2,34	2,33	2,12	2,11	2,31	2,25	2,42	2,35	2,34	2,31	2,43	2,53	2,31	2,46
Cr	0,00	0,00	0,00	0,00	0,00	0,00	0,00	0,00	0,00	0,00	0,01	0,00	0,01	0,00
Fe <sub>3</sub>	0,71	0,68	0,92	0,92	0,69	0,76	0,58	0,70	0,70	0,73	0,59	0,50	0,68	0,52
Mn	0,03	0,02	0,02	0,02	0,02	0,03	0,02	0,02	0,02	0,01	0,02	0,01	0,01	0,02
Mg	0,00	0,00	0,01	0,01	0,00	0,00	0,01	0,00	0,03	0,05	0,00	0,01	0,00	0,00
Ca	1,92	1,97	1,91	1,90	1,93	1,94	1,94	1,90	1,82	1,78	1,97	1,95	1,94	1,95
Na	0,00	0,00	0,00	0,00	0,00	0,00	0,00	0,00	0,00	0,00	0,00	0,00	0,00	0,01
K	0,00	0,00	0,00	0,00	0,00	0,00	0,00	0,00	0,00	0,00	0,00	0,00	0,00	0,00
Total	7,99	8,00	7,98	7,98	7,98	7,99	7,99	7,98	7,95	7,94	8,00	8,00	7,98	7,99
X <sub>Fe</sub>	0,23	0,23	0,30	0,30	0,23	0,25	0,19	0,23	0,23	0,24	0,20	0,16	0,23	0,17

X<sub>Fe</sub>=Fe/(Fe+Al); total Fe has been assumed to be Fe<sub>3+</sub>

Table 3. Selected representative analyses of garnets from biotite schist sample Gk 206.

Area	ORO	COO	IRO	ORC	COC	ORC	IRO	COO	ORO
SiO <sub>2</sub>	36,96	37,23	37,43	36,85	36,81	36,87	37,11	36,26	39,62
TiO <sub>2</sub>	0,00	0,02	0,00	0,00	0,04	0,03	0,07	0,03	0,00
Al <sub>2</sub> O <sub>3</sub>	19,62	20,85	20,67	20,73	20,86	20,84	20,75	20,50	21,50
Cr <sub>2</sub> O <sub>3</sub>	0,00	0,00	0,00	0,00	0,00	0,00	0,00	0,02	0,00
FeO	24,25	27,28	25,84	30,60	32,35	30,70	25,27	26,42	23,76
MnO	10,63	7,62	7,17	7,69	6,95	7,95	7,08	7,97	9,13
MgO	1,06	1,93	1,80	2,42	2,55	2,34	1,66	1,99	1,31
CaO	3,92	4,87	6,90	1,60	1,21	1,33	8,01	4,64	4,23
Na <sub>2</sub> O	0,94	0,06	0,03	0,01	0,03	0,02	0,01	0,06	1,11
K <sub>2</sub> O	0,03	0,01	0,01	0,00	0,00	0,01	0,00	0,01	0,08
Total	97,42	99,87	99,84	99,89	100,79	100,08	99,96	97,90	100,73
Cations on the basis of 12 oxygens									
Si	3,07	3,00	3,01	2,99	2,97	2,990	2,98	2,99	3,12
Ti	0,00	0,00	0,00	0,00	0,00	0,002	0,00	0,00	0,00
Al	1,92	1,98	1,96	1,98	1,98	1,992	1,97	1,99	1,99
Fe <sub>2</sub>	1,68	1,84	1,74	2,08	2,18	2,082	1,70	1,82	1,56
Mn	0,75	0,52	0,49	0,53	0,48	0,546	0,48	0,56	0,61
Mg	0,13	0,23	0,22	0,29	0,31	0,283	0,20	0,24	0,15
Ca	0,35	0,42	0,59	0,14	0,10	0,116	0,69	0,41	0,36
Na	0,15	0,01	0,00	0,00	0,01	0,003	0,00	0,01	0,17
K	0,00	0,00	0,00	0,00	0,00	0,001	0,00	0,00	0,01
Total	8,05	8,01	8,01	8,02	8,04	8,014	8,03	8,02	7,97
XAlm	0,58	0,61	0,57	0,68	0,71	0,69	0,55	0,60	0,58
XPyp	0,05	0,08	0,07	0,10	0,10	0,09	0,06	0,08	0,06
XGrs	0,12	0,14	0,20	0,05	0,03	0,04	0,22	0,14	0,13
XSps	0,26	0,17	0,16	0,17	0,15	0,18	0,16	0,18	0,23
Fe/Fe+Mg	0,93	0,89	0,89	0,88	0,88	0,88	0,90	0,88	0,91

ORO: outer rim of overgrown; COO; center of overgrown; IRO: inner rim of overgrown  
 ORC: outer rim of the core; COC: center of the core

Table 4. Selected representative analyses of biotite minerals from basement amphibolites, orthogneisses and schists and cover schists.

	Basement Orthogneisses				Basement Amphibolites				Basement Schists				Cover Schist				
	NK86-2	NK31	NK2	NK11	GK11-1	GK200	GK203	GK206	GK203	GK206	GK203	GK206	GK304	GK304			
SiO <sub>2</sub>	35,78	36,39	36,63	35,11	36,16	36,56	37,06	36,56	36,40	36,73	36,03	36,74	36,91	36,28	36,13	38,94	39,24
TiO <sub>2</sub>	2,20	1,71	2,10	2,39	2,78	1,88	1,94	1,99	2,10	2,31	2,01	1,23	1,50	1,54	1,62	1,29	1,37
Al <sub>2</sub> O <sub>3</sub>	15,76	15,83	16,34	16,04	15,88	16,60	16,19	16,16	16,28	15,99	16,79	16,54	16,61	17,42	17,87	14,23	14,69
Cr <sub>2</sub> O <sub>3</sub>	0,02	0,01	0,00	0,02	0,00	0,00	0,00	0,00	0,05	0,01	0,01	0,04	0,00	0,06	0,07	0,05	0,00
FeO	22,02	19,86	19,48	23,64	23,29	17,74	18,05	18,71	18,99	19,06	18,89	17,01	17,04	18,46	18,10	11,55	11,33
MnO	0,62	0,29	0,38	0,51	0,51	0,42	0,36	0,25	0,26	0,37	0,31	0,12	0,09	0,14	0,33	0,20	0,22
MgO	8,76	10,69	10,47	8,07	7,86	11,69	11,90	11,99	11,90	11,12	11,08	12,67	12,80	11,36	10,94	17,46	17,45
CaO	0,05	0,02	0,00	0,03	0,00	0,01	0,03	0,03	0,00	0,01	0,05	0,03	0,03	0,08	0,05	0,00	0,00
Na <sub>2</sub> O	0,08	0,06	0,13	0,08	0,08	0,08	0,06	0,18	0,15	0,14	0,13	0,11	0,09	0,19	0,21	0,07	0,06
K <sub>2</sub> O	9,04	9,52	9,60	8,60	9,38	9,62	9,59	9,05	9,43	9,45	9,26	9,07	9,14	8,87	9,21	10,06	10,01
Total	94,32	94,37	95,14	94,47	95,94	94,60	95,17	94,91	95,55	95,20	94,56	93,56	94,20	94,38	94,52	93,85	94,39
Cations on the basis of 11 oxygens																	
Si	2,80	2,81	2,80	2,76	2,80	2,79	2,81	2,79	2,77	2,80	2,76	2,81	2,80	2,77	2,76	2,91	2,90
Ti	0,13	0,10	0,12	0,14	0,16	0,11	0,11	0,11	0,12	0,13	0,12	0,07	0,09	0,09	0,09	0,07	0,08
Al	1,45	1,44	1,47	1,49	1,45	1,49	1,45	1,45	1,46	1,44	1,52	1,49	1,49	1,57	1,61	1,25	1,28
Cr	0,00	0,00	0,00	0,00	0,00	0,00	0,00	0,00	0,00	0,00	0,00	0,00	0,00	0,00	0,00	0,00	0,00
Fe <sub>2</sub>	1,44	1,28	1,25	1,55	1,51	1,13	1,15	1,19	1,21	1,22	1,21	1,09	1,08	1,18	1,15	0,72	0,70
Mn	0,04	0,02	0,02	0,03	0,03	0,03	0,02	0,02	0,02	0,02	0,02	0,01	0,01	0,01	0,02	0,01	0,01
Mg	1,02	1,23	1,19	0,94	0,91	1,33	1,35	1,36	1,35	1,26	1,27	1,45	1,45	1,29	1,24	1,94	1,93
Ca	0,00	0,00	0,00	0,00	0,00	0,00	0,00	0,00	0,00	0,00	0,00	0,00	0,00	0,01	0,00	0,00	0,00
Na	0,01	0,01	0,02	0,01	0,01	0,01	0,01	0,03	0,02	0,02	0,02	0,02	0,01	0,03	0,03	0,01	0,01
K	0,90	0,94	0,94	0,86	0,93	0,94	0,93	0,88	0,91	0,92	0,91	0,89	0,89	0,86	0,90	0,96	0,94
Total	7,80	7,84	7,82	7,79	7,79	7,83	7,82	7,83	7,85	7,82	7,82	7,82	7,82	7,80	7,81	7,88	7,86
XMg	0,41	0,49	0,49	0,38	0,38	0,54	0,54	0,53	0,53	0,51	0,51	0,57	0,57	0,52	0,52	0,73	0,73

$$XMg = Mg / (Mg + Fe)$$

Table 5. Selected representative analyses of amphiboles from amphibolites.

Sample	GK203				NK11-1			
	core	rim	core	rim	core	rim	core	rim
SiO <sub>2</sub>	43,56	41,96	43,08	42,71	43,54	41,56	42,59	41,47
TiO <sub>2</sub>	0,52	0,56	0,56	0,54	1,32	0,56	0,87	0,39
Al <sub>2</sub> O <sub>3</sub>	12,87	14,21	12,99	13,55	11,47	13,28	11,88	13,25
Cr <sub>2</sub> O <sub>3</sub>	0,05	0,03	0,03	0,01	0,00	0,01	0,05	0,04
FeO	15,97	16,44	15,77	15,62	17,90	18,85	18,22	19,25
MnO	0,38	0,32	0,37	0,26	0,52	0,52	0,55	0,47
MgO	10,71	9,95	10,75	10,24	9,71	8,57	9,24	8,34
CaO	11,38	11,18	11,41	11,18	11,46	11,38	11,37	11,49
Na <sub>2</sub> O	1,52	1,72	1,44	1,51	1,29	1,45	1,32	1,45
K <sub>2</sub> O	0,35	0,45	0,41	0,41	0,64	0,66	0,92	0,67
Total	97,31	96,81	96,81	96,03	97,84	96,84	97,00	96,82

Cation occupation on the basis of 23 oxygens

Si	6,424	6,248	6,381	6,383	6,477	6,274	6,420	6,275
Al(IV)	1,576	1,752	1,619	1,617	1,523	1,726	1,580	1,725
Al(VI)	0,660	0,740	0,650	0,770	0,489	0,636	0,530	0,638
Ti	0,058	0,062	0,062	0,060	0,147	0,063	0,099	0,044
Fe <sup>+3</sup>	0,508	0,534	0,553	0,433	0,432	0,581	0,460	0,584
Cr	0,006	0,003	0,004	0,001	0,000	0,002	0,005	0,005
Mg	2,354	2,208	2,374	2,282	2,152	1,928	2,075	1,881
Fe <sup>+2</sup> (C)	1,415	1,452	1,358	1,454	1,779	1,790	1,831	1,847
Mn(C)	0,000	0,000	0,000	0,000	0,000	0,000	0,000	0,000
Mg	0,000	0,000	0,000	0,000	0,000	0,000	0,000	0,000
Fe <sup>+2</sup> (B)	0,047	0,061	0,043	0,066	0,016	0,008	0,006	0,004
Mn(B)	0,048	0,041	0,046	0,033	0,065	0,066	0,071	0,060
Ca	1,799	1,784	1,810	1,790	1,826	1,841	1,836	1,863
Na(B)	0,107	0,115	0,101	0,111	0,093	0,085	0,087	0,073
Na(A)	0,328	0,381	0,313	0,325	0,278	0,338	0,299	0,353
K	0,065	0,085	0,077	0,079	0,121	0,128	0,177	0,128
Total A	0,393	0,466	0,390	0,404	0,399	0,466	0,475	0,482
XMg	0,62	0,59	0,63	0,60	0,55	0,52	0,53	0,50

Calculation method by Schumacher (1997)

Table 6. Representative analyses of muscovites/phengites from the basement orthogneisses and the cover schists.

	Basement Orthogneisses						Basement Schists		Cover Schists	
	NK2		NK31		NK86-2		GK206		GK304	
SiO <sub>2</sub>	48,20	46,78	46,62	46,25	47,29	51,15	46,59	49,21	49,79	49,39
TiO <sub>2</sub>	0,08	0,29	0,14	0,24	1,21	0,42	0,40	0,51	0,37	0,51
Al <sub>2</sub> O <sub>3</sub>	28,04	29,07	28,48	29,07	29,62	27,00	32,52	25,21	23,79	23,49
Cr <sub>2</sub> O <sub>3</sub>	0,00	0,00	0,00	0,05	0,05	0,01	0,00	0,04	0,05	0,04
FeO	5,94	7,54	5,73	6,79	5,36	5,00	2,69	6,48	6,00	6,39
MnO	0,00	0,07	0,04	0,09	0,05	0,08	0,00	0,10	0,10	0,09
MgO	1,91	1,55	2,22	1,86	1,57	2,56	1,42	3,18	3,75	3,59
CaO	0,01	0,00	0,00	0,02	0,00	0,01	0,01	0,00	0,00	0,07
Na <sub>2</sub> O	0,11	0,21	0,15	0,19	0,28	0,19	0,57	0,12	0,11	0,09
K <sub>2</sub> O	10,70	10,25	10,91	10,19	10,06	9,78	10,36	10,32	10,36	10,01
Total	94,98	95,76	94,29	94,74	95,48	96,19	94,55	95,17	94,31	93,66
Cation occupation on the basis of 11 oxygens										
Si	3,30	3,20	3,22	3,19	3,20	3,41	3,15	3,37	3,43	3,43
Ti	0,00	0,01	0,01	0,01	0,06	0,02	0,02	0,03	0,02	0,03
Al	2,26	2,34	2,32	2,36	2,37	2,12	2,59	2,03	1,93	1,92
Cr	0,00	0,00	0,00	0,00	0,00	0,00	0,00	0,00	0,00	0,00
Fe <sub>2</sub>	0,34	0,43	0,33	0,39	0,30	0,28	0,15	0,37	0,35	0,37
Mn	0,00	0,00	0,00	0,01	0,00	0,00	0,00	0,01	0,01	0,01
Mg	0,20	0,16	0,23	0,19	0,16	0,25	0,14	0,32	0,39	0,37
Ca	0,00	0,00	0,00	0,00	0,00	0,00	0,00	0,00	0,00	0,01
Na	0,01	0,03	0,02	0,02	0,04	0,02	0,08	0,02	0,01	0,01
K	0,93	0,89	0,96	0,90	0,87	0,83	0,89	0,90	0,91	0,89
Total	7,04	7,07	7,10	7,08	7,00	6,94	7,02	7,05	7,05	7,03
XMg	0,36	0,27	0,41	0,33	0,34	0,48	0,48	0,47	0,53	0,50

XMg=Mg/(Mg+Fe<sub>2+</sub>); all Fe has been assumed to be Fe<sub>2+</sub>

Table 7. Results of Rb-Sr dating on muscovite and biotite separates.

Sample	Rb ( $\mu\text{g/g}$ )	Sr ( $\mu\text{g/g}$ )	$^{87}\text{Rb}/^{86}\text{Sr}$	$^{87}\text{Sr}/^{86}\text{Sr}$	Age (Ma)
<b>Kırklareli metagranite</b>					
K1(WR)	233,67	77,84	8,7108	0,738796	
K1(Bt)	1215,29	3,99	1084,2040	3,080426	153,2 $\pm$ 1,5*
K2(WR)	161,49	101,91	4,5923	0,724478	
K2(Bt)	1050,23	2,91	1339,9260	3,646080	153,9 $\pm$ 1,5*
K2(Ms)	599,35	7,40	247,3130	1,285593	162,6 $\pm$ 1,6*
K3(WR)	189,22	83,30	6,5869	0,731029	
K3(Bt)	1077,08	2,27	1917,1510	4,773714	148,9 $\pm$ 1,4*
<b>Hbl-Bt granite gneiss</b>					
HBG1(WR)	37,75	218,38	0,5002	0,710005	
HBG1(Bt)	312,31	3,66	258,7802	1,221822	139,4 $\pm$ 1,3*
HBG2(WR)	66,17	337,10	0,5682	0,710675	
HBG2(Bt)	359,87	1,93	597,1190	1,850316	134,4 $\pm$ 1,3*
<b>White mylonitic gneiss</b>					
WMG1(WR)	274,21	64,15	12,4327	0,763225	
WMG1(Ms)	728,76	15,27	146,2300	1,316260	290,5 $\pm$ 3,0*
WMG2(WR)	223,19	49,50	13,1134	0,763604	
WMG2(Ms)	719,90	19,07	114,1029	1,164795	279,2 $\pm$ 3,0*
<b>Biotite schist</b>					
MS1(WR)	62,57	286,01	0,6335	0,715350	
MS1(Bt)	473,73	4,44	328,8366	1,378453	142,1 $\pm$ 1,4*
MS1 (Ms)	208,74	57,50	10,5310	0,736328	149,1 $\pm$ 2,1*
MS2(WR)	188,34	307,63	1,7726	0,714919	
MS2(Bt)	389,45	8,14	142,2624	0,993520	139,5 $\pm$ 1,3*
<b>Biotite schist</b>					
MS3(WR)	116,58	213,92	1,5778	0,714517	
MS3(Ms)	364,14	17,45	61,1911	0,848146	157,7 $\pm$ 1,5*
MS4(WR)	39,99	510,20	0,2268	0,707188	
MS4(Bt)	373,71	6,77	165,1434	1,061114	151,0 $\pm$ 1,4*
<b>Bt-Mc granite gneiss</b>					
BMG1(WR)	128,18	176,37	2,1055	0,721414	
BMG1(Ms)	602,49	13,58	135,5085	1,282625	295,6 $\pm$ 2,8*
BMG2(WR)	92,28	245,76	1,0871	0,714743	
BMG2(Bt)	412,87	20,86	57,9109	0,824941	136,4 $\pm$ 1,3*
<b>Bt mylonite</b>					
GK127(WR)	101,88	135,33	2,1797	0,714944	
GK127(Bt)	680,40	5,04	424,2448	1,579272	144,1 $\pm$ 1,4
GK128(WR)	84,97	430,20	0,5715	0,709319	
GK128(Bt)	502,56	15,18	97,5861	0,901420	139,3 $\pm$ 1,3
GK129(WR)	92,09	448,58	0,5941	0,709374	
GK129(Bt)	598,79	10,35	173,4460	1,074460	148,6 $\pm$ 1,4
GK131(WR)	81,97	455,27	0,5210	0,710099	
GK131(Bt)	547,90	8,43	194,9987	1,085982	136,0 $\pm$ 1,3
<b>Ms mylonite</b>					
GK130(WR)	166,12	89,24	5,3976	0,730247	
GK130(Ms)	540,24	10,13	159,9481	1,080387	159,4 $\pm$ 1,5
GK134(WR)	199,11	93,10	6,2035	0,733686	
GK134(Ms)	562,56	19,70	84,1507	0,899454	149,6 $\pm$ 1,5
GK135(WR)	111,82	93,22	3,4772	0,727350	
GK135(Ms)	546,55	35,17	45,4823	0,824641	162,9 $\pm$ 1,6
GK136(WR)	104,98	284,78	1,0670	0,711537	
GK136 (Ms)	542,80	74,36	21,2246	0,758051	162,3 $\pm$ 1,6

WR: Whole-rock, Bt: Biotite, Ms: Muscovite, Hbl: Hornblende

\* Ages recalculated after Vonderschmidt (2004) according to the following errors;

2  $\sigma$  error on  $^{87}\text{Rb}/^{86}\text{Sr}$  is 1%; 2  $\sigma$  error on  $^{87}\text{Sr}/^{86}\text{Sr}$  is 0.003%



Fig 1

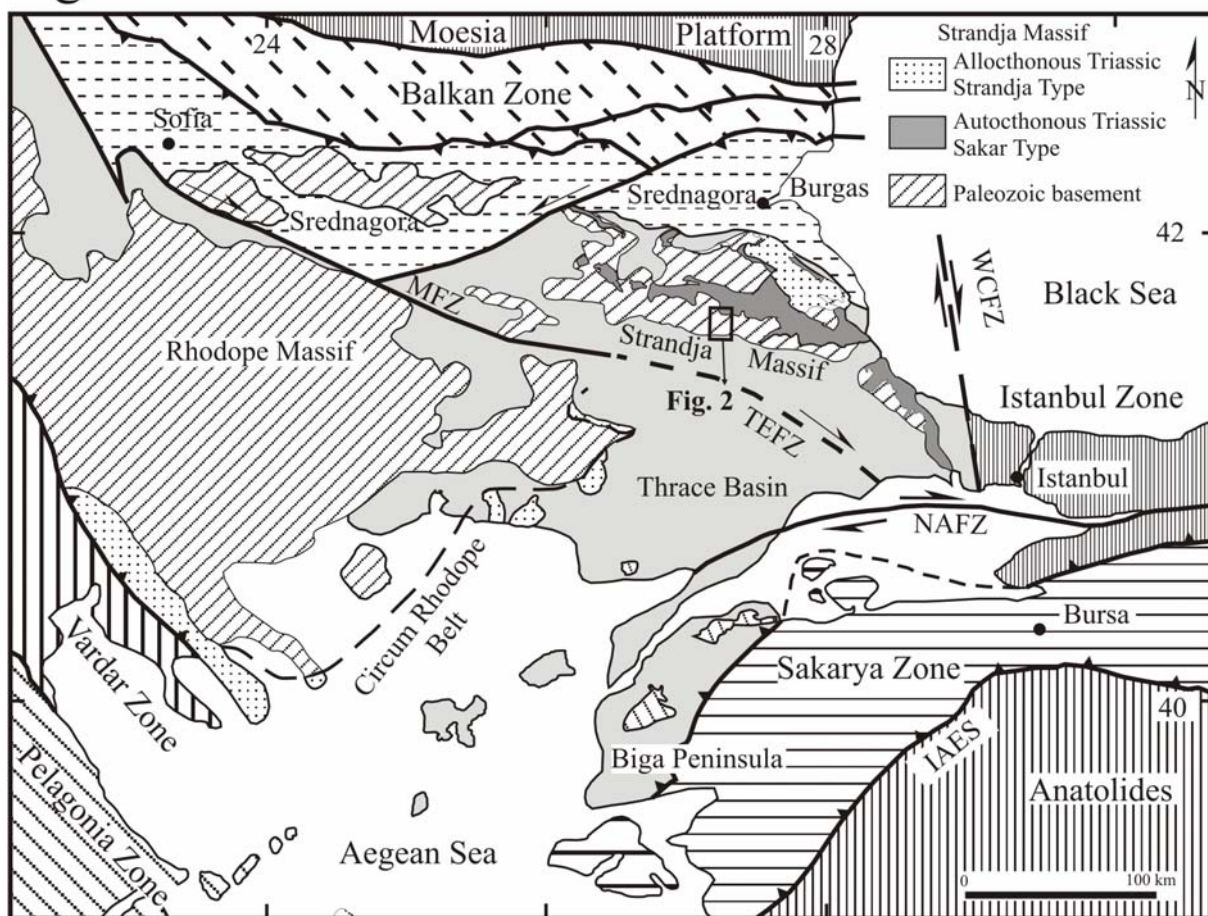


Fig. 2

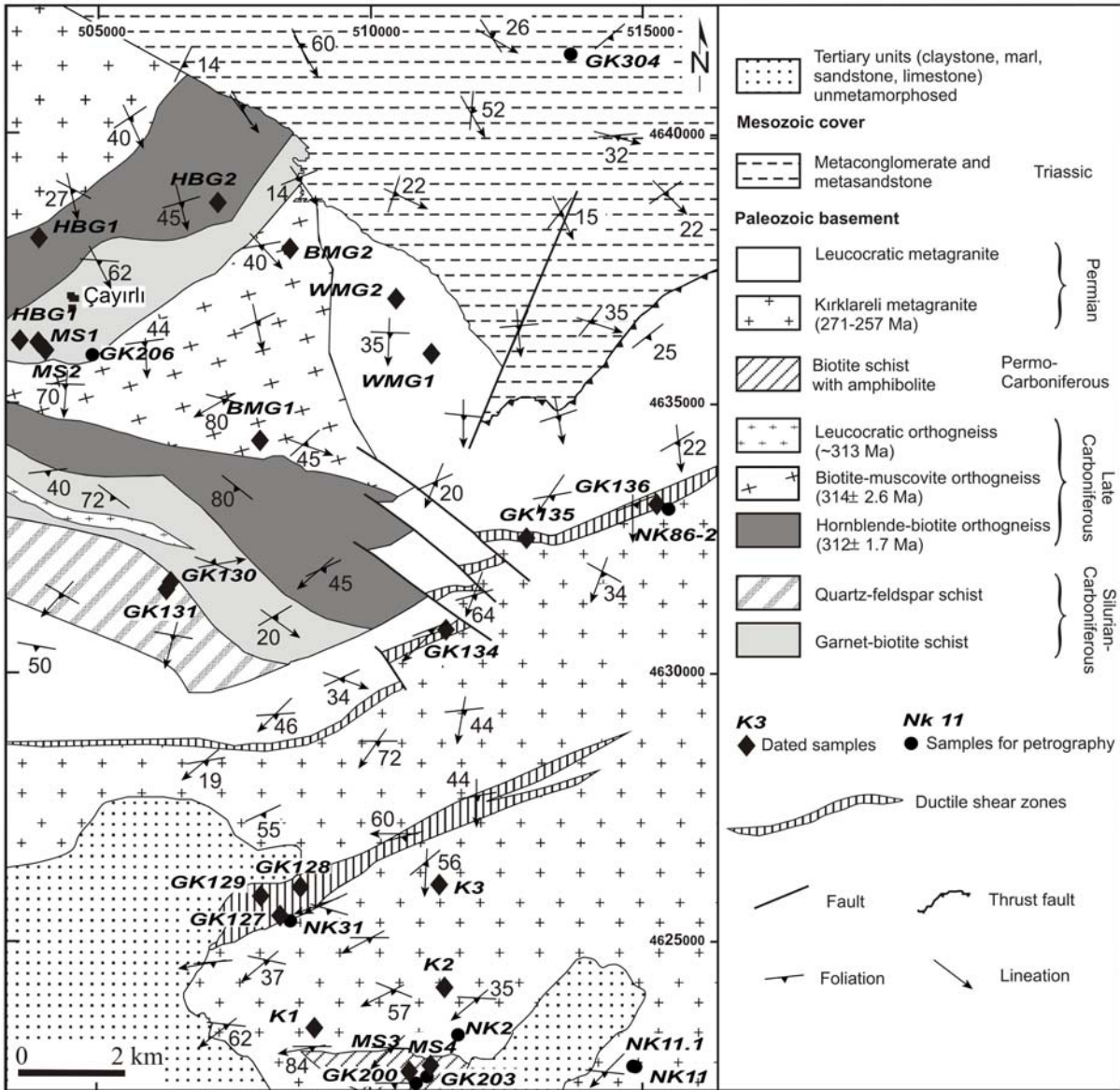


Fig. 3

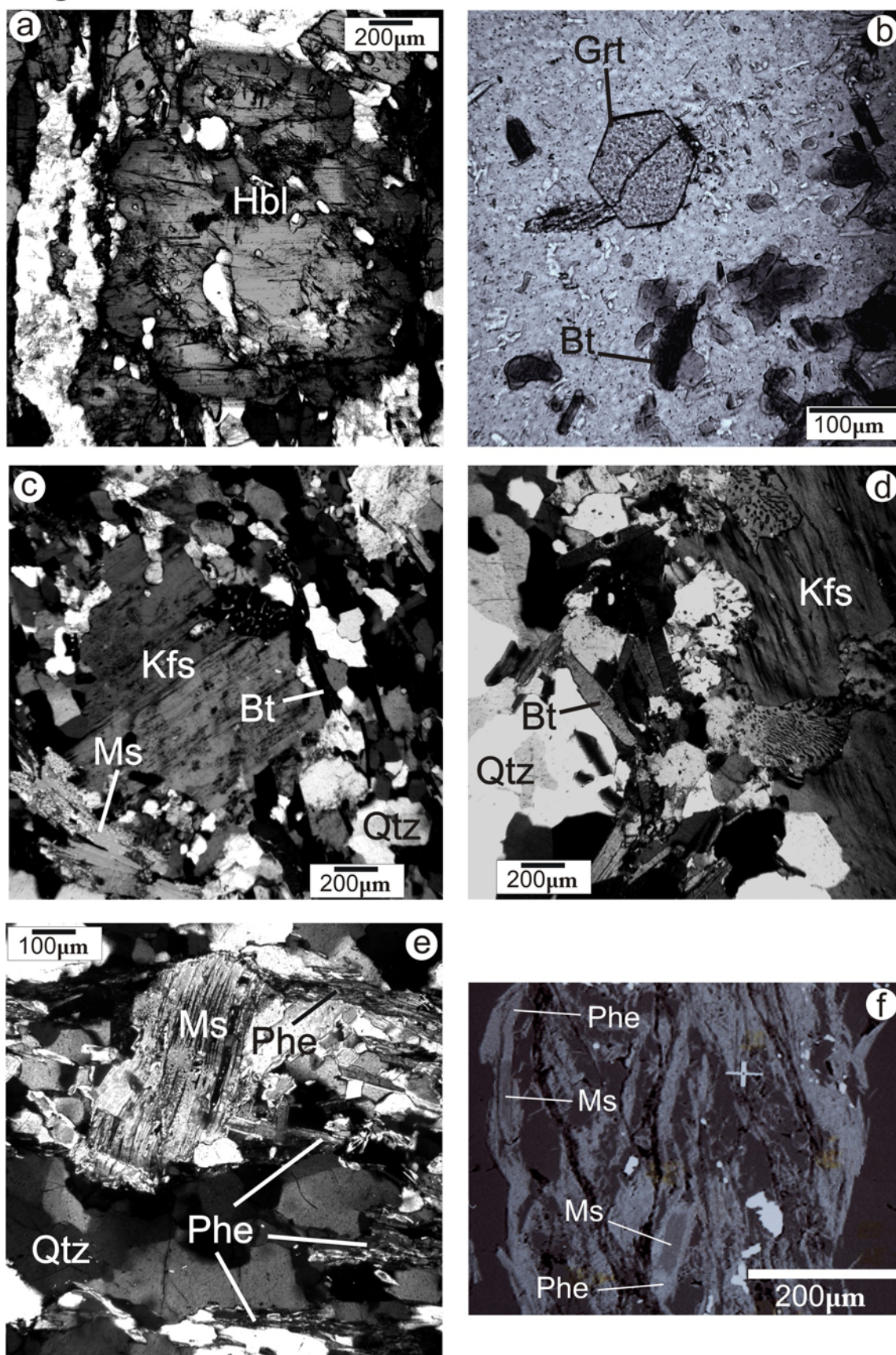


Fig. 4

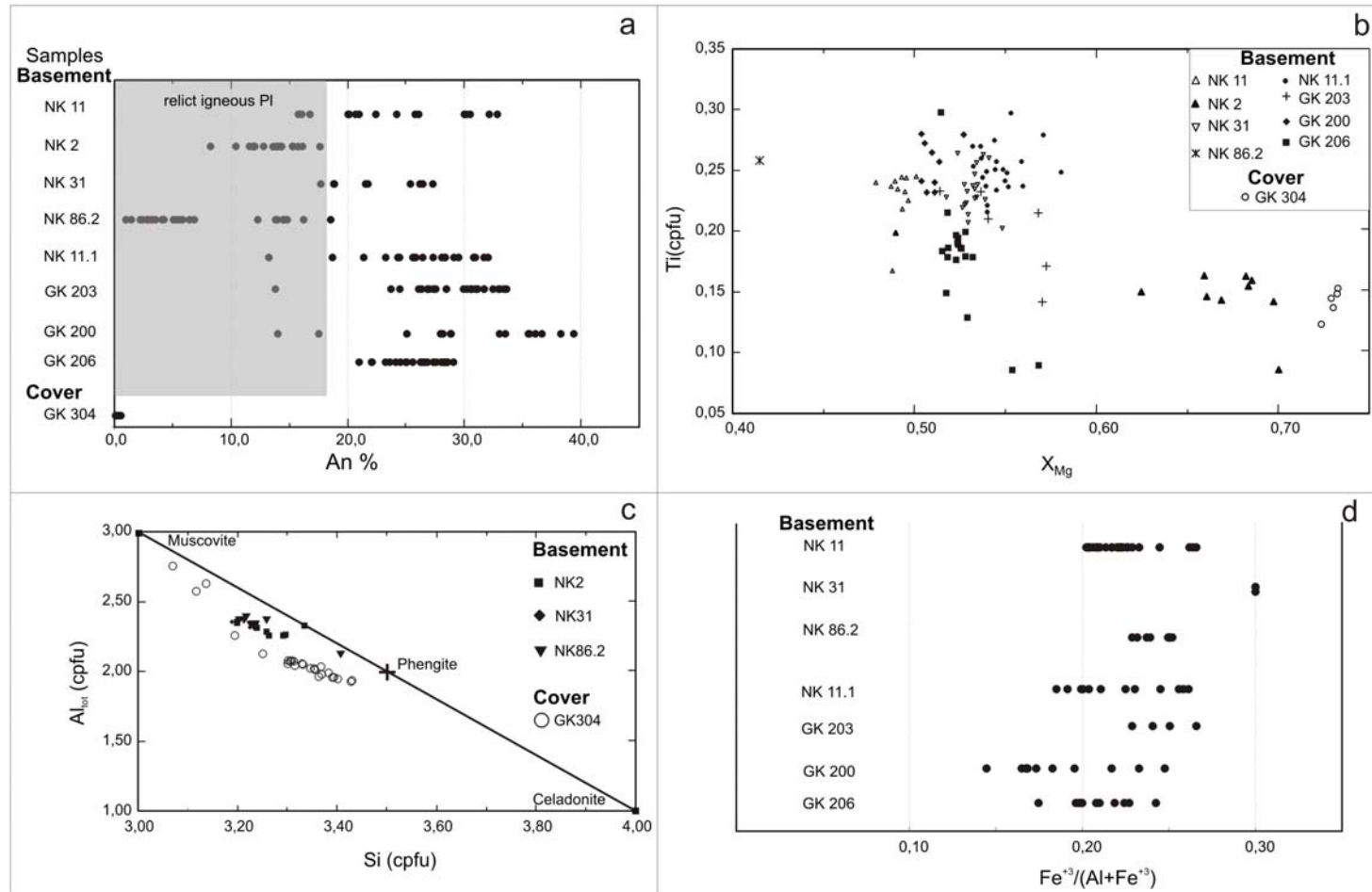


Fig. 5

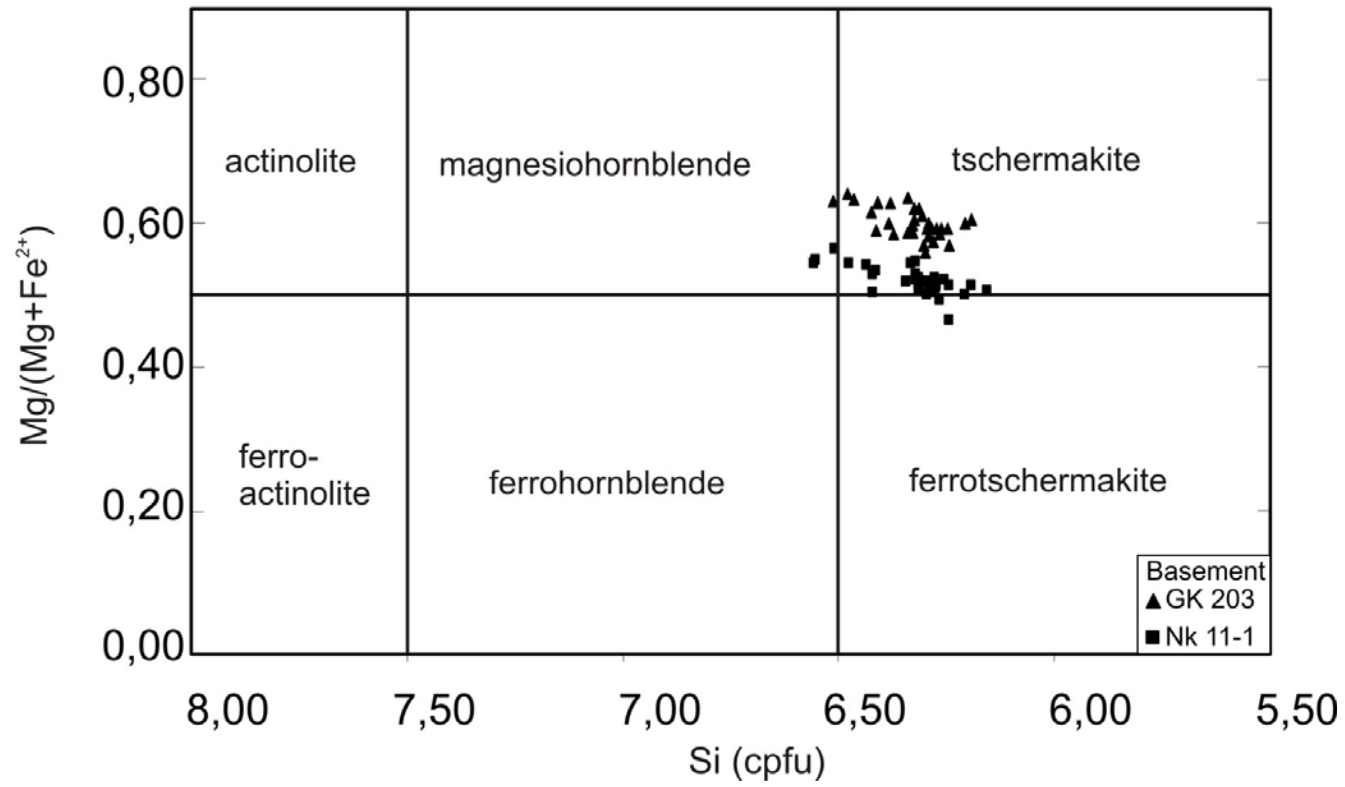


Fig.6

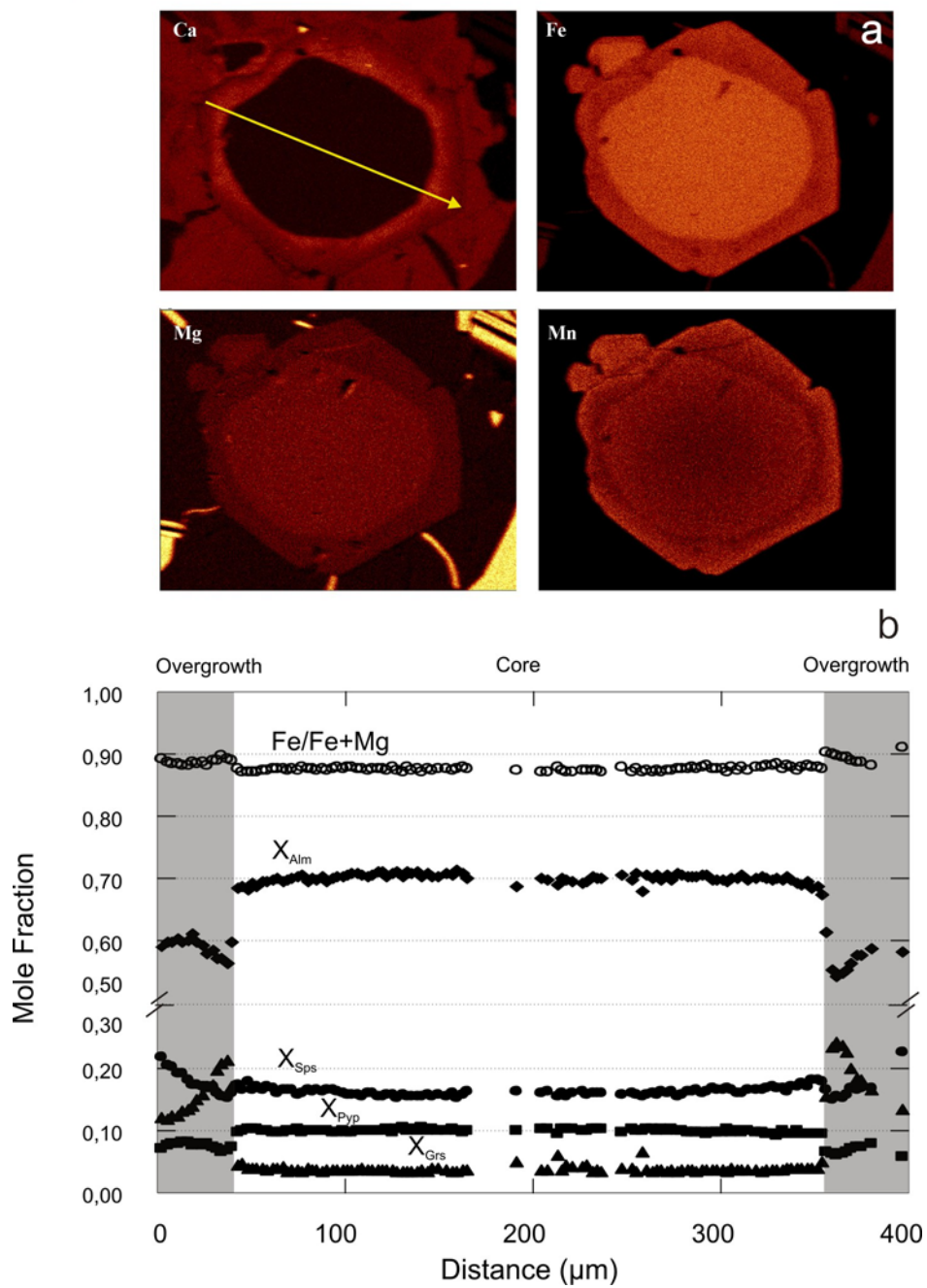


Fig. 7

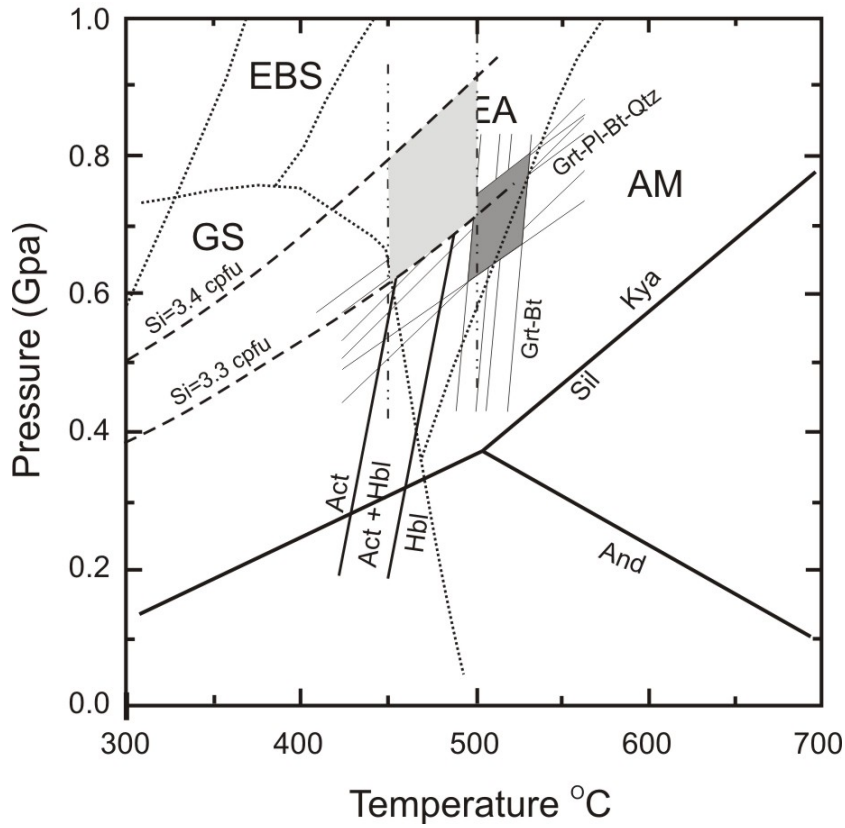


Fig. 8

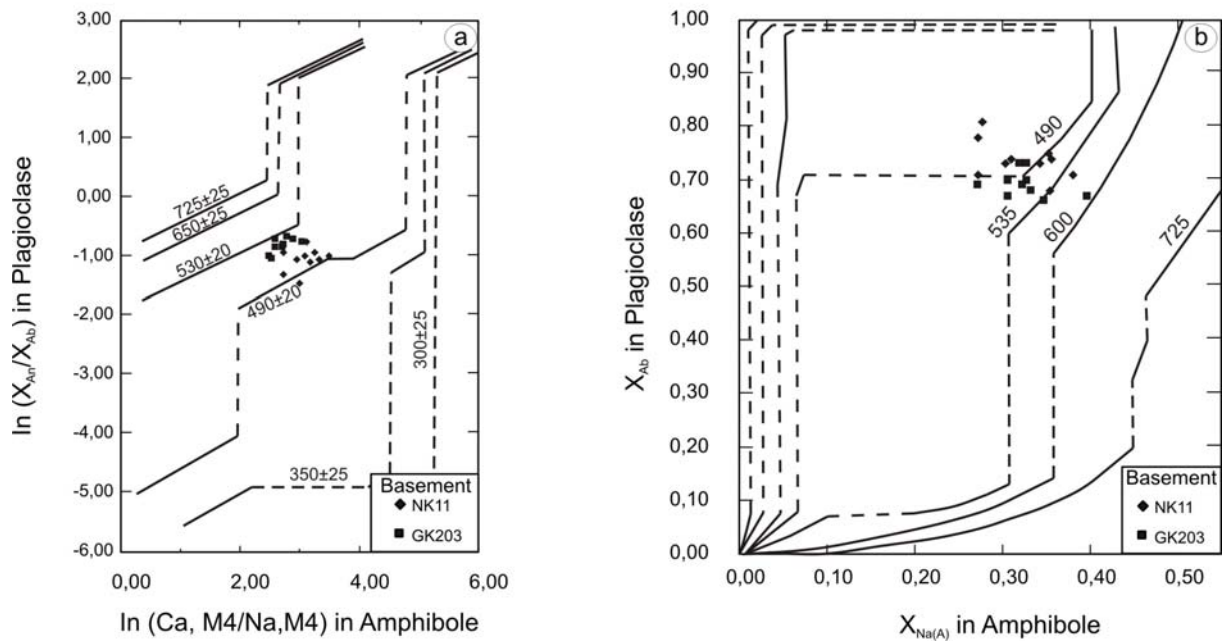
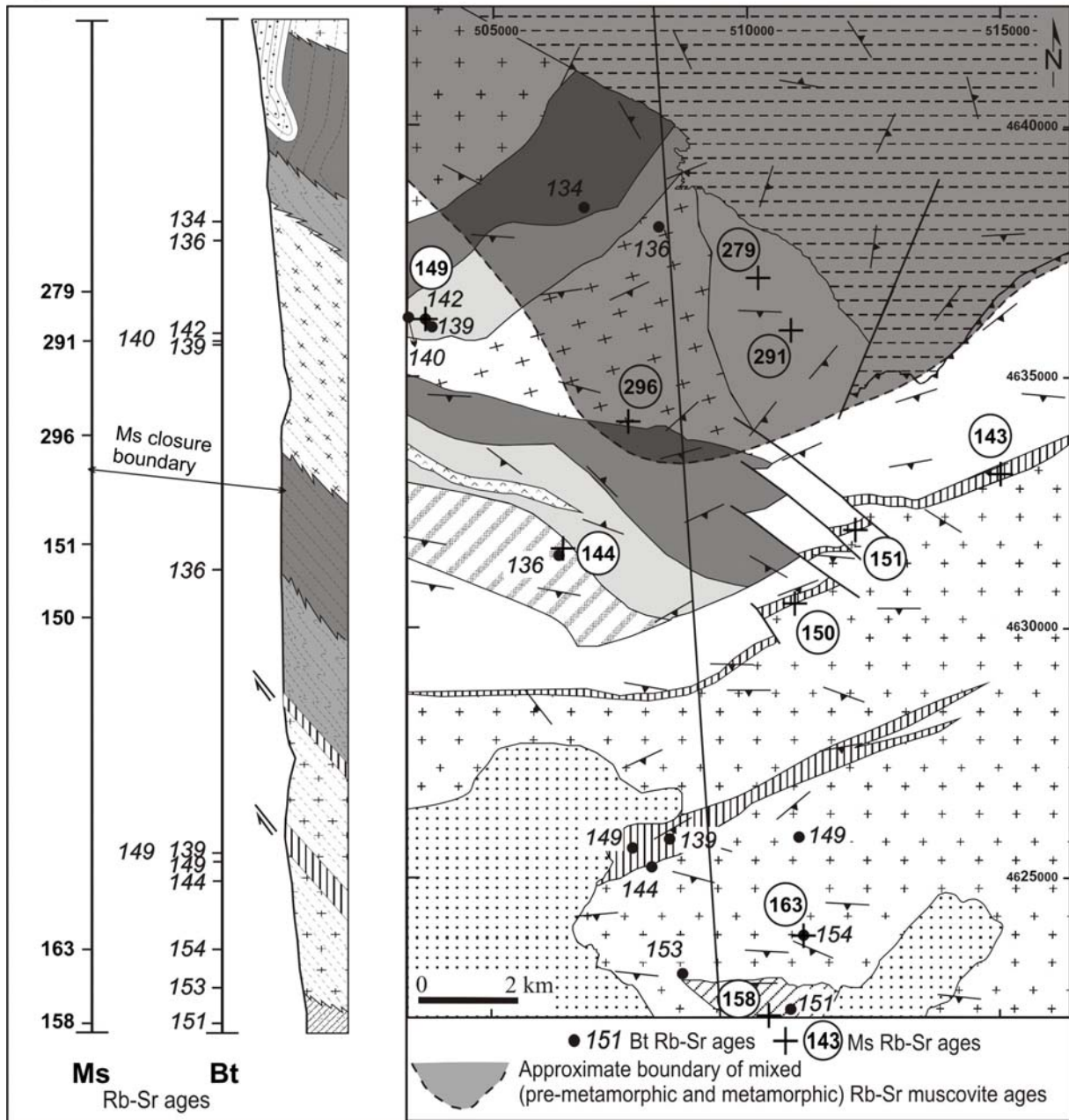


Fig. 9





## Curriculum Vitae

24.03.1970 Date of Birth

1989-1994 B.S. Geology: Istanbul Technical University, Mining Faculty, Department of Geology.

1994-1995 English Preparing School, İstanbul Technical University.

1995-1998 M.S. Geology: Istanbul Technical University, Science and Technology Institute

2001- PhD. Universität Tübingen, Institut für Mineralogie, Petrologie und Geochemie.

## **EIDESSTATTLICHE VERSICHERUNG**

Hiermit erkläre ich, dass ich die vorliegende Arbeit selbstständig verfasst habe und keine anderen als die von mir angegebenen Quellen und Hilfsmittel benutzt habe.

Ferner erkläre ich, dass ich nicht anderweitig mit oder ohne Erfolg versucht habe, eine Dissertation einzureichen.

Tübingen, 16 December 2008

A handwritten signature in black ink, appearing to be 'G.S.' or similar, written in a cursive style.

Gürsel Sunal